FINAL REPORT

LUNAR PHOTO STUDY

Contract NAS9-3826

1 December 1964 - 1 October 1965

Z-3841

Prepared by

EASTMAN KODAK COMPANY
Apparatus and Optical Division
Rochester, New York, 14650

For

NASA Manned Spacecraft Center
Lunar Surface Technology Branch/ET33
Advanced Spacecraft Technology Division
2101 Webster-Seabrook Road
Houston, Texas, 77058

Prepared by: George T. Keene

Approved by: W. H. Allaman

Frederick S. Oder

1 October 1965

FORWARD

This work represents the Final Report on the Lunar Photo Study for the National Aeronautics and Space Administration, Manned Spacecraft Center, Houston, Texas, under Contract NAS9-3826 to the Eastman Kodak Company, Rochester, New York.

Beginning 1 December 1964 the contract authorized a ten-month study to investigate the photometric properties of realistic lunar models and to examine the interpretation of photographs of these models taken under a variety of conditions. The study was conducted under the cognizance of the Advanced Spacecraft Technology Division, with Mr. Robert L. Jones of the Lunar Surface Technology Branch serving as Technical Representative.

SUMMARY

This work studied the effect of several photographic parameters on the detection and identification of lunar surface details. The investigation was accomplished by having three readers evaluate photographs of models dusted with copper oxide to match the lunar photometric function. A slide projector of 1/2 degree subtense simulated the sun and could be set at sun elevations from 0° to 90°. Combinations of lens and film quality were selected to yield systems having limiting high contrast resolution of 53 lines/mm, 92 lines/mm, and 220 lines/mm.

Two kinds of models were dusted with copper oxide and photographed. The first contained both concave and convex cones and hemispheres, while the second (KLM6-65) was a realistic lunar landscape based on measurements from pictures taken by Rangers 7 and 9. The ability of the readers to detect and identify objects was the same for both geometric shapes and craters. In general, stereo and oblique photography revealed only slightly smaller objects than could be identified in a single picture taken perpendicular to the model.

A graph of universal value relates phase angle (angle between sun and observer) to the ratio of object size to pitch of the limiting tri-bar resolution. Such a plot contains zones of detection and identification and shows that maximum information is obtained from pictures exposed at phase angles of 70° to 85°. Under these conditions objects equal in size to the limiting system resolution may be detected, while objects twice this size may be identified.

A motion picture was made using KLM6-65 and other models to show the view from the landing LEM during the last 10,000 feet of the descent.

Several areas are suggested for additional study.

TABLE OF CONTENTS

TABLE OF CONTENTS CONT'D.

LIST OF FIGURES

LIST OF FIGURES CONT'D.

LIST OF FIGURES CONT'D.

LIST OF TABLES

INTRODUCTION

This study investigated the photometric properties of realistic lunar models and examined the interpretation of photographs of these models taken under a variety of conditions. Results and conclusions from this study have been reported in four bimonthly reports and in two oral presentations at the Manned Spacecraft Center, Houston, Texas. This report summarizes the findings from the investigation over the past 10 months and concludes with specific recommendations for a continuing effort.

This report is divided into the following six sections:

A. Lunar Photometry and Prior Work

B. Materials and Techniques

C. Geometric Shapes

D. Kodak Lunar Model 6-65

E. Motion Picture

F. Proposed Follow-On Work

A. LUNAR PHOTOMETRY AND PRIOR WORK

As viewed from the earth, the moon reflects light in a peculiar fashion, unlike either a diffuse or a specular reflector. The apparent luminance of the lunar surface is primarily a function of the phase angle - the angle between the observer and the sun as seen from the lunar surface. Figure A-1 compares lambert diffuse reflection with simulated lunar reflection.

This mode of reflection makes all areas of the moon reach maximum apparent brightness at full moon independent of their location on the moon. Figure A-2 shows the relative luminance of semi-specular, diffuse and lunar

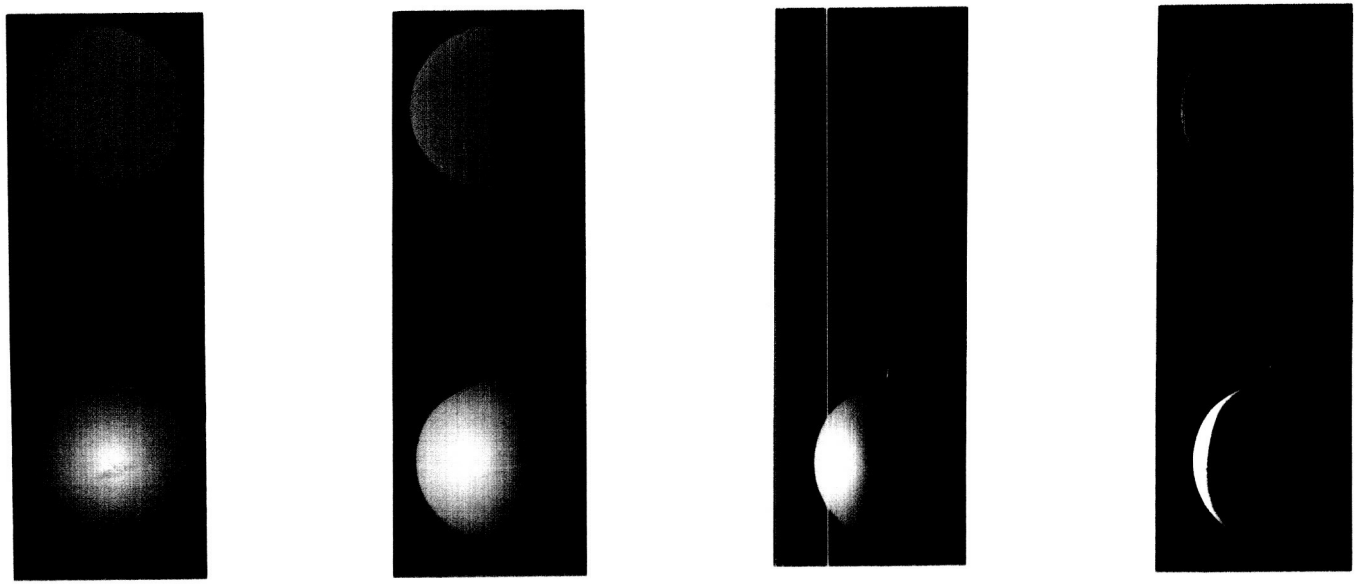

Phase Angle 3° 45° 90° 155°

Comparison of Lambert reflection vs. Simulated Lunar Photometric Function reflection. The lower ball is a diffuse reflector that reflects about 6% of the incident light. The upper ball has been dusted with copper oxide to simulate the Lunar photometric function (approximately 6% albedo). It should be noted that near full moon (3 degree phase angle) the lower ball (diffuse reflector) is brighter near the center than at the edge giving it a rounded appearance, but the upper ball (Lunar photometric function) is nearly the same brightness at the edge as it is at the center making it appear more like a disk than a ball. Also the upper ball (Lunar photometric function) darkens very quickly with increasing phase angle compared with the diffuse ball. The light source subtends one-half degree.

Figure A-1

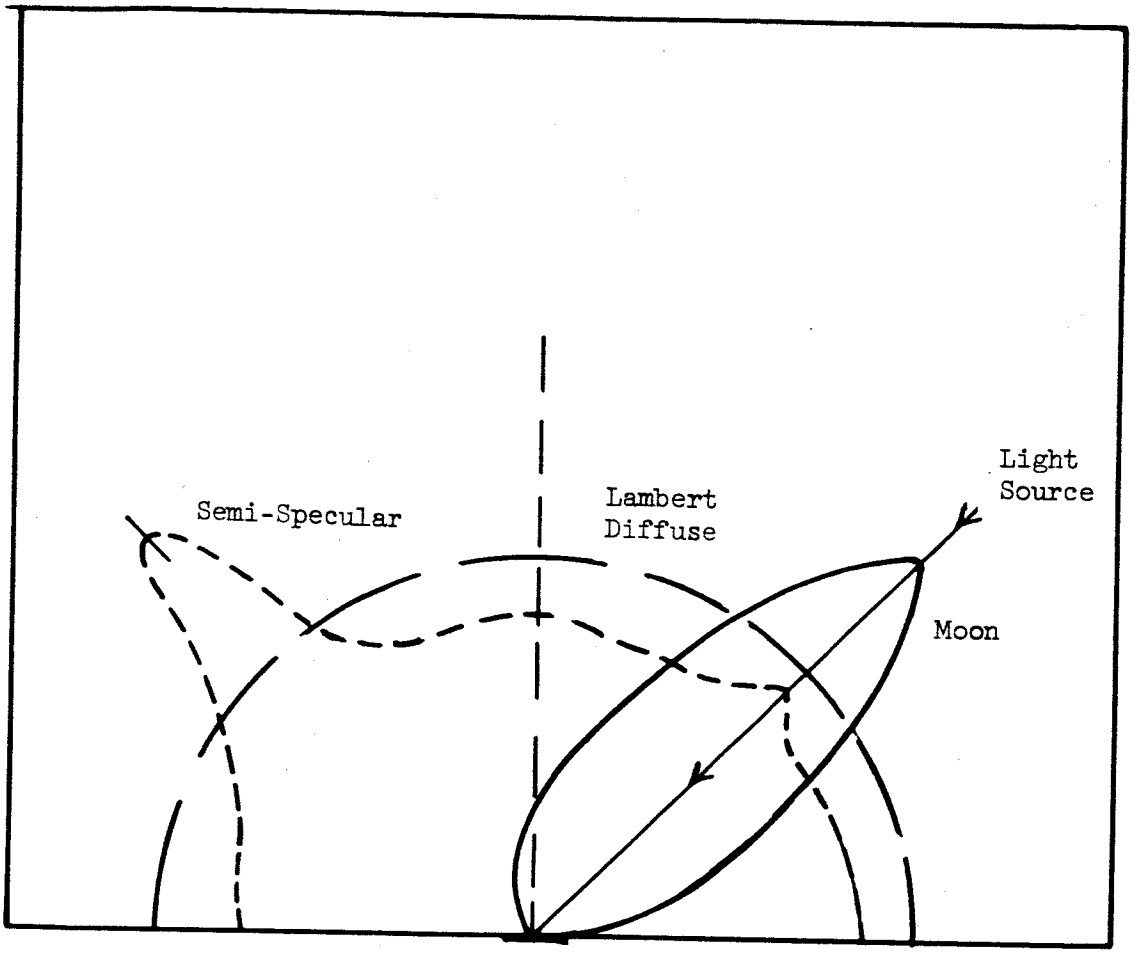

Relative reflectance of diffuse, lunar, and semi-specular reflectors under light incident 45 degrees to the vertical.

Figure A-2

reflectors of similar albedo when illuminated at 45° to the surface normal. The lunar surface shows substantial back scatter and a lack of specular reflection, both features characteristic of highly structured surfaces. This structure may be of any size as long as it is slightly larger than the wavelength of light and elements in the structure are not resolved by the viewer.

Light reflected from the moon is best characterized by the lunar photometric function - the ratio of the brightness at "full moon" to that seen at lower sun elevations. Figure A-3 shows this function as measured by several observers; all areas of the moon are remarkably similar in this property. Van Diggelen pointed out the similarity between the moon's reflectance and that of vegation having a branched and detailed structure. Variations in lunar albedo, the inherent reflectance of an object, range from 6% to 18%. The photometric function, however, causes a change of over 15 times in the luminance of any given area.

While resolution of lunar details from earth is no better than about 1 mile, there is now general agreement that the lunar photometric function is probably caused by the first 0.1 to 0.3 millimeter thickness of a layer of dust covering all the lunar surface. In recent years several workers have produced laboratory simulations of the lunar reflectance curves. Most applicable to the Kodak study is the work of Gold and Hapke at Cornell University and that of Halajian at the Grumman Aircraft Engineering Corp. Along with other materials, these workers used certain dusts (notably copper oxide) to produce the close match to the lunar photometric function shown in Figure A-2.

As described in Section B, Kodak has successfully dusted realistic lunar models with copper oxide without losing details as small as 1/8 inch in diameter. While these models accurately match the form of lunar details at a size of 1 to 30 feet, we do not know if the fine detail of the lunar surface has the same photometric function as that observed from earth.

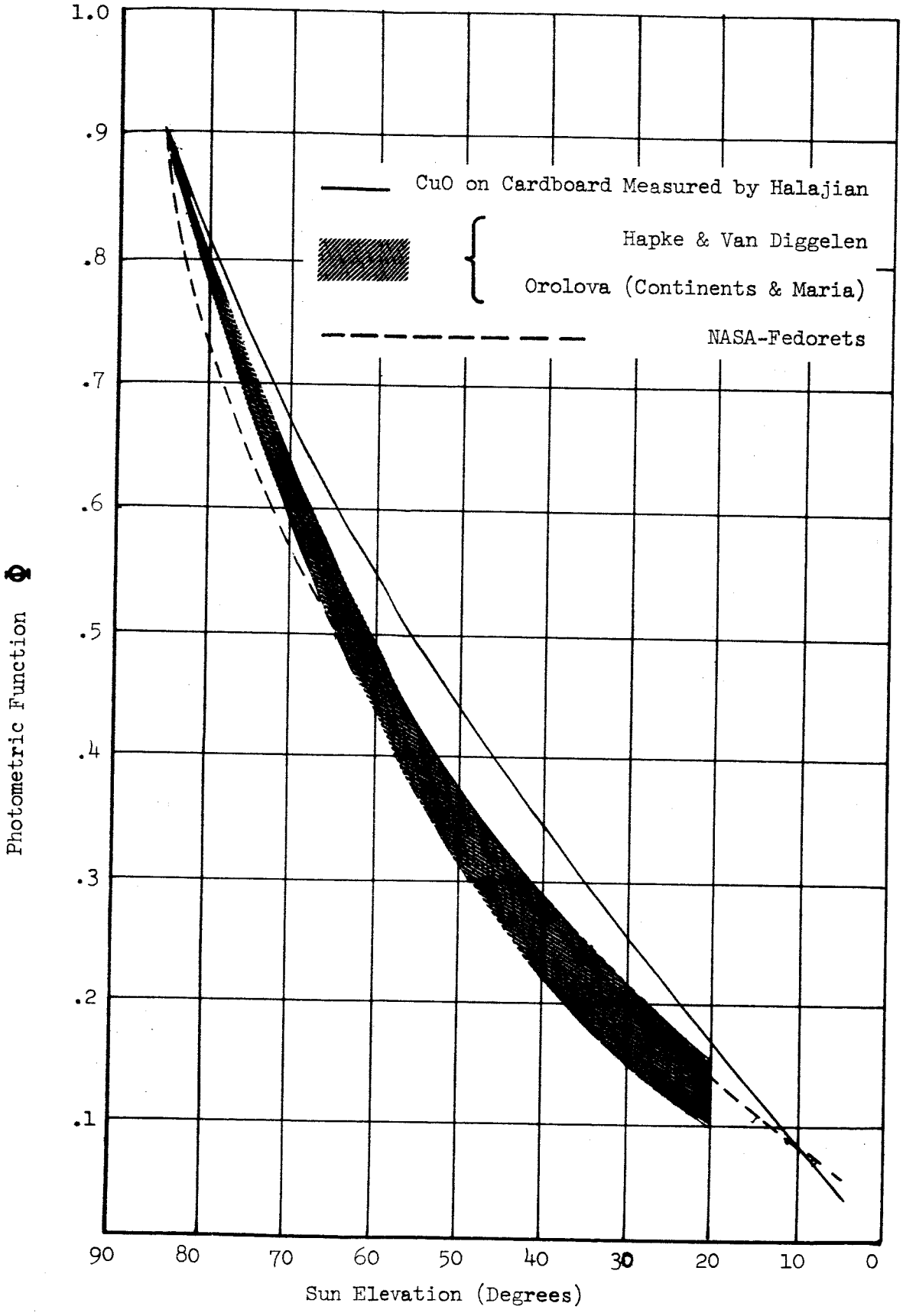

Figure A-3 Photometric Measurements of Simulated Lunar Surfaces

In addition, there are undoubtedly local variations in albedo, color, and dust-cover that our models do not correctly simulate. Despite these uncertainties, the Kodak models reflect as realistically as possible the measurements and theories of many lunar investigations and form a suitable medium for the study of high resolution lunar photography.

B. MATERIALS AND TECHNIQUES

1. Dusting Materials

This Lunar Photography Study is based upon creating in the laboratory geometric shapes and simulated lunar surfaces that will reflect the light in the same manner as the Lunar surface. Some of these shapes will be on the order of 0.1 inch and smaller in size so that the material which is used to provide this reflectance or back scatter must be small compared to these dimensions; in other words it could be a dust with very small particles.

Measurements of the back scatter of many materials have been done at Grumman Aircraft under a NASA contract by Mr. John Halajian with a photometer especially designed to measure the photometric function of materials. It was agreed that this photo study would use a material and dusting technique reported by Mr. Halajian. To coordinate this effort a visit was made to Grumman Aircraft in January of 1965 where Mr. Hallock and Mr. Lambity demonstrated the Grumman photometer and showed auto-plotted curves of many materials. Most of these Grumman measured materials were too large for use with the proposed Kodak models. Their CuO (obtained from Fisher Scientific Company) has a low albedo (0.07) but matches the lunar photometric function; and its albedo is higher than the CuO (obtained from Will Corporation) used by Kodak (0.03) in our early work.

In our search for a material with higher albedo but with the lunar photometric function Mr. Halajian suggested that we might try alternate layers of varnish and powder of high albedo to obtain a light material with intricate surface structure. This suggestion is based upon a theory he has

developed using both horizontal and vertical surfaces in a honeycomb-like structure. He shows in one of his reports that these surfaces can have a high albedo and still have a photometric function matching that of the moon. This scheme was never tried because this photo study needed very small, dust-like particles that would cover but not distort the small surfaces of the proposed lunar models.

Grumman has measured only two other dust type materials - silver chloride and volcanic ash. The first material, silver chloride, darkens with age, has an albedo of about 0.13 after aging and has a photometric function matching that of the moon. It is considerably more expensive than copper oxide, and commerical silver chloride will not pass through a 400 mesh screen (particle size used in dusting). It cannot be used for dusting unless each crystal is first coated with a thin layer of gelatin. Photometric measurements of silver chloride are described in section B2.

The second material, volcanic ash, has a lower albedo (0.05) in large chunks and gives a good photometric match to the moon. However, as this material is ground finer and finer the albedo rises to 0.13 or higher and its photometric function approaches that of a Lambert surface.

Since Halajian is primarily interested in determining the load bearing capability of the lunar surface, most of the materials measured by the Grumman photometer are too large to consider for dusting the small details on Kodak models.

It was agreed by NASA that the Kodak models would be dusted with CuO using Halajian dusting techniques.

a. Copper Oxide Study

The difference in albedo between Fisher CuO and Will CuO is probably caused by differences in manufacture of the material and may come from particle size alone.

Will Corporation CuO is made by converting copper concentrate in a hot oxidizing atmosphere to cupric oxide. Fisher CuO is made by igniting a copper salt (copper carbonate or copper nitrate) in a roasting process. Chemically they are alike and have identical proportions of copper oxide and similar impurities. Photomicographs of dusted samples do not show real differences. However, Figure B1-1 shows photomicrographs of the particles that were separated by a 400 mesh screen. About 93% of the Will CuO passed through this screen, but only 41% of the Fisher CuO would pass through the screen.

Will CuO that is dusted through a 400 mesh screen has a tendency to build up a textured surface (Figure B4-1) that has been observed to have peak to valley dimensions of about 300 microns. This is nearly 9 times the maximum particle size that passes through the sieve.

Fisher CuO dusted in the same manner has a smoother surface (Figure B4-3) with an observed peak to valley dimension of 100 microns, or only 3 times the maximum particle size that passes through the sieve.

Photometric measurements of these copper oxides are described in Section B2. Table B1-1 summarizes the copper oxide measurements.

2. Photometric Measurements

Photometric measurements of copper oxide and silver chloride were made in a darkened work area using a SPECTRA PRITCHARD PHOTOMETER #119 with a 15 minute arc aperture and a simulated solar source at 21 feet. These measurements are tabulated in Table B2-1 along with the calculated photometric function and albedo. Figure B2-1 shows the lunar photometric function as measured by several workers in the field and as given by NASA from Fedorets' data. This figure shows the curve for copper oxide on cardboard as measured by Halajian and reported in "Photometric Measurements of Simulated Lunar Surfaces," November 1964, Interim Report on NASA Contract NAS9-3182, also shown are points measured by Kodak on Fisher copper oxide as dusted on the background plane of the geometric shapes. The agreement

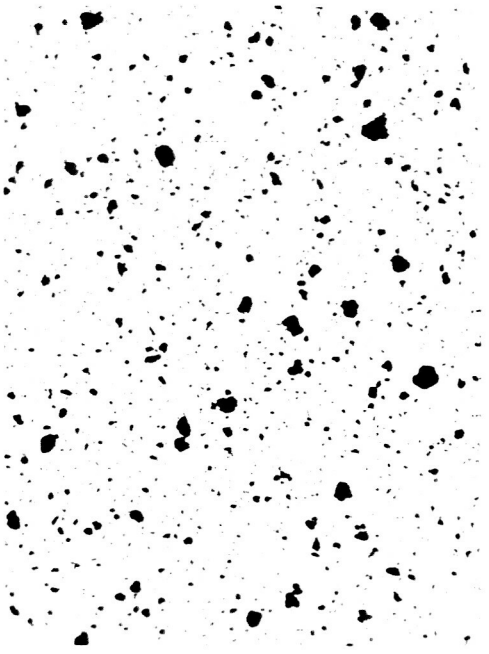

93% by weight passed through 400 mesh screen

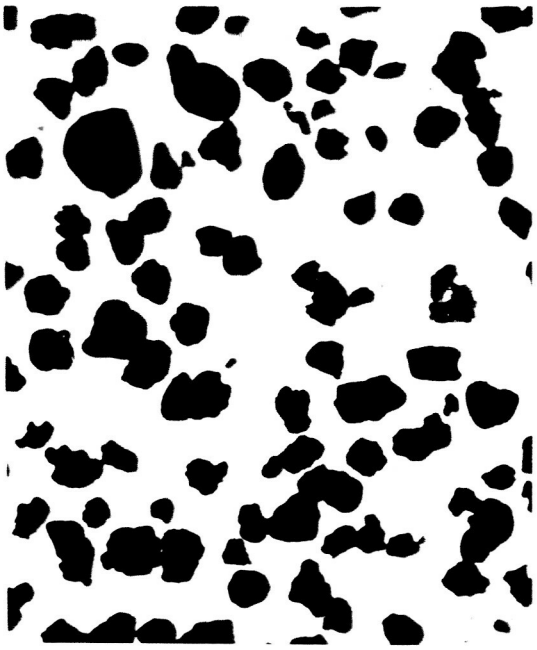

7% by weight was retained by 400 mesh screen

WILL CuO

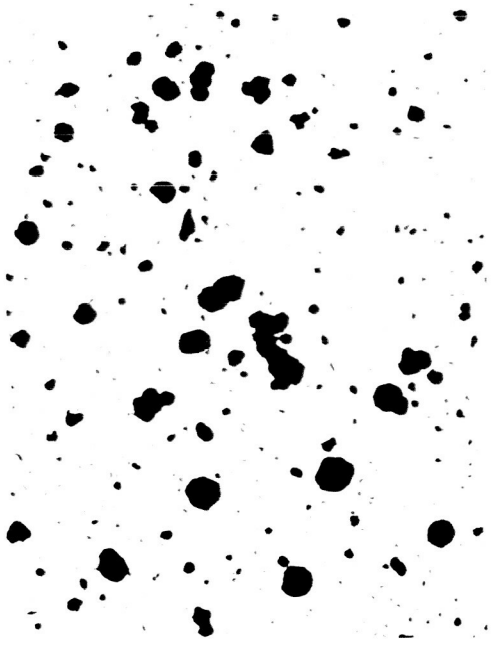

41% by weight passed through 400 mesh screen

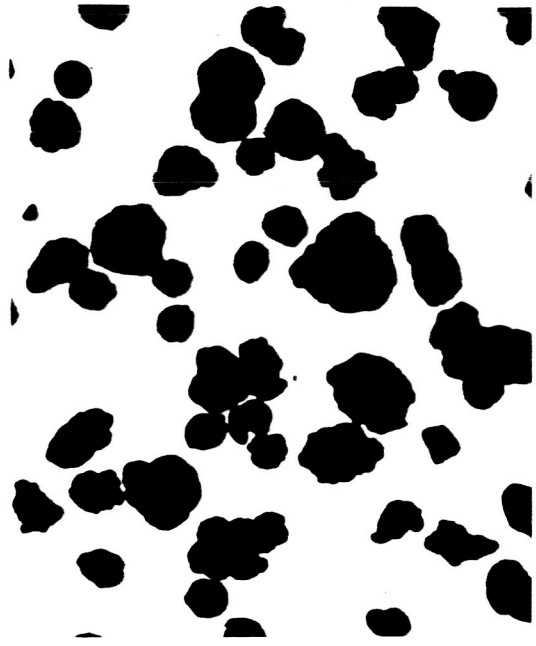

59% by weight was retained by 400 mesh screen

FISHER CuO

Photomicrographs of copper oxide particles at 100 times magnification. The left photographs show the shape and size of the particles that passed through the 400 mesh screen. The right photographs show the shape and size of the particles that were retained by the 400 mesh screen.

Figure B1-1

Copper Oxide Measurements

Copper Oxide	Albedo*	Visual Appearance	Manufacture Method	Observed peak to valley on dusted surface, microns	Particle size microns Average	Max.	Separation by a 400 mesh screen % by weight ** % Pass	% Retained
Will	.048	Textured	roasting copper concentrate	300	20-45	110	93	7
Fisher	.055	Smooth	roasting copper salt	100	50-105	225	41	59

* These values are slightly different from those quoted earlier in this report.
The early albedo of .03 for Will was measured by a less reliable method.
The value of .07 for Fisher was measured using the Grumman Photometer.
The values in the table are obtained from the Kodak work described in Section B2.

** Openings in 400 mesh screen are 37 microns.

Table No. B1-1

Sun Elevation Degrees	Magnesium Oxide	Copper Oxide Fisher		Copper Oxide Will		Silver Chloride		Silver Chloride one hour later		Mixture AgCl + CuO	
	Ft-L	Ft-L	Φ	Ft-L	Φ	Ft-L	Φ	Ft-L	Φ	Ft-L	Φ
89	43	2.38	1.05	2.06	1.05	19.8	1.08	13.2	1.13	7.6	1.06
85*		2.06	.91	1.79	.91	16.6	.91	10.64	.91	6.48	.91
84		1.98	.88	1.72	.87	15.8	.87	10.0	.86	6.2	.87
75		1.72	.76	1.33	.68	12.8	.70	7.3	.63	5.4	.76
60		1.30	.57	.96	.49	9.9	.54	5.4	.46	4.3	.60
45		.88	.39	.65	.33	7.4	.41	4.0	.34	3.5	.49
30		.58	.256	.39	.20	5.1	.28	2.7	.23	2.7	.38
15		.27	.12	.18	.092	2.2	.12	1.4	.12	1.65	.23
10		.18	.08	.122	.062	1.5	.082	.92	.079	1.24	.17
5		.09	.04	.043	.024	.69	.038	.46	.039	.69	.097
Calculated Albedo		.055		.048		.46		.307		.177	
Figure No.		B2-1		B2-2		B2-3		B2-4		B2-5	

* The Photometric function, Φ, was interpolated for 85° and set equal to .91 to agree with the NASA-Fedorets' data

Photometric measurements and calculations of dusting materials. Reflectance measurements made with Spectra Pritchard Photometer #119 with 15 minute aperture. Sample illuminated from a simulated solar source.

Table B2-1

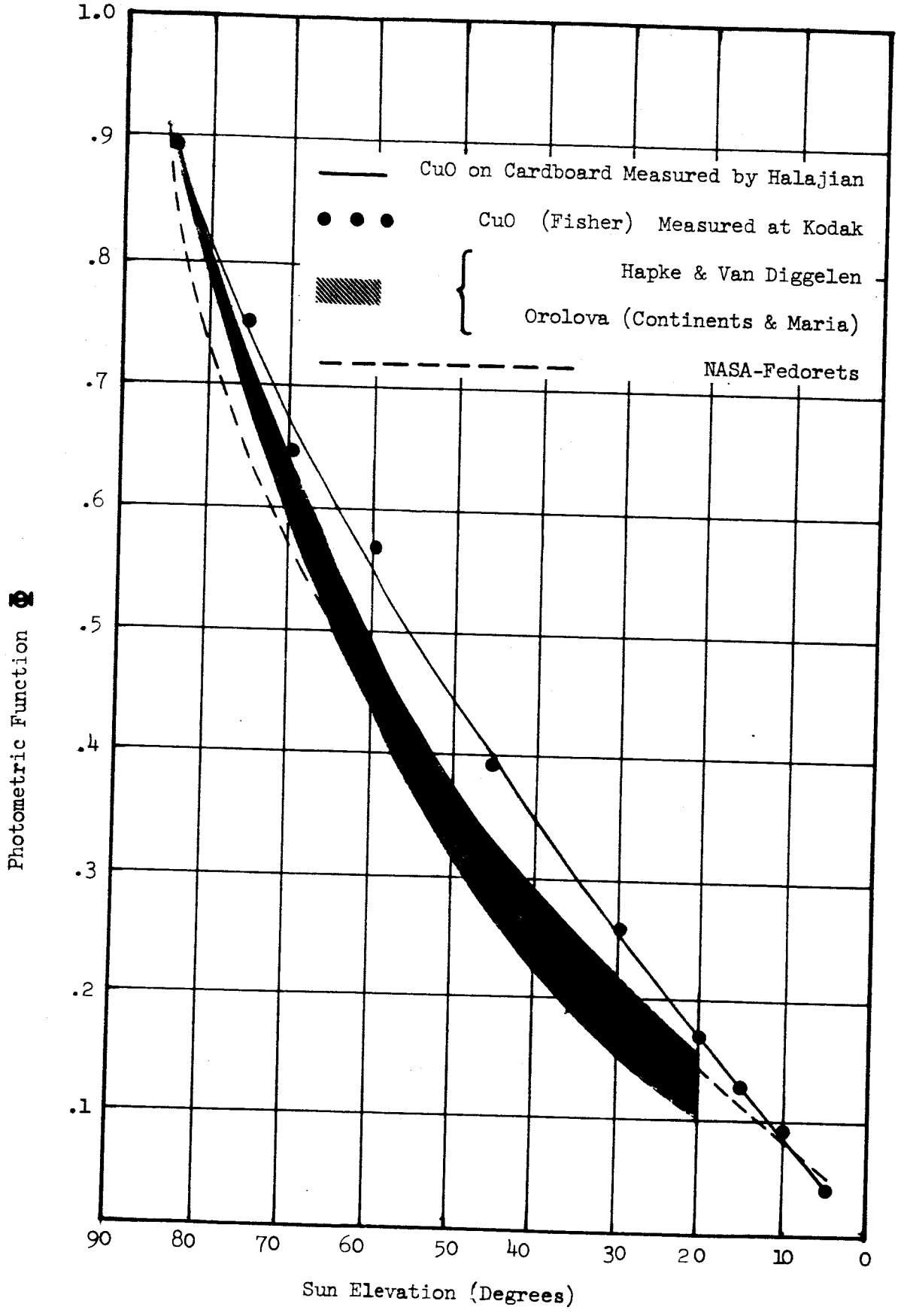

Figure B2-1 Photometric Measurements of Simulated Lunar Surfaces

between the measurements made by Halajian and Kodak was considered close enough so that a return visit to Grumman Aircraft Corporation to check dusting techniques and back scatter measurements was unnecessary.

Figure B2-2 shows the photometric function of Fisher CuO and Will CuO along with the NASA Fedorets data. This curve shows that either dust is a good photometric match to the Lunar Photometric function, and both are near the range of the average lunar albedo (0.07). Fisher CuO was used for all Kodak dusted models except the early Ranger VII model which was dusted with Will CuO.

To obtain silver chloride that would pass through the 400 mesh screen it was necessary to precipitate silver chloride from solution and coat each crystal with gelatine in order to keep the soft silver chloride from conglomerating in the sieve. A sample of silver chloride made in this manner was dusted on a plastic sheet and exposed to strong light for several minutes; then the reflectance measurements were made. A second set of measurements was made after about one hour during which time the sample had been exposed to direct sunlight for about 20 minutes. The results of these measurements are tabulated in Table B2-1 and plotted in Figure B2-3. The photometric function was calculated from the data and is plotted in Figure B2-4. The albedo of silver chloride changed from 0.307 to 0.177 during this period of time and should approach Halajian's measurement of 0.13 as a limit. Unfortunately any disturbances of the surface uncovered unexposed silver chloride that was much brighter than the exposed grains. The variable albedo characteristic of silver chloride makes this a poor material for dusting models even though the photometric function is correct. If reliable high albedo with a lunar photometric function is desired in future lunar studies silver grains should be tried as a dusting material, since well exposed silver chloride is mostly silver.

In some of our later work, silver chloride was dusted over the copper oxide to obtain a higher albedo. The reflectance for such a mixture was measured and used to calculate the photometric function plotted in

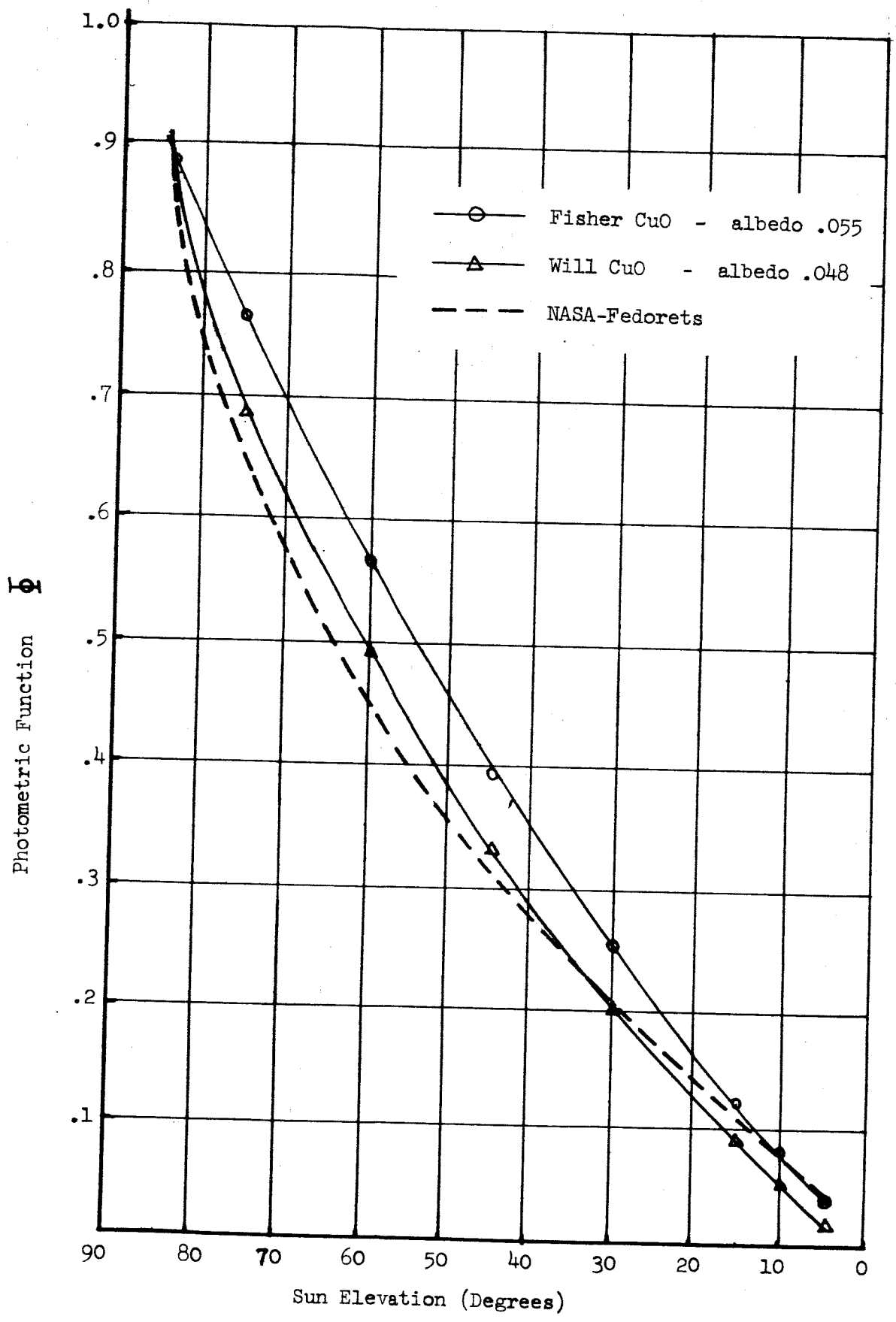

Figure B2-2 Photometric Function of Fisher CuO and Will CuO Compared to NASA-Fedorets Data.

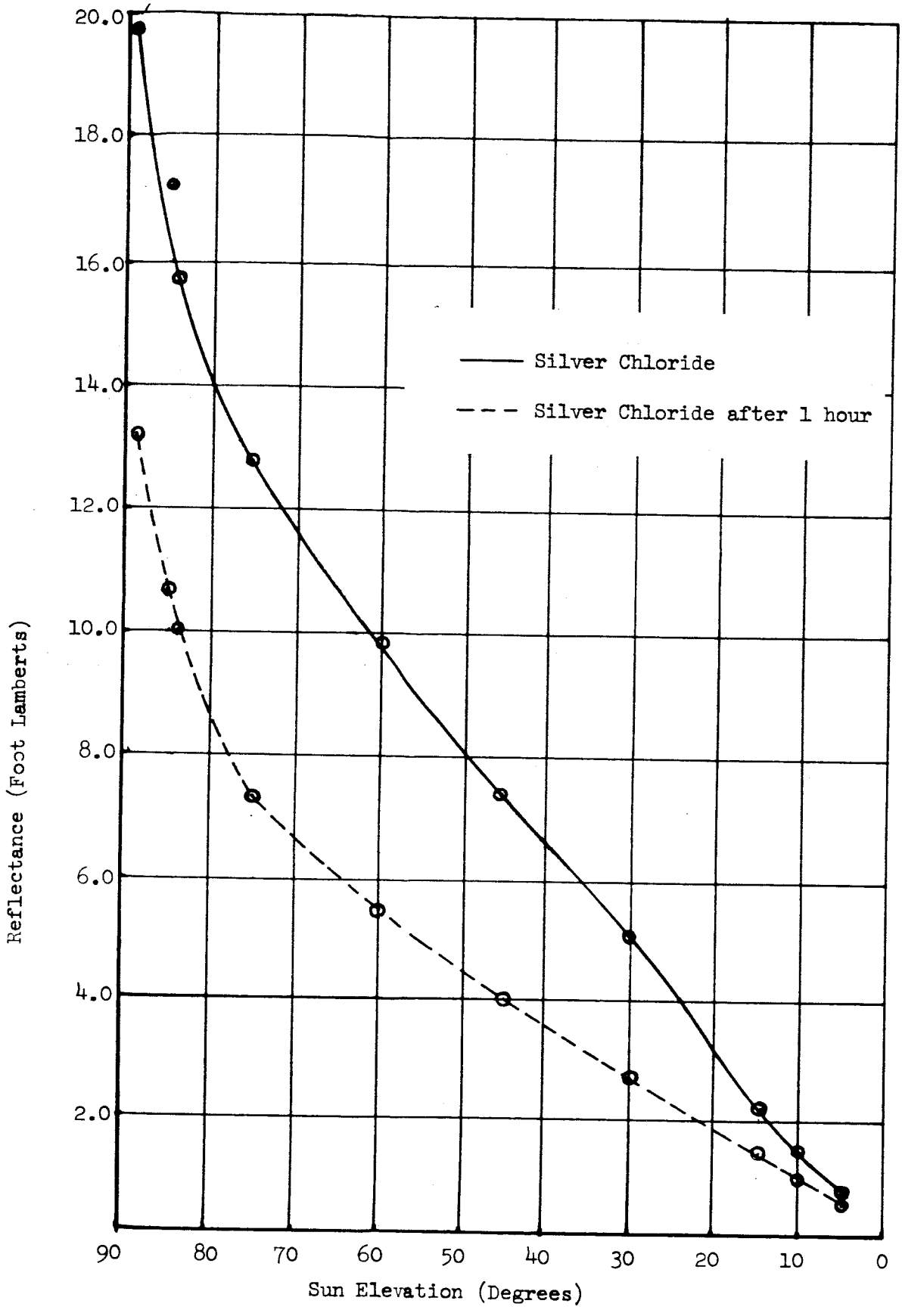

Figure B2-3 Reflectance of Silver Chloride with a Moderate Exposure and After One Hour with an Additional Exposure.

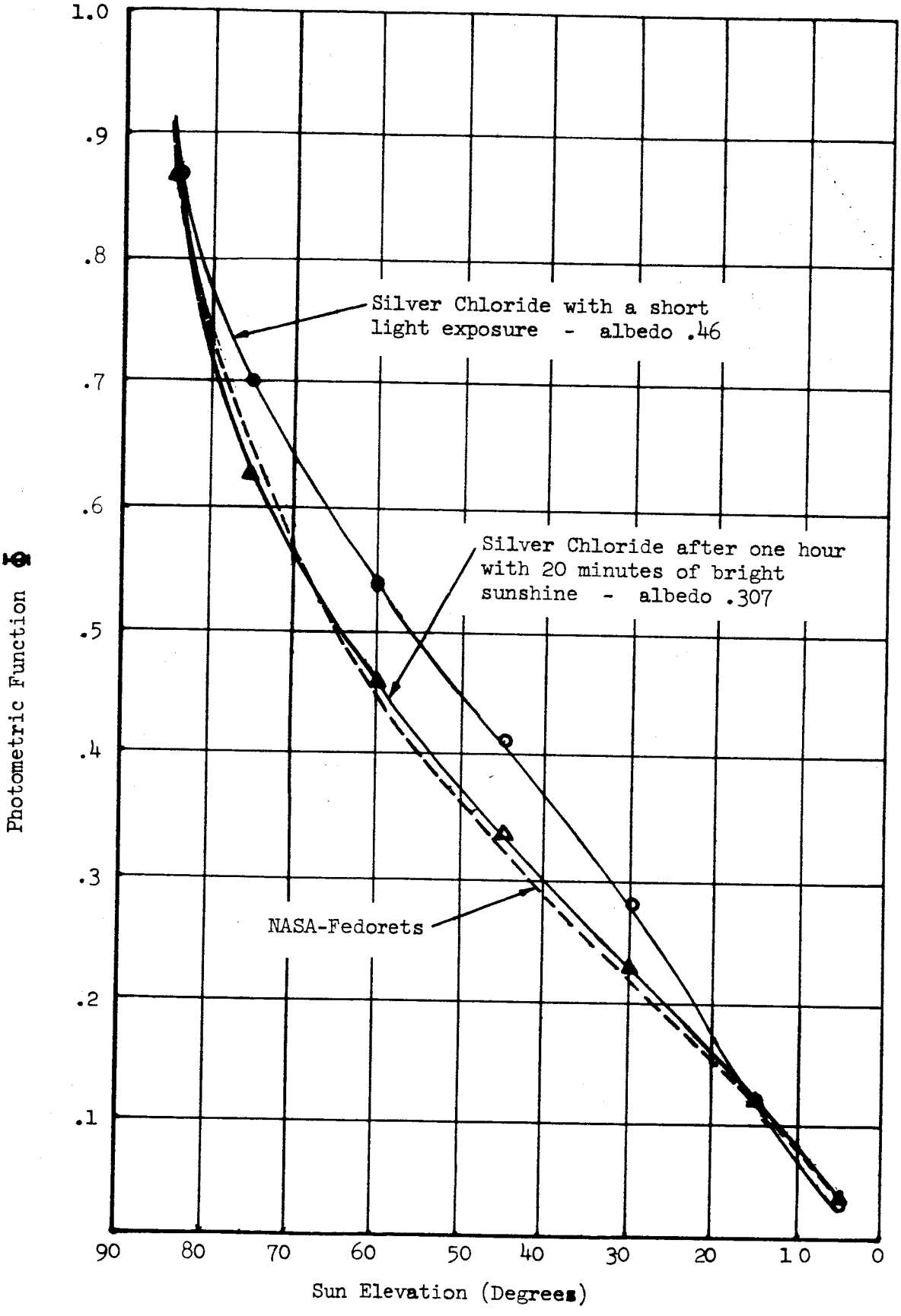

Figure B2-4 Photometric Function of Silver Chloride after a short light exposure and after one hour including a 20-minute exposure to bright sunshine.

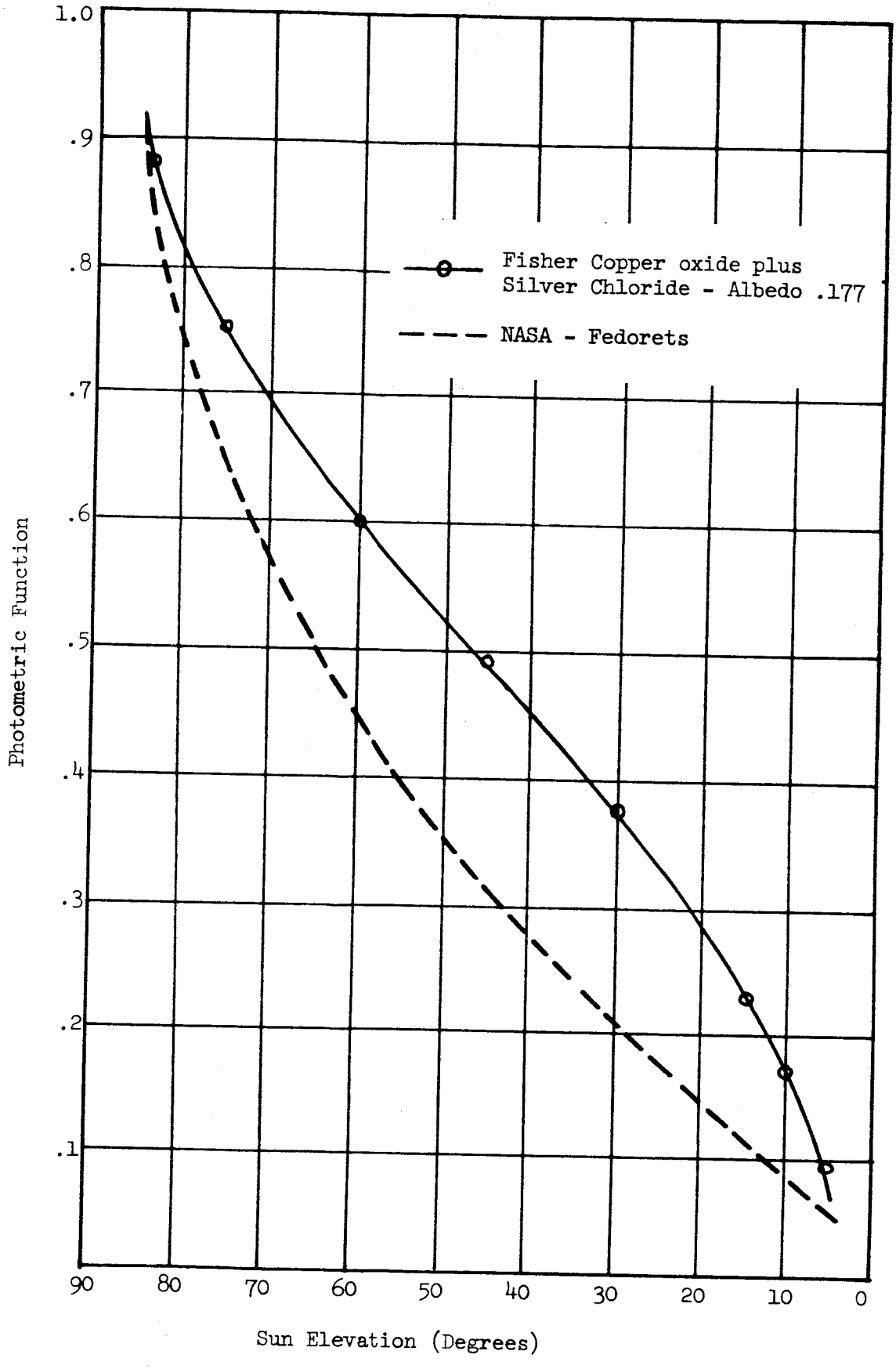

Figure B2-5 Photometric Function of a mixture of Copper oxide and Silver Chloride.

Figure B2-5. The comparison with the lunar curve shows a high back scatter at all sun elevations.

a. Conclusions from Photometric Measurements

1. Photometric function of the dusted Fisher CuO measured at Kodak agrees with the measurements made and reported by Halajian at Grumman.

2. The photometric function of dusted copper oxide is a good match to the lunar photometric function and the albedo is near the average albedo of the moon.

3. Dusted silver chloride is a good photometric match to the lunar photometric function but it does not have a stable albedo.

4. Mixtures of copper oxide and silver chloride show too bright a back scatter at all sun elevations. The mixture also has variable albedo until the silver chloride darkening has gone to completion.

3. Dusting Techniques

Basically, dusting the models follows the method described by J. D. Halajian in Grumman Research Report Number RM-250. The copper oxide is obtained from Fisher Scientific Company, Cat. No. C-472. Copper (ic) oxide is sifted through a W. S. Taylor Company, Standard Sieve, A.S.T.M. No. 400 (400 mesh 37 micron openings or 0.0015 inch). In order to dust the model, an area 40 inches by 40 inches, with a uniform coat of dust, it is necessary to hold the sieve about 4 or 5 feet above the model during the dusting operation. If the sieve is held closer than this the dust builds up nonuniformly in small piles.

The vertical surfaces of the hemispheres require special attention. Ordinary dusting from the vertical position will build up the dust thickness at the edges of the domes or craters leaving very little material sticking to the sides. We were able to obtain a uniform coat of dust on these surfaces by painting or spraying them with a solvent that

softens the plastic and dusting them immediately. The model is lifted and turned so that the surfaces that would be vertical during normal dusting are essentially horizontal during this operation. Some of the copper oxide sticks to the softened plastic and provides a tooth for the material which later falls on the model. After these vertical edges are dusted, the model is placed on a modified drafting board in a horizontal position and the remainder of the model is dusted.

It is necessary to build a skirt around the model during the dusting operation to prevent drafts from blowing the dust. A skirt of plastic sheeting eight feet high is placed around the model before dusting starts. The duster climbs to the top of this structure and sifts the copper oxide. Dusting continues until all parts of the model are covered with a uniform coat and the plastic surface of the model is no longer visible. All incident light which reaches the model must be absorbed before it escapes in the direction of the camera if the copper oxide is to be the controlling factor in this experiment.

After the model is dusted, the skirt is removed and the model is photographed in a vertical position.

If the dust is not relatively thin and uniform, slugs of dust may be dislodged during this part of the experiment and form avalanches which uncover much of the model. Repairs after an avalanch have been unsuccessful and the model must be cleaned and redusted if it is to be free from fault-like discontinuities, an example of which is visible in Figure B4-4 at 10° sun elevation. The solvent technique helps to hold the dust on some of the more critical areas, and will even hold dust on the underside of the horizontal surfaces. The thickness of the dusted surface of the geometric models have been estimated at 150 μ to 200 μ.

The plastic solvent found to be successful with the Royalite material is xylol. It tends to soften the surface so that the copper oxide particles can stick to it, but will evaporate long before any photographs are made.

A thin acrylic resin was used as an adhesive whenever copper oxide was dusted on the 1/4 inch and 1/8 inch shapes since they were not made of plastic. It should be noted that either the solvent or the adhesive only affects the underlayers. The material that reflects the incident light to the camera is copper oxide dust at least 150μ thick with no foreign material visible.

In three areas, Kodak dusting techniques differ from those used at Grumman Aircraft:

1. To obtain uniformity, Kodak dusted from 5 feet above the model; on the other hand, Halajian dusted from several inches above the cardboard background.

2. Kodak photographed with the background in a vertical plane whereas Halajian's measurements were made in a horizontal plane.

3. A solvent was used to "stick" the copper oxide to the vertical surfaces of the plastic model, and acrylic resin was used over the metal geometric shapes.

The photometric measurements of the Fisher CuO were made with the dusted surface in a vertical position. Since these measurements match those made of the same material by Halajian, no difference in the photometric function is caused by dusting from different heights or by photographing the model in either a vertical or a horizontal position. Measurements and photographs show no difference in photometric function caused by the application of plastic solvents or acrylic resin.

4. Model Making

The first geometric shapes made by Kodak for study as lunar models were convex metal cones and domes. Positive and negative replicas made from these shapes were dusted, illuminated and photographed during our preliminary evaluation.

a. Kodak Model #2 (Ranger VII)

The first lunar surface model simulating the area depicted in the last "A" frame of Ranger VII was made using modeling clay. Attempts to dust this model proved unsuccessful since oil in the clay wet the copper oxide dust and changed its photometric properties. Shellacing the surface or spraying with Krylon or other materials was unsuccessful, since the oil would invariably seep out through pin holes and wet the dust. A negative replica was made of this surface in plaster and a positive made out of Royalite sheet plastic by vacuum forming. This plastic was dusted and photographed at various sun angles. Figure B4-1 shows the model illuminated from the left at a sun angle of 23°. Note the texture of the surface caused by the Will CuO used to dust this model.

b. Geometric Shapes

The scale of the geometric shapes is made 1 to 48 lunar size. The photographic scale from model to film is 1 to 1270 making the representative lunar photographic scale 1 to 61,000.

Table B4-1 gives the dimensions of the objects that are included in the geometric shape model. The geometric shapes were divided into three classes: large, small and tiny. The large and the small shapes were each made by vacuum forming 20 inch x 40 inch sheets of 1/16 inch Royalite over the convex metal forms. One side of the sheet provides the convex forms and a similar sheet, mounted upside down provides the concave forms. The combination provides a model 40 inches x 40 inches. The convex tiny shapes were made of metal and mounted on a metal plate. The concave tiny shapes are a plastic casting of these shapes.

Table B4-2 identifies and Figure B4-2 shows the location of each shape in the models. Figure B4-3 is a record photograph of the large and tiny geometric shapes taken with sun elevation of 84°, 64°, 30° and 10° and Figure B4-4 is a similar photograph of the small geometric shapes taken at the same sun elevation.

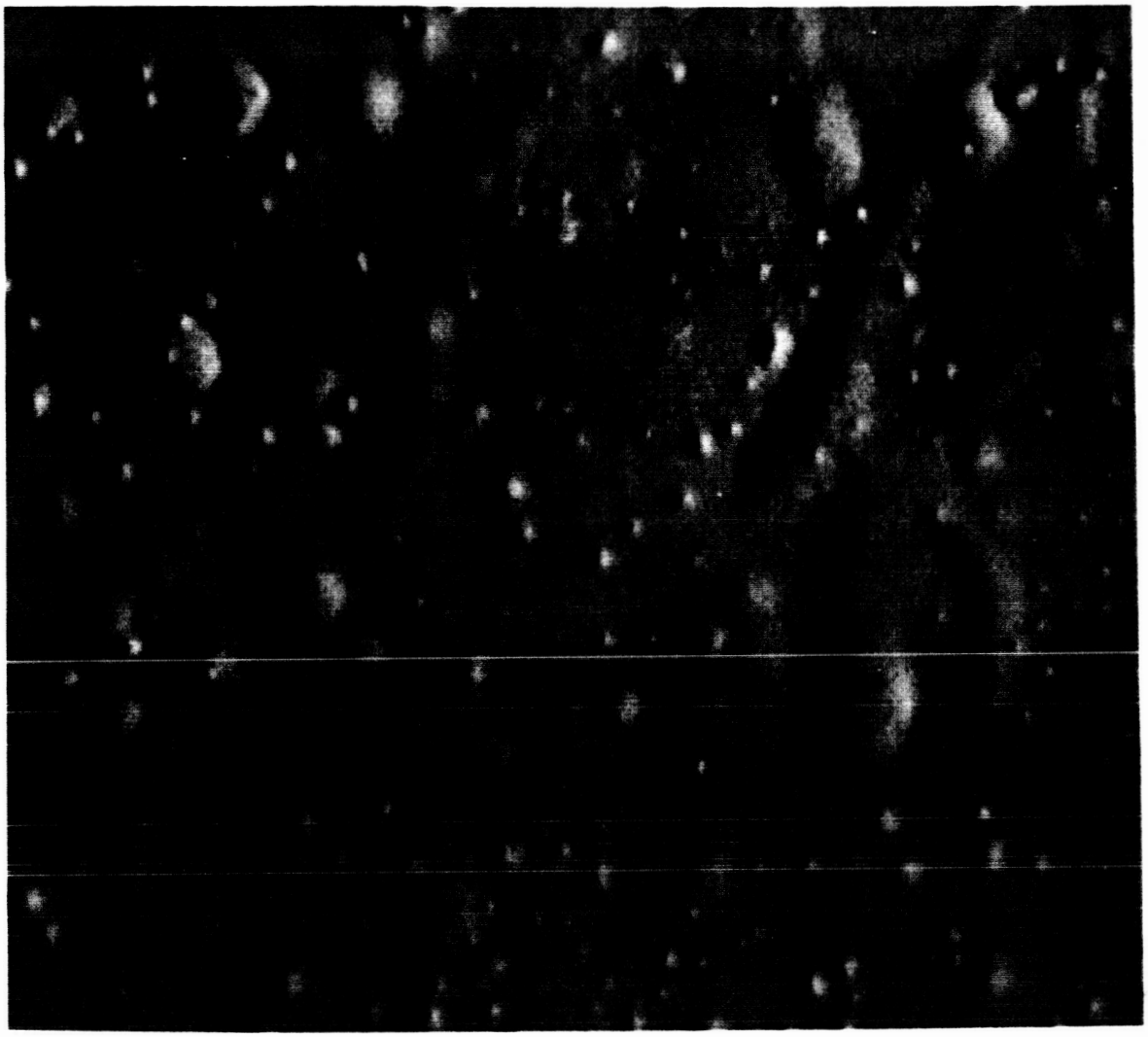

Kodak Model No. 2A Lunar Surface Model with Sun Elevation 23° sun from the left. Note the texture of the surface. WILL CuO was used to dust this model.

Figure B4-1

Height of Geometric Shapes in Inches

Diameter In.	Spherical Diameter to Height Ratio 2:1	4:1	8:1	Conical Cone Angle 7°	26°	
.13	.06	.032	.015	.007	.03	Tiny
.25	.13	.063	.032	.013	.06	
.50	.25	.13	.063	.026	.12	Small
1.0	.50	.25	.13	.052	.24	
2.0	1.0	.50	.25	.105	.49	Large
4.0	2.0	1.0	.50	.21	.97	

Table No. B4-1

Large Shapes				Small Shapes				Tiny Shapes			
Shape Position	Surface Type*	Diameter	Diameter to Depth Ratio or Slope	Shape Position	Surface Type*	Diameter	Diameter to Depth Ratio or Slope	Shape Position	Surface Type*	Diameter	Diameter to Depth Ratio or Slope
1	SV	2"	2:1	1	SV	1"	8:1	1	SΛ	1/8"	8:1
2	CV	1"	26°	2	SV	1"	4:1	2	SΛ	1/8"	4:1
3	SV	4"	4:1	3	SV	1"	2:1	3	SΛ	1/8"	2:1
4	SV	4"	8:1	4	CV	1/2"	26°	4	CΛ	1/8"	26°
5	CV	4"	26°	5	CV	2"	7°	5	CΛ	1/8"	7°
6	CV	4"	7°	6	CV	2"	26°	6	CV	1/8"	7°
7	SV	4"	2:1	7	CV	1/2"	7°	7	CV	1/8"	26°
8	CV	1"	7°	8	SV	1/2"	8:1	8	SV	1/8"	2:1
9	SV	2"	8:1	9	SV	1/2"	4:1	9	SV	1/8"	4:1
10	SV	2"	4:1	10	SV	1/2"	2:1	10	SV	1/8"	8:1
11	CΛ	1"	7°	11	CΛ	1/2"	7°	11	SΛ	1/4"	2:1
12	SΛ	2"	8:1	12	SΛ	1/2"	8:1	12	SΛ	1/4"	4:1
13	SΛ	2"	4:1	13	SΛ	1/2"	4:1	13	SΛ	1/4"	8:1
14	SΛ	2"	2:1	14	SΛ	1/2"	2:1	14	CΛ	1/4"	26°
15	SΛ	4"	4:1	15	CΛ	1/2"	26°	15	CΛ	1/4"	7°
16	SΛ	4"	8:1	16	CΛ	2"	7°	16	CV	1/4"	7°
17	CΛ	4"	26°	17	CΛ	2"	26°	17	CV	1/4"	26°
18	CΛ	4"	7°	18	SΛ	1"	8:1	18	SV	1/4"	8:1
19	SΛ	4"	2:1	19	SΛ	1"	4:1	19	SV	1/4"	4:1
20	CΛ	1"	26°	20	SΛ	1"	2:1	20	SV	1/4"	2:1

* CΛ - conical convex
CV - conical concave
SΛ - spherical convex
SV - spherical concave

Identification of Geometric Shapes

Table No. B4-2

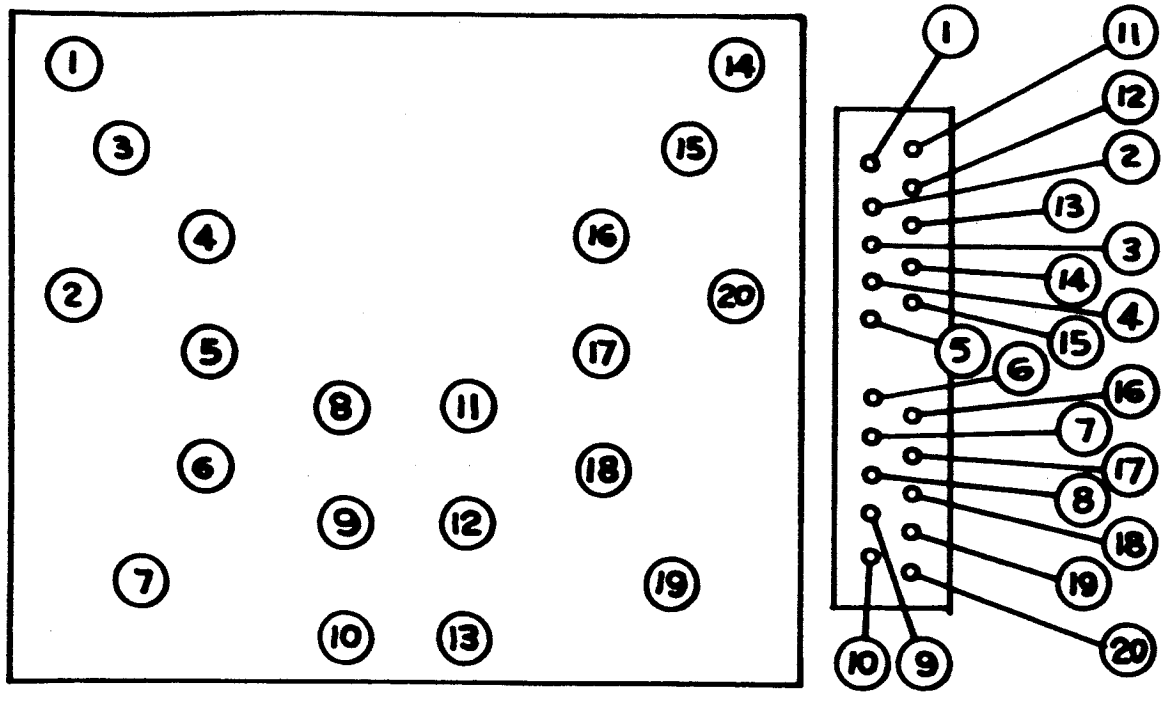

Large Geometric Shapes

Tiny Geometric Shapes

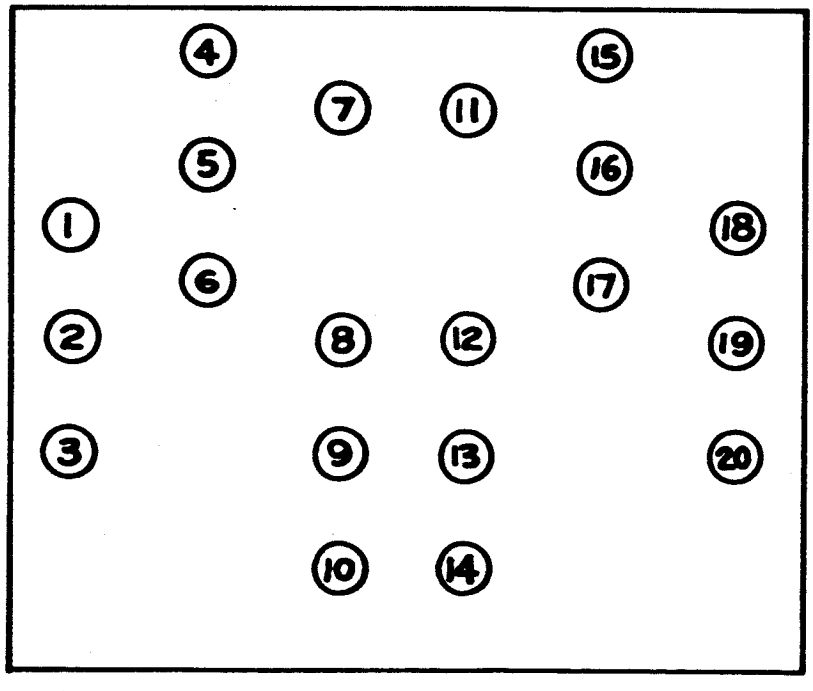

Small Geometric Shapes

Figure B4-2 Shape Locations on Lunar Model

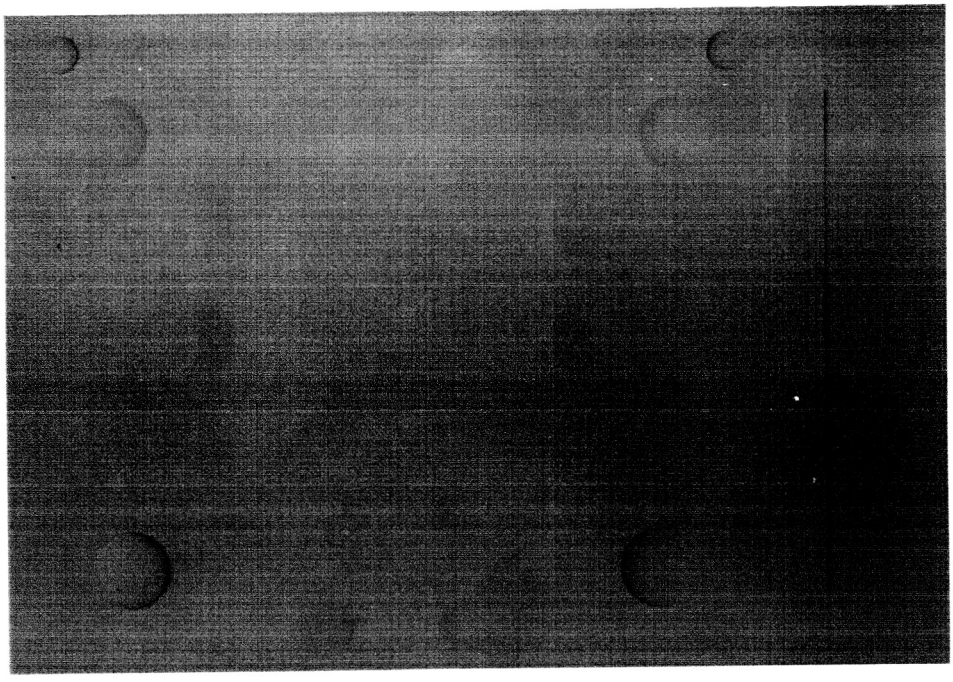

Sun Elevation = 84°

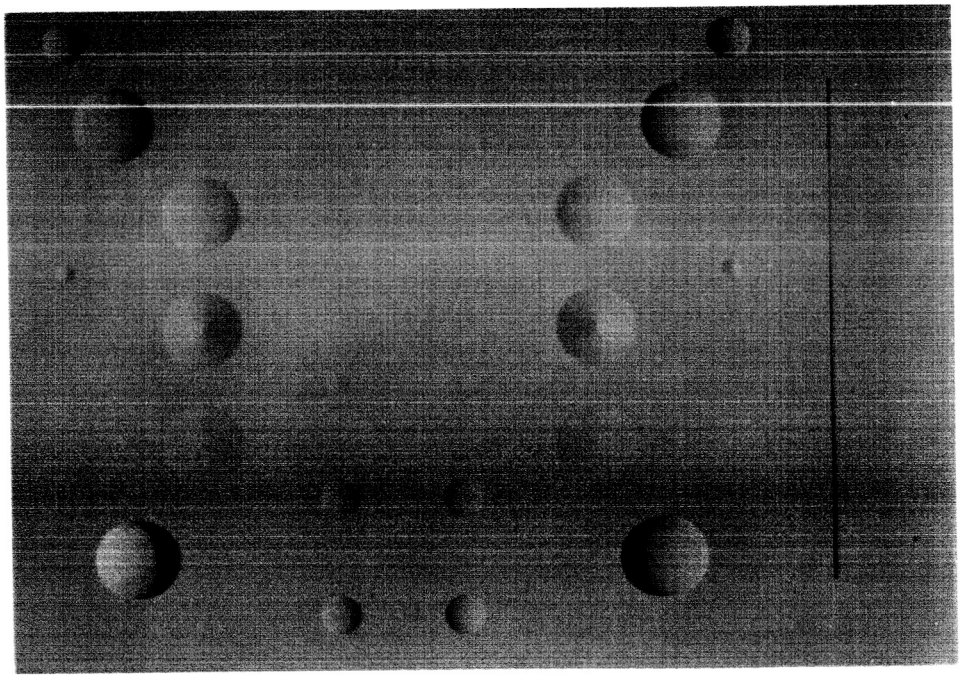

Sun Elevation = 60°

Photographs of Large and Tiny Geometric Shapes

Figure B4-3

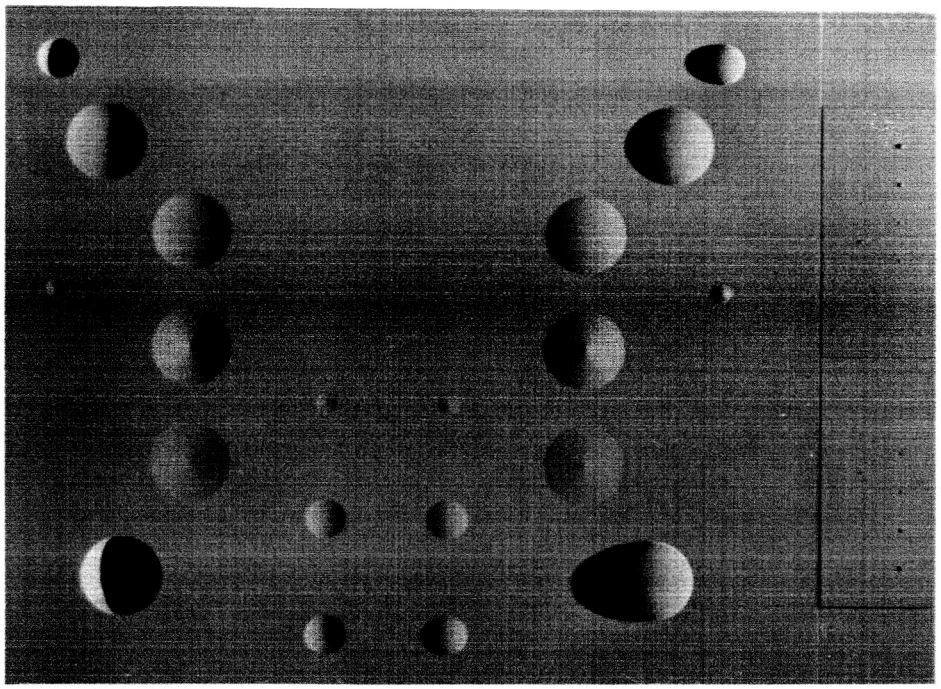

Sun Elevation = 30°

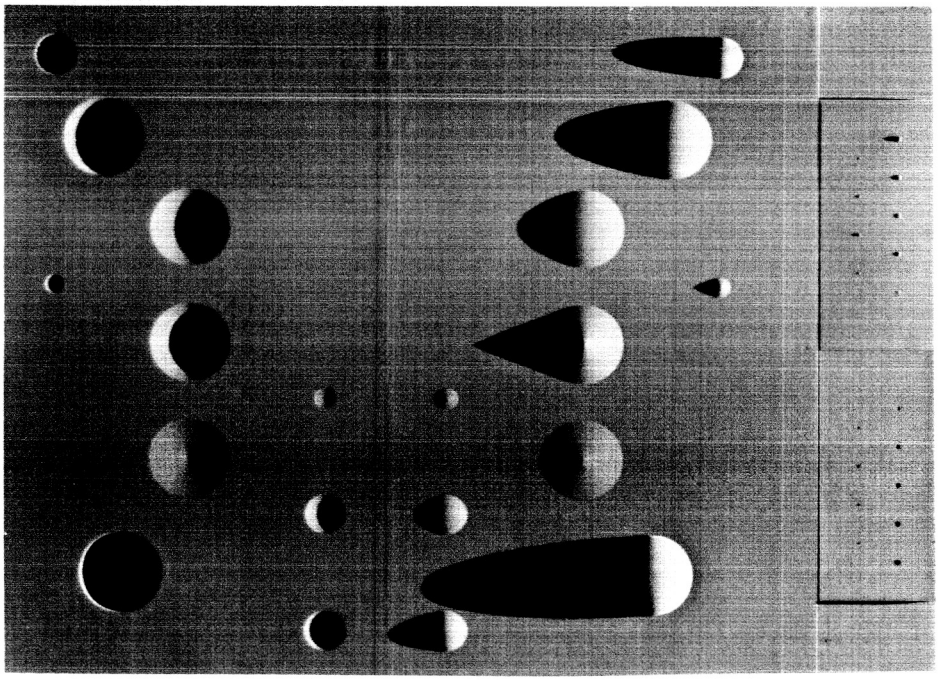

Sun Elevation = 10°

Photographs of Large and Tiny Geometric Shapes

Figure B4-3

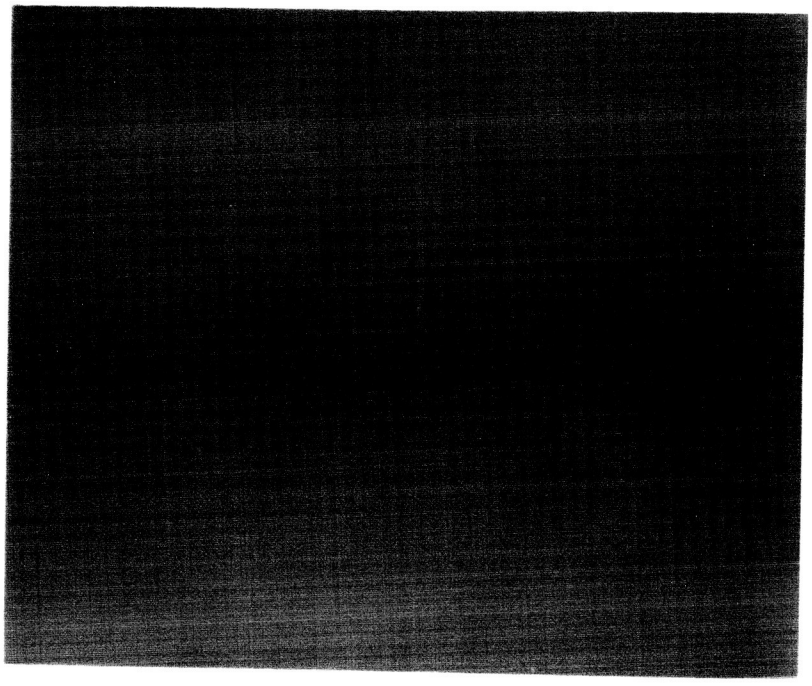

Sun Elevation = 84°

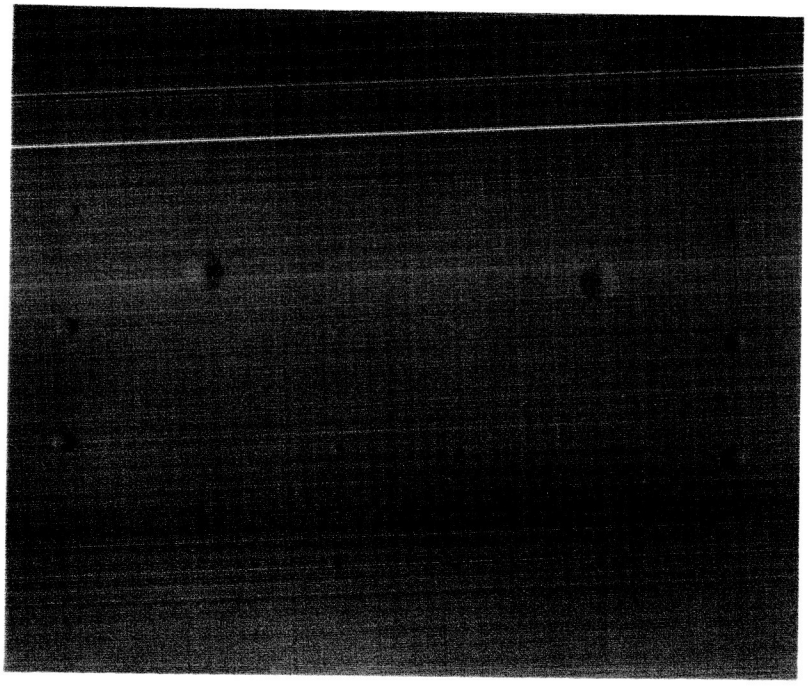

Sun Elevation = 60°

Photographs of the Small Geometric Shapes

Figure B4-4

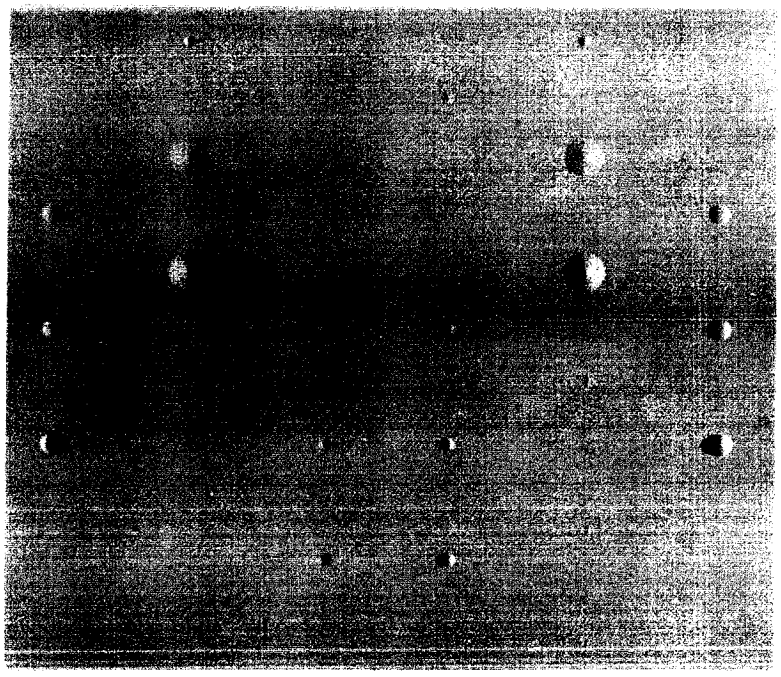

Sun Elevation = 30°

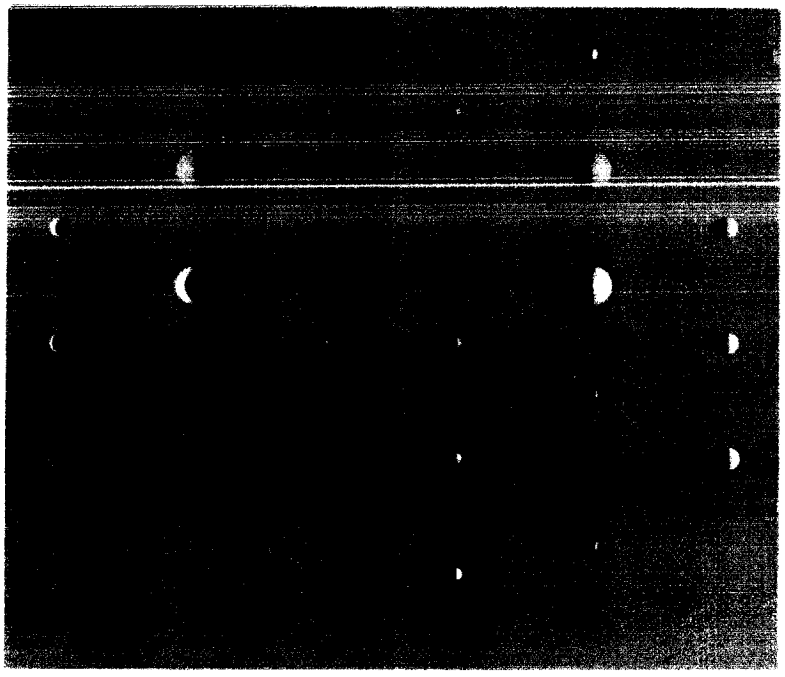

Sun Elevation = 10°

Photographs of the Small Geometric Shapes

Figure B4-4

c. Kodak Lunar Model 6-65 (KLM 6-65)

1) A Study of Ranger Photographs

Photographs from Ranger VII and IX were studied to obtain information from which to build a realistic model of the lunar surface. Measurements of crater diameter, number of craters per square mile for given size craters, and crater shadow length were used to prepare Figures B4-5 and B4-6. A description of model KLM 6-65 is given later in this section.

Figures B4-7, B4-8 and B4-9 have been made to assit in the analysis of these Ranger Data.

Figure B4-7 shows the cross section of an idealized crater with a sun elevation of 23°. Many of the craters in the photographs made with Ranger VII show no distinct shadow and are only slightly darker on the side toward the sun. They, therefore, have slopes less than 23°. Those craters that do cast a shadow have an average shadow length of about 33 percent of their diameter. The depth of the craters at the tip of the shadow is:

$$d = S \tan 23^\circ$$

$$= 0.33\ D \tan 23^\circ$$

The diameter-to-depth ratio then becomes:

$$\frac{D}{d} = \frac{\cot 23^\circ}{0.33} \quad \text{or about 7 to 1.}$$

There are at least two reasons why the true depth (d_t) is greater than the calculated depth (d). First, the end of the shadow is probably longer than the measured length since the tip of the shadow is probably not resolved. Secondly, if the true shape approaches a spherical surface, then the depth at the center, d_t, is greater than the calculated depth, d. This will shift the calculated diameter-to-depth ratio in the direction of smaller values (deeper craters).

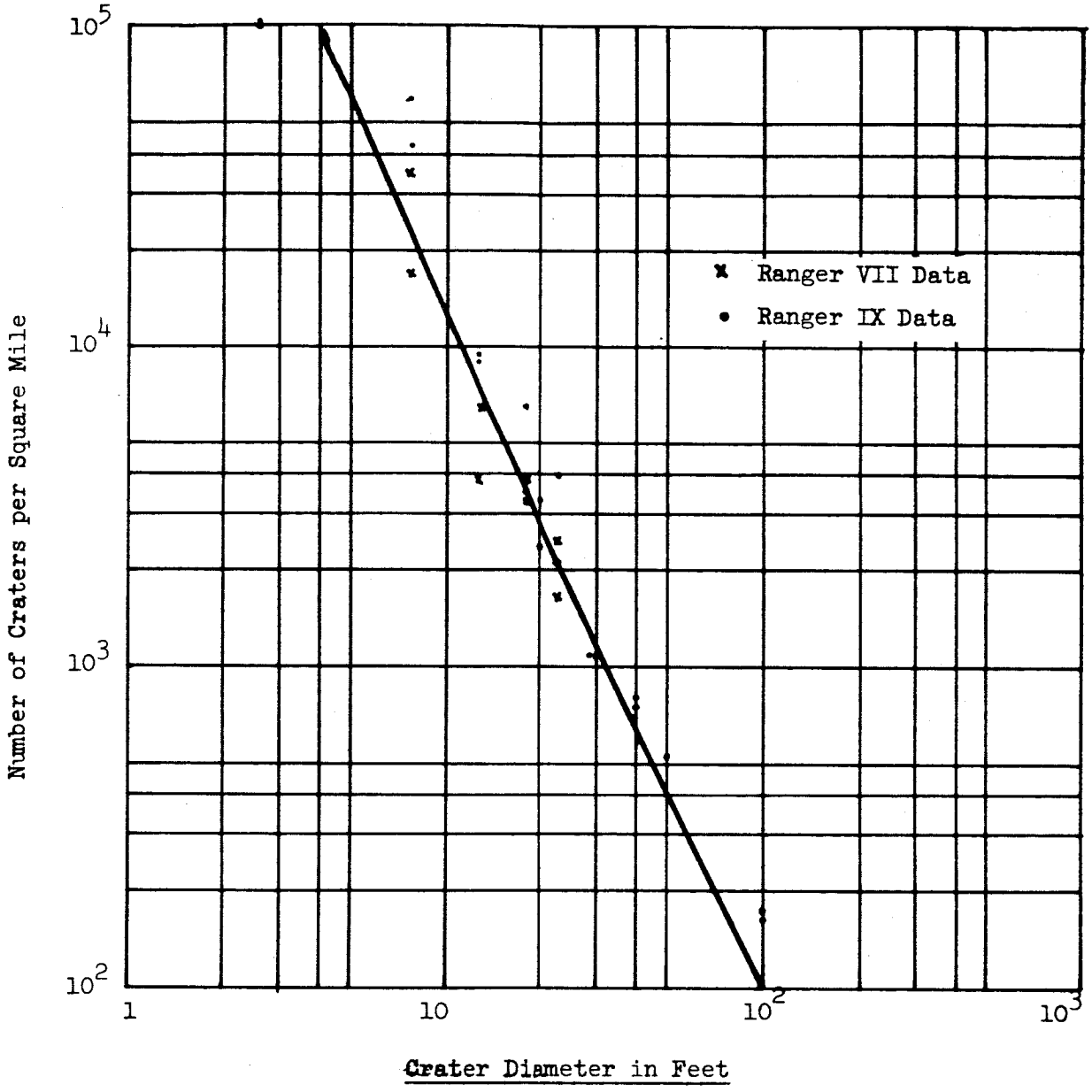

Figure B4-5 Number of Lunar Craters per Square Mile for Several Crater Diameters. Data Obtained from Ranger VII and Ranger IX Photographs.

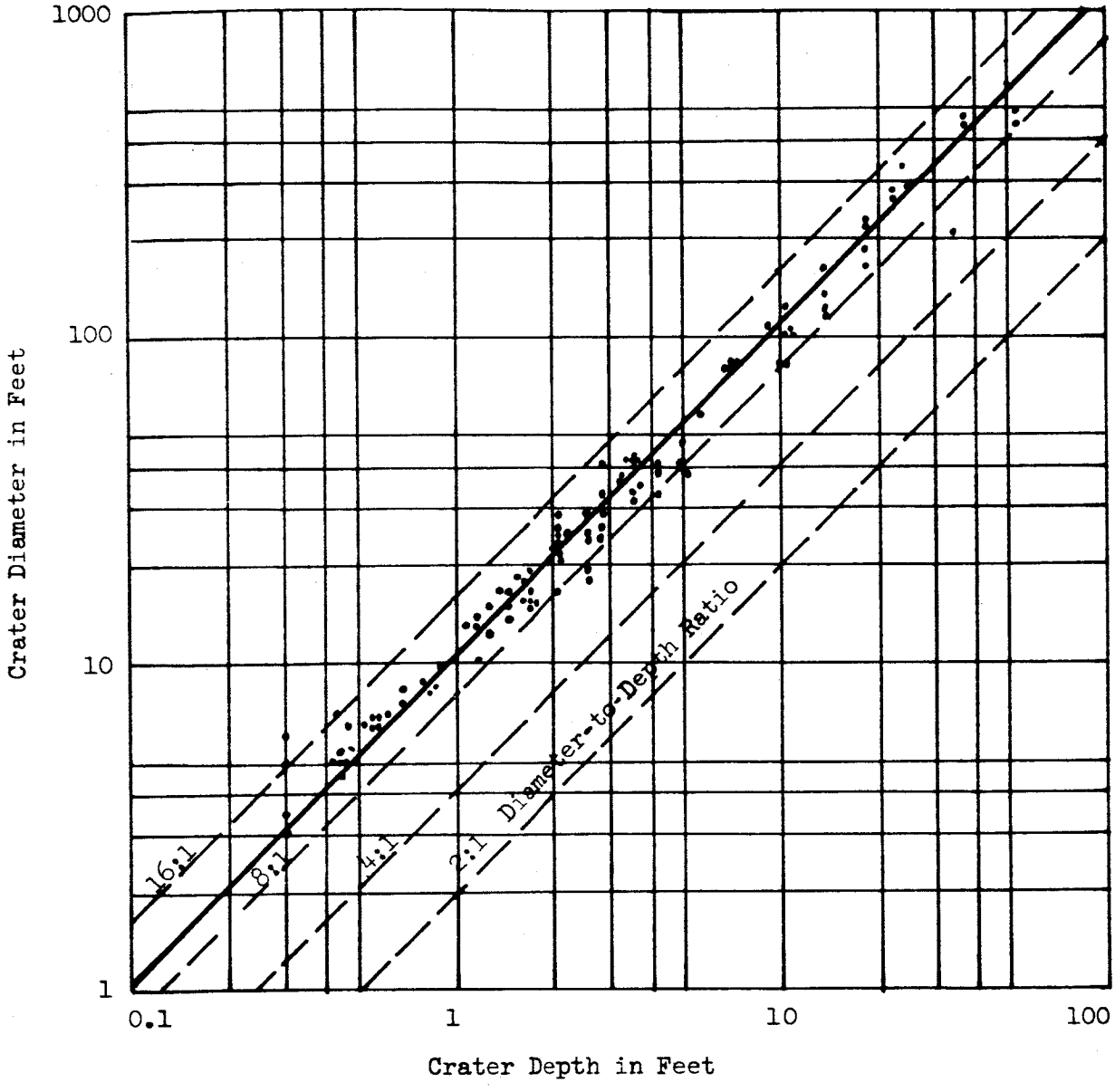

Figure B4-6 Diameter and Depth of Craters on the Moon. Obtained from Photographs Taken by Ranger VII and IX.

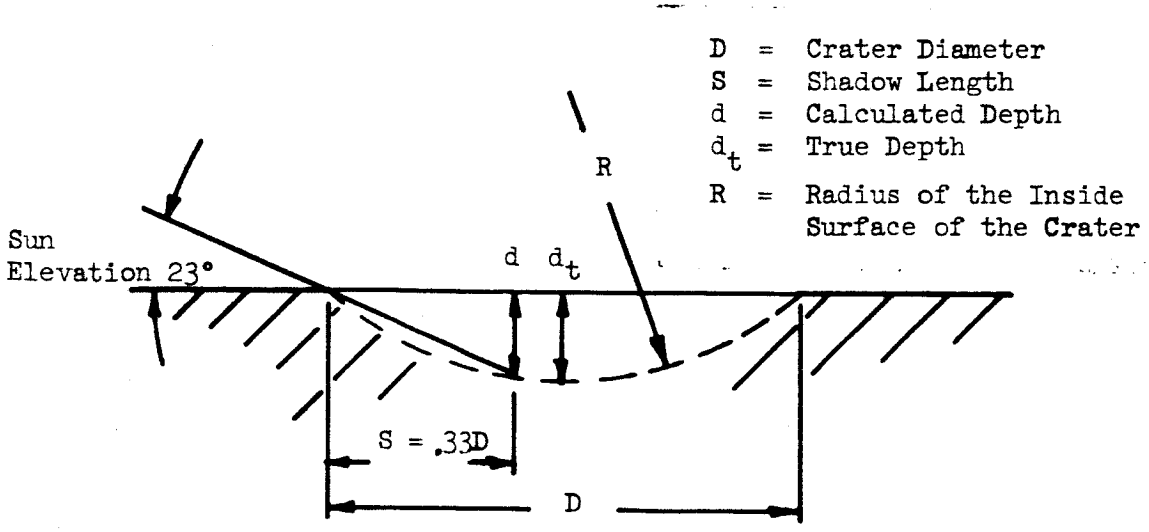

Figure B4-7 Crater Analysis for Ranger VII Conditions

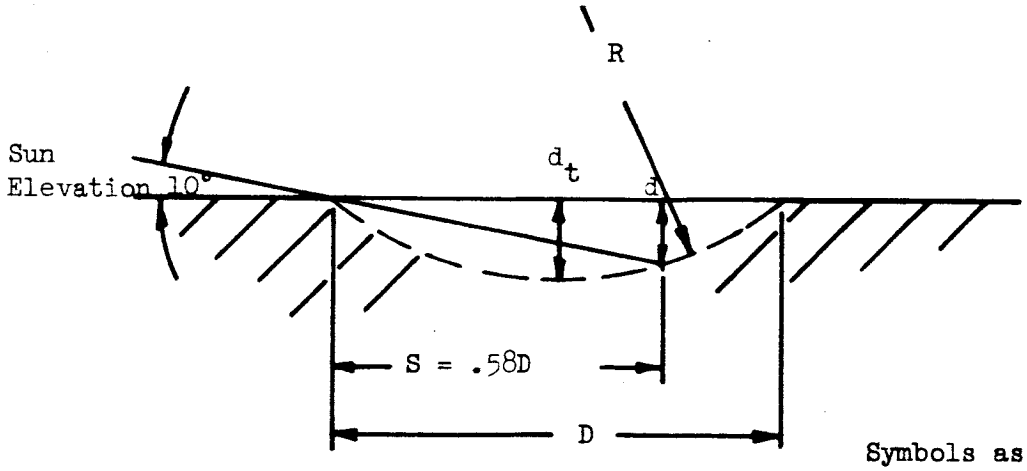

Symbols as in Figure B4-7

Figure B4-8 Crater Analysis for Ranger IX Conditions

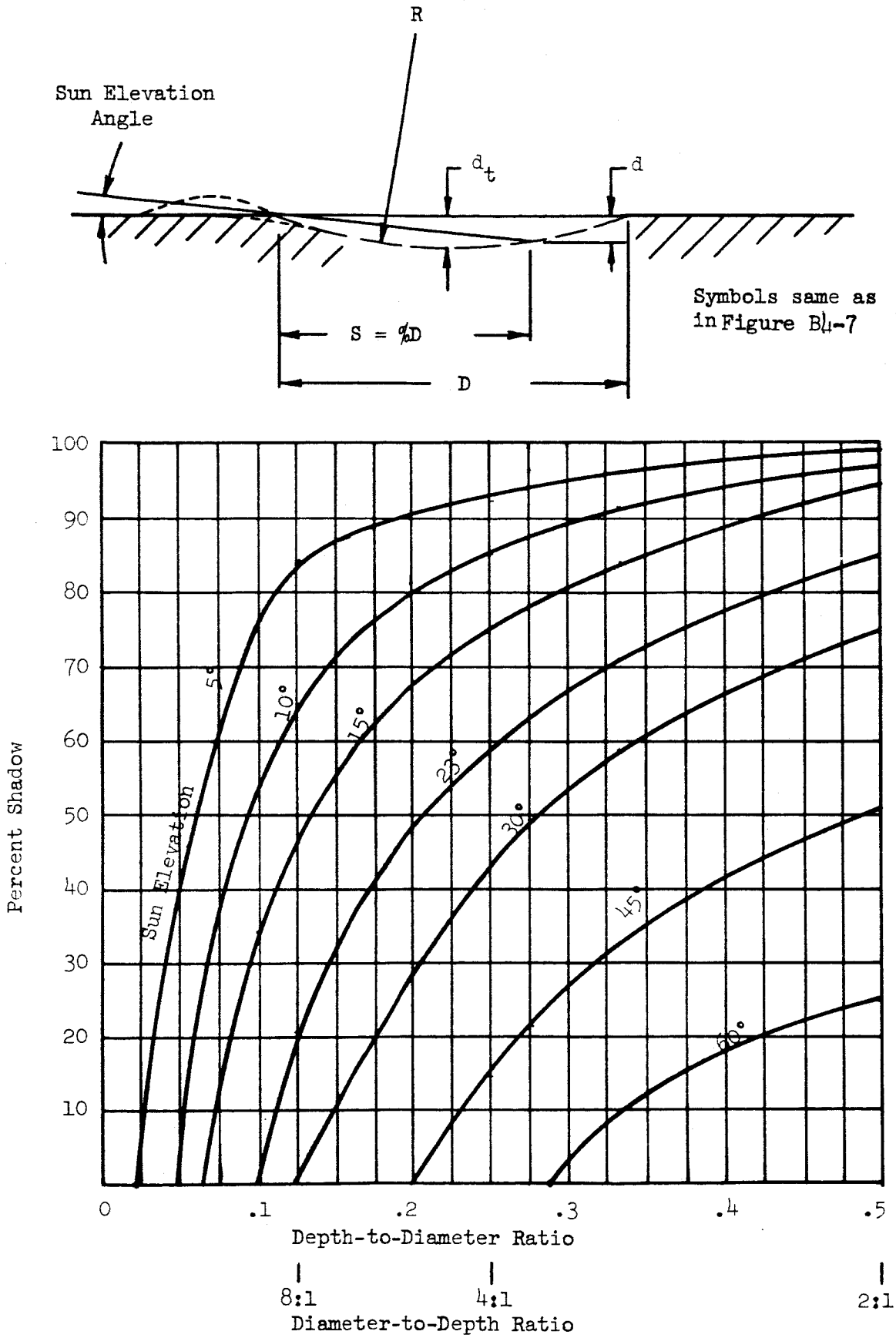

Figure B4-9 Percent Shadow vrs. Diameter to Depth Ratio for Several Sun Elevation Angles

Figure B4-8 shows the cross section of a typical crater with a sun elevation of 10°. The shadow lengths of the smaller craters found in the photographs of Ranger IX were measured at 55 to 60 percent of the crater diameter with an average of about 58 percent. The diameter-to-depth ratio can be calculated from:

$$\frac{D}{} = \frac{\cot 10^\circ}{0.58} = 9.8 \qquad \text{or about 10 to 1}$$

The true depth, d_t, is probably greater than this calculated depth for the reasons mentioned above.

Another method of analyzing these photographs is shown in Figure B4-9 where a spherical surface of radius R is assumed for the shape of the crater. Then the following expression gives the relationship between the parameters:

$$R = \frac{D}{8} \left(K + \frac{4}{K}\right)$$

Where R = radius of the inside of the crater surface.

D = diameter of the crater

K = diameter-to-depth ratio

The curves of Figure B4-9 plot shadow length as a function of the diameter-to-depth ratio for various sun elevations. Ranger VII photographs taken with a sun elevation of 23° show a crater shadow length of 33 percent, giving a diameter-to-depth ratio of about 7:1. Since many of the craters did not show any distinct shadows, many must have had diameter-to-depth ratios of 10:1 or larger (very shallow). The Ranger IX data with shadow lengths of 55 to 60 percent give calculated diameter-to-depth ratios between 9:1 and 10:1.

The results of the two methods of analysis agree quite well. However, for the second method a multiplying factor is easily calculated to give the true depth. If we assume the crater to be a portion of a spherical

surface of radius R, then it can be shown * that for the conditions of Ranger VII:

$$d_t = 1.12d$$

and for the conditions of Ranger IX,

$$d_t = 1.03d$$

This will change the calculated diameter-to-depth ratio very little, but will shift it in the direction of deeper craters.

The rims of the craters observed in the Ranger photographs differ from the idealized geometry by: (1) rounded rims and (2) built-up rims, as shown in the dotted lines of Figure B4-9. These changes in shape will affect the calculated diameter-to-depth ratio very little, depending of course upon how much rounding or build-up has occurred. It can be seen that a rounding of the crater rims will cause the shadow to fall short, but the start of the shadow will be moved nearly a corresponding amount. Therefore, the shadow length will measure nearly the same. The diameter will be measured slightly larger in this case, and since the shadow length is nearly unchanged, the diameter-to-depth ratio will shift to a slightly larger value (shallower craters).

If a moderate buildup is present around the crater then the diameter will be larger and the shadow length longer, leaving the diameter-to-depth ratio nearly unchanged. The depth will be assumed to be measured downward from the crater rim rather than from the undisturbed lunar plane.

Photographs of the Kodak geometric shapes were studied at sun angles of 10° (Ranger IX) and 23° (Ranger VII). The model with geometric shapes has craters with diameter-to-depth ratios of 2:1, 4:1, and 8:1. The shadow appearance of the 8:1 craters closely matches the shadow detail of the Ranger photographs. Figures B4-5, B4-6, and Table B4-3 show the results of many measurements from Ranger VII and Ranger IX.

* See Figure B4-9

Data from Ranger Photography				Kodak Lunar Model 6-65		
Crater Diameter on Moon in Feet	Crater Depth in Feet	Representing Crater Diameter Range	Number of Craters per Square Miles of Lunar Surface	Crater Diameter in Inches	Crater Depth in Inches	Number of Craters
2.5	.24	1 - 5 ft.	100,000	0.63	0.06	100
7.5	.73	5 - 10 ft.	50,000	1.9	0.18	50
12.5	1.2	10 - 15 ft.	9,000	3.1	0.30	9
17.5	1.7	15 - 20 ft.	5,000	4.4	0.43	5
22.5	2.2	20 - 25 ft.	2,500	5.6	0.55	2
27.5	2.7	25 - 30 ft.	1,000	6.9	0.68	1
35.0	3.4	30 - 40 ft.	800	8.8	0.85	1

Crater Data for Kodak Lunar Model 6-65 from Ranger Photographs

Table No. B4-3

Although Kodak Model #2 was made from a Ranger VII photograph taken at a sun elevation of 23°, when the model was photographed at a sun elevation of 10°, the pictures showed remarkably similar shadow detail to that in the Ranger IX photographs.

Boulders were found in three photographs from Ranger IX and a count of their number and size is given in Table B4-4.

Other surface features have been noted in distant Ranger pictures. These include the (1) tree bark effect, (2) rills, (3) fault lines, (4) variable albedos (halos, rays), (5) wrinkles, (6) mountains, etc.

Except for changes in albedo, these details are probably too large with respect to KLM 6-65 to be included on the Kodak model. In the following section, the measurements from the Ranger pictures are used to specify the details of Kodak's next lunar model.

2) Parameters for the Kodak Lunar Model 6-65 (KLM 6-65)

The largest model that can be uniformly illuminated with the simulated sun (2 inch diameter at 21 feet) is about 40 inches x 40 inches. Even a model of this size will show a change in sun elevation of 10° across the model. At a scale of 1/4 inch equals one foot on the moon, this model will represent a lunar area 160 feet on a side.

The original KLM 6-65 was modeled in clay and served as a mold for a plaster casting. Over the surface of the plaster casting, a sheet of plastic was vacuum formed to produce a replica of the original clay model. Since a 20-inch x 40-inch sheet is the largest size that can be conveniently formed by the available equipment, two 20-inch x 40-inch panels were made and fastened together to form the 40-inch x 40-inch model. This method offers an inexpensive way to create replicas of the KLM 6-65. The formed plastic sheets were mounted on plywood and dusted in preparation for photography.

Extrapolated from Last Ranger IX B Frame (Partially Scanned)
Last Frame P-3 and Last Frame P-1

Boulder Diameter Feet	Number of Boulders	Estimated Number of Boulders per Sq. Mi. of Lunar Surface	Boulder Diameter in Inches on KIM 6-65	Number of Boulders on KIM 6-65
0.5 - 1.5	3	2,000	0.25	2
1.5 - 2.5	0	0	0.5	
2.5 - 3.5	2	1,300	0.75	2
3.5 - 4.5	3	1,300	1.0	1
4.5 - 5.5	1	700		
5.5 - 6.5	4	700	1.37	1

Height of Boulders Ranged from 0.2 Feet to 1.7 Feet

Height Feet	Number in Interval	Number on KIM 6-65
.2 to .5	4	3
.5 to 1.5	4	2
1.5 to 2.5	1	1

RANGER - BOULDER DATA

Table No. B4-4

Figure B4-10 is a photograph of KLM 6-65 showing the location of prominent features. Figure B4-11 shows the appearance of KLM 6-65 at four sun altitudes from 10° to 84°.

3) Summary of KLM 6-65 Features

Size	- 40" x 40"
Material	- Plastic sheet, vacuum formed over a sculptured plaster surface
Model Scale	- 1/4 inch on model represents 1 foot on the moon, 1 to 48
Photographic Scale	- 1/4 inch on model photographs as 1/200mm on the film (1 to 1270), representing a Lunar photographic scale of 1 to 61,000

Surface Features:

(a) Craters - Number and size as shown in Table B4-3. A study of the small craters in the Ranger photography indicates that a buildup of material around the edges of craters is not characteristic of the majority of these small craters. There are some that have a buildup of a little material. In KLM 6-65, 10 percent of the craters have some buildup to form rims, and the remainder are essentially rimless.

(b) Boulders - Number and size as shown in Table B4-4. Measurements of bolder diameters and heights indicate that the boulders large enough to be seen by Ranger may not be hemispherical. They are either low protusions or are round but not supported on the surface; e.i., they have penetrated far enough into the lunar surface to find support or have been surrounded by lunar debris and dust. The diameter-to-height ratio is about 3:1 or 4:1. It is possible that the shadows are actually longer than measured, as the tip of the shadow may be lost in the photographic background making the shadow measurement shorter than

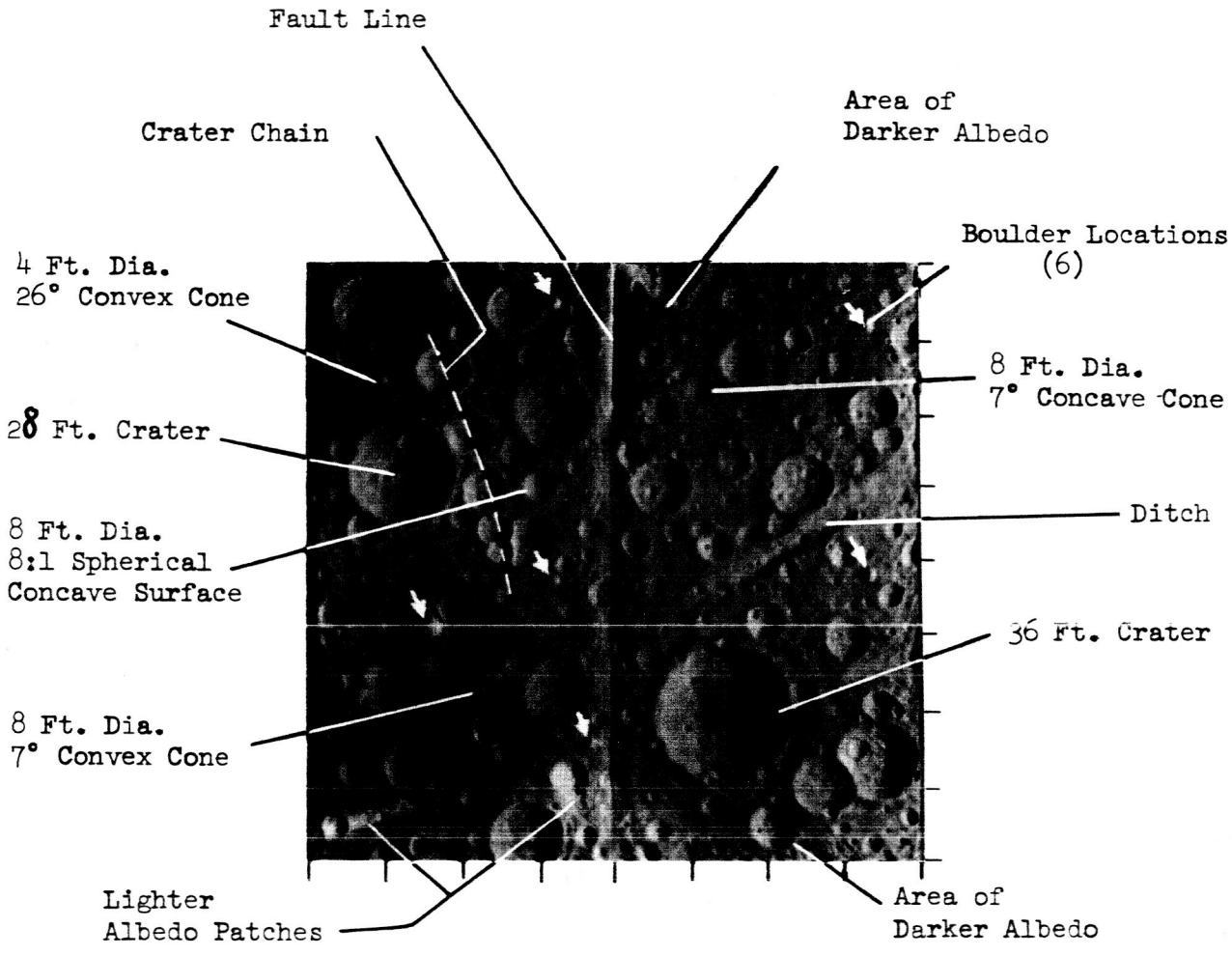

Scale - KLM6-65 is 160 feet on a side - each division along the bottom and right side represents 20 feet

Photograph of KLM6-65 with Sun Elevation of 15°
Showing the Location of Lunar Features

Figure B4-10

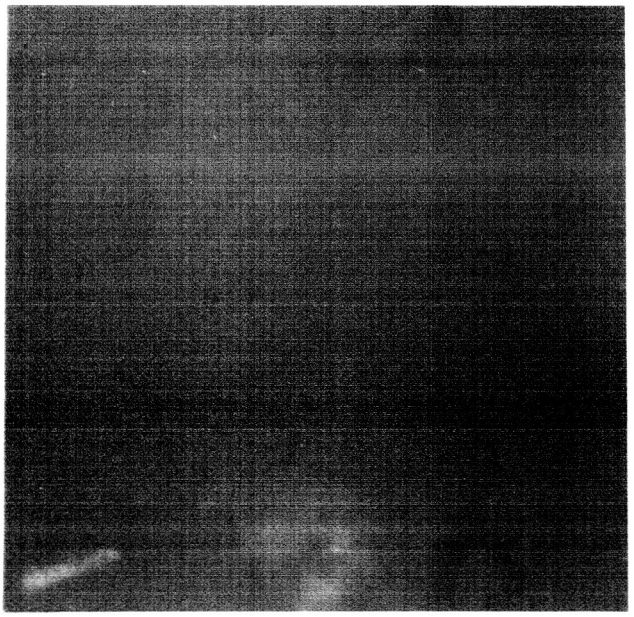

Sun Elevation = 84°

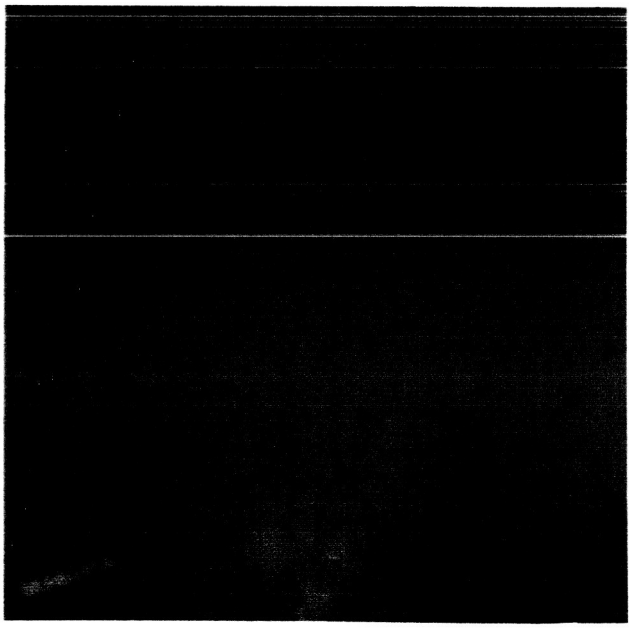

Sun Elevation = 60°

Record Photographs of Kodak Lunar Model 6-65
at Several Sun Elevations

Figure B4-11

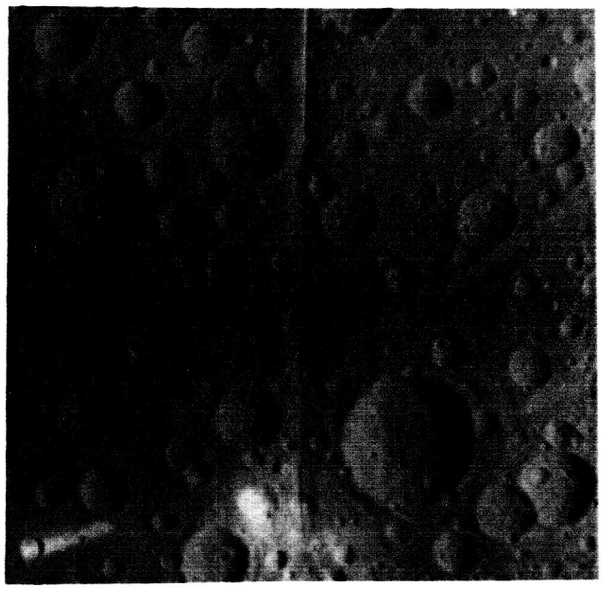

Sun Elevation = 30°

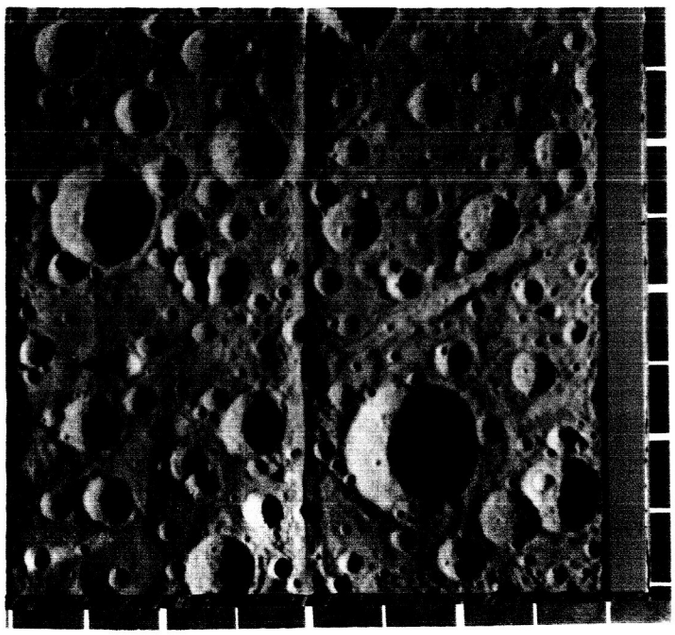

Sun Elevation = 10° with scale
along the bottom and right side

Figure B4-11 KLM6-65

it should be. The boulders on the model must have a diameter-to height-ratio of about 3:1 to account for this effect.

(c) Tree Bark - This effect has appeared as a feature with a pitch of about 100 to 1000 feet, a size too large to influence the KLM 6-65 model of only landing-site size.

(d) Rills and Fault Lines - All rills and fault lines observed in the Ranger photographs are on a large scale. In the model, there are no rills but there is a fault line 5 inches with a 1/2 inch difference in elevation. After several days of photography the left and right half of the model separated forming a very contrasty fault line down the middle.

(e) Variations in Albedo - A bright material, silver chloride was dusted over the copper oxide in two areas to show changes in albedo. These areas in the lower left corner of the model were named "the streak" and "the blob" by the readers. In addition, Will CuO was dusted in two places to provide areas of darker albedo.

(f) Wrinkles, Troughs, Ridges - Large wrinkles, troughs, and ridges are easily identified in the distant Ranger photographs. The Kodak model has an undulating surface but is not large enough to show these features clearly.

(g) Crater Chains - The model included one small chain of five craters starting with 3 inches in diameter and reducing to 1 1/2 inches in diameter spaced about 1 1/2 diameters apart.

(h) Geometric shapes - To bridge the work done previously, four geometric shapes are included in the model as follows:

(1) 1-inch diameter, 26° slope, conical convex surface
(2) 2-inch diameter, 7° slope, conical concave surface
(3) 2-inch diameter, 8:1 spherical concave surface
(4) 2-inch diameter, 7° slope conical convex surface

5. Solar Simulators, Working Space and Control of Stray Light

a. Solar Simulators

1) Light Source Requirements

The light that simulates the sun and illuminates the models should appear to come from an infinitely distant source that subtends 1/2 degree, if shapes are to appear as though they were on the surface of the moon.

The moon is illuminated by three sources with the following approximate values:

Sun	-	12,000 foot candles
Earth	-	2.4 foot candles (at brightest earth shine)
Sky	-	0.0004 foot candle

For realism, the shadow areas of any models should have less than 3×10^{-7} of the brightest illumination from the simulated solar source. However, if the shadows receive less than 10^{-3} of the maximum illumination, then the exposure on the film will be below the threshold of sensitivity and will be insignificant. To insure that the shadows were black enough, the photography was performed in a darkroom.

The source should be as bright as possible to keep the photographic exposure times short and should be mobile so that sun elevation can be readily changed.

2) Light Sources

(a) The sun itself is an excellent light source but it does have several disadvantages:

(1) Sun elevation is not under direct control.

(2) Clouds in the sky would scatter light into the shadow areas and give a false impression of the lunar reflectance.

(3) The sky would also scatter blue light into the shadow areas. (This condition could be minimized with a red filter at the expense of increased exposure time).

(4) The models would be subject to wind or air drafts which could change the model appearance during the experiment thus making comparisons difficult.

(b) Small bright sources projected by lenses or mirrors to meet the angular and brightness requirements. It is possible with a mirror or lens to project a small light source over a reasonable size model, however, the mirror or lens must be of high quality and at least as large as the maximum dimension of the model. Large 60 inch mirrors are available on the surplus market and could be incorporated into such an optical system. Search lights may be rented but these would be difficult to move, will scatter light from objects illuminated by the source, and will generate smoke which scatters light.

(c) An array of small collimated light sources will not meet the 1/2 degree requirement over a large model and would make objects appear different from similar objects on the lunar surface.

(d) Flashbulbs and an electronic flash lamp were considered but are not as convenient to control and are not as easy to use in a darkroom as are continuous sources.

(e) Carbon arcs, zirconium arcs and other small arcs require special power supplies and may be relatively unstable compared to a tungsten lamp.

(f) Sun guns, projector lamps, etc. with projector optics. These light sources could be used if the size of the source subtends an angle of 1/2 degree. The model size will need to be small or the sun elevation will change as seen from different points on the surface of the model. As an example, a 2-inch diameter projection lens at 21 feet will subtend 1/2 degree. However, each 4 inches on the model will change the sun elevation by 1 degree at a sun elevation of 90 degrees. Despite this problem, objects in the model will appear like similar objects on the lunar surface.

3) Light Source Selected

A 500-watt projector with a projection lens 2 inches in diameter is a convenient, mobile*, solar simulator and will satisfy all the requirements except for the small change in sun elevation with position on the model.

b. Working Space and Stray Light Control

The area selected for photography of the models is a darkroom with 59 feet between model and camera. Normally, a storage area, this room has been modified for this work by draping large overlapping black plastic sheets to build a darkroom 30 feet square by 16 feet high with a long corridor to include the tripod mounted camera. As discussed previously, the light reaching the shadow areas must be less than 1/1000 of the incident light reaching the target. Measurements of the brightness levels show that the illumination from the simulated sun source is 30 foot candles and the illumination reaching the shadow areas is less than 0.05 foot candle (measured by a Weston Illumination Meter Model 756). This ratio is satisfactory for the photo study. During the summer months photography was done at night to insure low illumination in the shadow areas.

6. Photographic Systems

The ability of a photo system to faithfully record information in the object space is usually limited by one or more of the following factors:

a. Optical quality of the system components.

b. Nature of light (diffraction limit of the optics).

c. Film capabilities.

d. Image motion.

e. Atmospheric discontinuities.

* Solar altitudes studied were 5°, 10°, 15°, 30°, 45°, 60°, 75°, 84° for monophotography and a similar number of angles for stereo photography.

For this study it was decided to provide three photo systems that would record 200 lines/mm, 100 lines/mm and 50 lines/mm. These systems should have similar image quality at limiting resolution and, if possible, should use the same lens. The camera will be held rigidly on a tripod eliminating image motion, and the steady air in the work space should keep atmospheric discontinuities to an insignificant value. Therefore, the lens and film are the primary factors in determining photo system quality.

Camera Focus and Shutter Tests

A 35mm camera was procured for this study and the lens mount was modified by adding an extended scale and pointer. Each division of this focus scale represents a displacement of 0.00066 inch and it is possible to focus the lens to within 1/6 of a division or 0.0001 inch. Several resolution tests were made with this equipment and accurate focus settings were found to be repeatable.

Shutter tests were made with a Berkeley Interval Timer which counted the period of time during which light can pass through a narrow slit near the image plane. The slit was placed in three positions in the image plane: center, left and right. This test showed that the errors marked shutter speeds of 1/60 second and longer were from -12 percent to +9 percent. All exposures longer than one second were made by turning the light source on and off with a Microflex Eagle Signal Corporation Timer which can be controlled at 1/10 second. These shutter tests revealed error tolerances which were acceptable for this photo study.

Film Selection - Exposure Values - Characteristic Curves

Photographs of resolution targets were made on SO-243 film using the 15mm f/2.5 Cine Kodak Lens at several apertures. The results of this test are tabulated in Table B6-1 and shown in Figure B6-1. It can be seen from the figure that this photo system can provide 200 lines/mm at f/2.5 and at f/7.5, and that at settings slower than f/8.0 it is essentially diffraction limited. An f stop of 3.5 was selected to insure a high

Measured Resolution in Lines Per mm of a High Contrast Tri-Bar Chart for Three Films With a Kodak Cine Ektar 15mm f/2.5 Lens

f/#	SO-243 Resolution lines/mm	Plus-X Pan Resolution lines/mm	Tri-X Pan Resolution lines/mm
2.5	207	75	50
2.8	207	67	55
4.0	237	89	62
5.6	237	94	78
8.0	188	89	78
11.0	151	78	75
16.0	106	67	70
22.0	71	55	55

Table No. B6-1

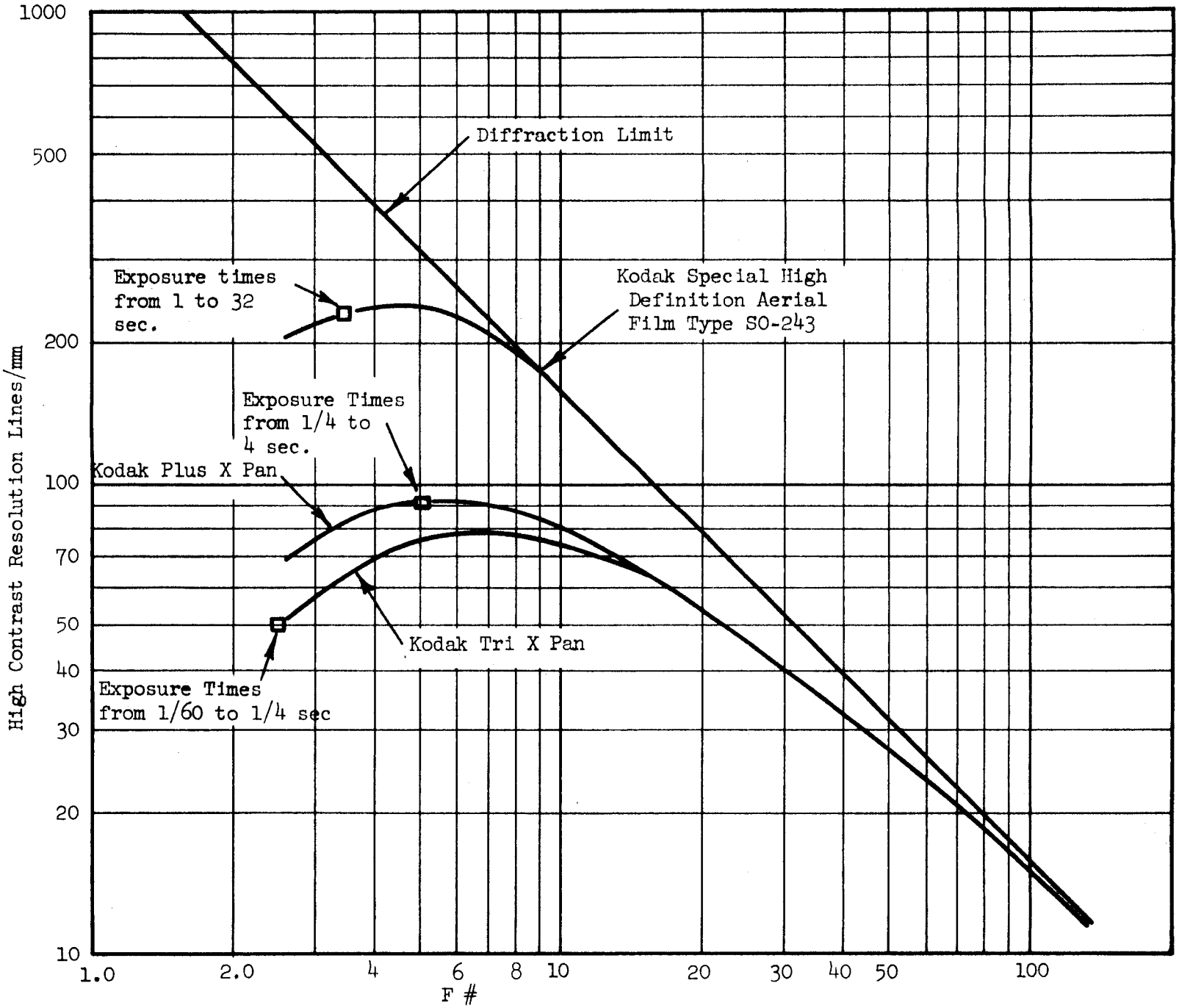

Figure B6-1 Resolution vs F Stop for Three Photographic Materials With Kodak Cine Ektar Lens 15mm f/2.5

resolution system yielding slightly better than 200 lines/mm. The nominal exposures using SO-243 film at this f stop for the dusted models at the expected sun angles with this system ranged from 1 second at 84° sun elevation to 32 seconds at 5° sun elevation. However, if the lens is stopped down to f/16 to obtain 100 lines/mm the exposure times would range from 21 seconds to 670 seconds, while 50 lines/mm would require f/32 with a maximum exposure time of 2680 seconds. Since these exposure times are too long, two other films, Plus-X Pan and Tri-X Pan were tried. The results of these tests are tabulated in Table B6-1 and plotted in Figure B6-1. From these last tests the 100 lines/mm system was selected using Plus-X Pan film at f/5.0 where the nominal exposures are 1/4 second at the high sun angle, and 4 seconds at the low sun angle. The 50 lines/mm system was selected using Tri-X Pan film at f/2.5 with nominal exposure times from 1/60 second to 1/4 second.

Figure B6-2 has been made from the negatives obtained in the resolution tests. SO-243 has been enlarged 200X, the Kodak Plus-X Pan enlarged 100X and the Kodak Tri-X Pan enlarged 50X. Since the ratio of grain size to target bar size is similar in all three systems, direct comparison of results among the three photo systems is possible.

The average resolution of the system selected after many photographs were made with the above parameters turned out to be 220 lines/mm, 92 lines/mm and 53 lines/mm. The remainder of this report will identify the system with these values.

Table B6-2 shows the exposure times required to give satisfactory background densities (near 0.8) in pictures of a surface dusted with copper oxide and illuminated with the 500 watt slide projector.

Figure B6-3 shows typical characteristic curves for the three photographic materials used in this study.

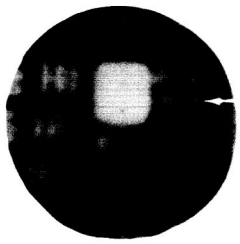

200X
Enlargement

200 Line/mm System
SO-243 Film
f/3.5

100X
Enlargement

100 Line/mm System
Plus-X Pan Film
f/5.0

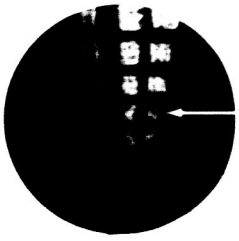

50X
Enlargement

50 Line/mm System
Tri-X Pan Film
f/2.5

Limiting Resolution for Three Photo Systems Selected for this Photo Study. All Photographs were made with the Kodak Cine Ektar 15mm f/2.5 Lens from a Distance of 59 Feet.

Figure B6-2

Nominal Exposure Values
Seconds

Sun Elevation		84°	75°	60°	45°	30°	15°	10°	5°
Film	F/#								
SO-243	3.5	1	2	2	4	4	8	16	32
Plus-X-Pan	5.0	1/4	1/2	1/2	1/2	2	2	4	4
Tri-X-Pan	2.5	1/60	1/60	1/30	1/30	1/15	1/8	1/8	1/4

Table No. B6-2

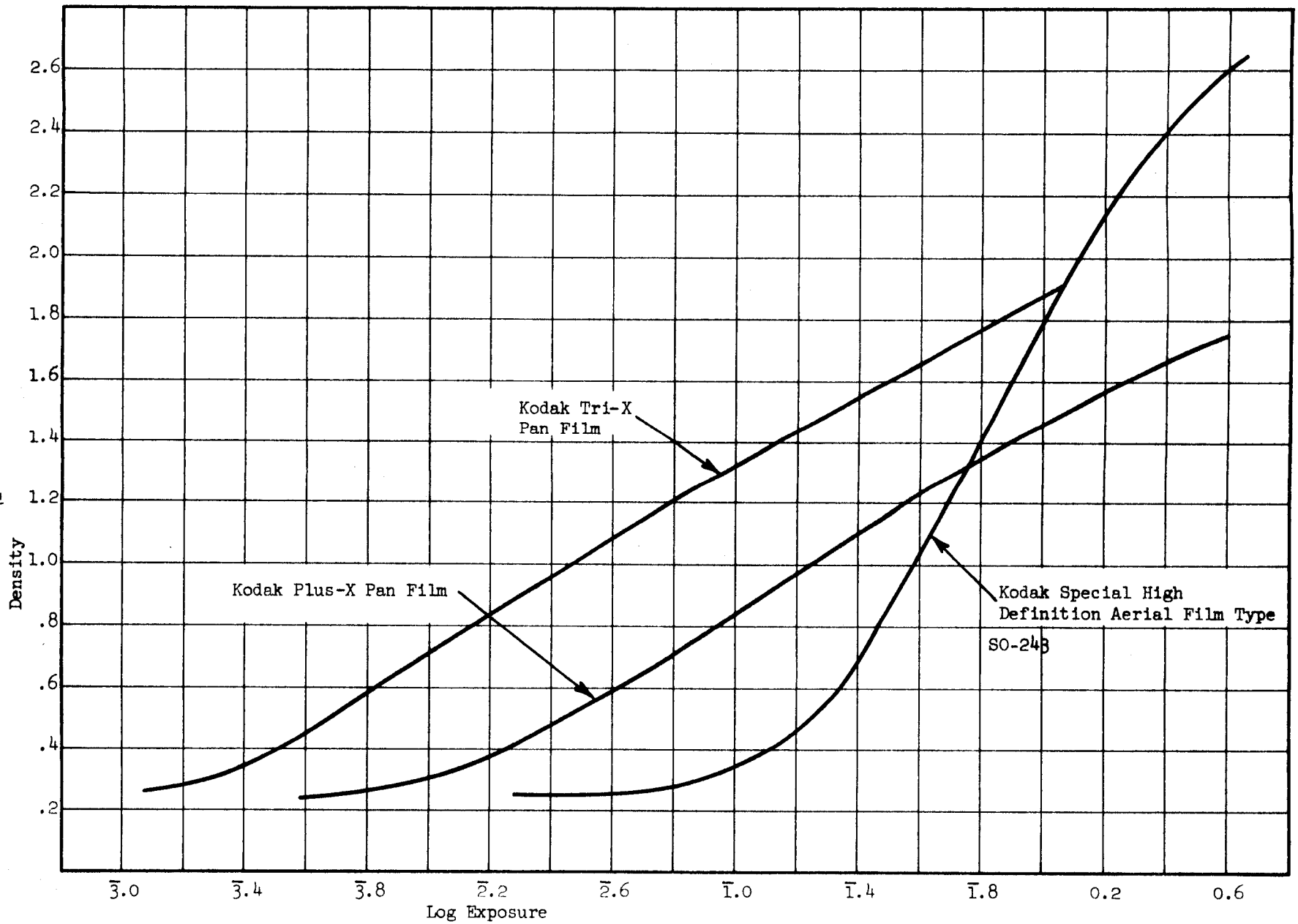

Figure B6-3 Typical Characteristic Curves for the Three Photographic Materials Used in This Study

7. Reader Equipment and Reader Selection

a. Mono Photography - The size of the image of the 40" x 40" targets taken through the 15mm lens at 59 feet is a little smaller than one millimeter square on the film. Six of these photographs have been magnified by a 40X enlargement and are shown in Figure B7-1 to illustrate the size and quality of the detail in KLM 6-65 photography. A 16mm objective with 10 X eyepiece providing 100 X magnification was the prime instrument used in the evaluation of the mono photography in this photo study. The reader was encouraged to change magnification if this would yield more information; a few changes were made.

b. Stereo Photography - It was originally hoped that a Bausch & Lomb Zoom 70 Stereoscope, Model II, could be used for the evaluation of stereo negative pairs. However, the capability of this instrument proved to be inadequate.

It was decided to secure two microscope bodies with 16mm objectives and 10 power eyepieces and build a frame to hold these microscopes, with a fine adjustment for the interocular distance. A bright light source from the laboratory was added, and the entire instrument was mounted on a tilting drafting board. Clips were mounted on the observation table to hold the individual cardboard-mounted slides. In use, the operator adjusts these slides in rotation and translation to bring the two images into coincidence.

The new instrument has worked satisfactorily during evaluation of the stereo photography for the 220 lines/mm system by the three readers.

c. Reader Selection - Three readers were selected from the Photo Science group for reading the photography in this photo study. Two of these readers are experienced in evaluating tri-bar resolution targets; the third reader had limited experience in

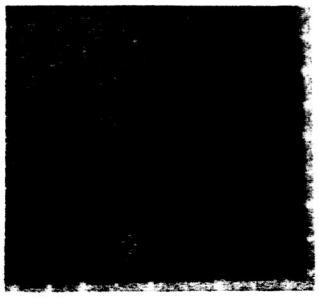

53 l/mm

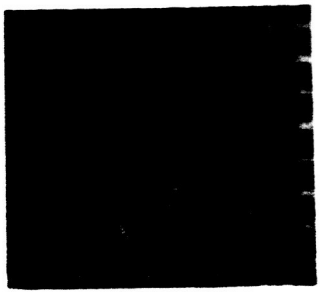

Sun Elevation 75°

Sun Elevation 15°

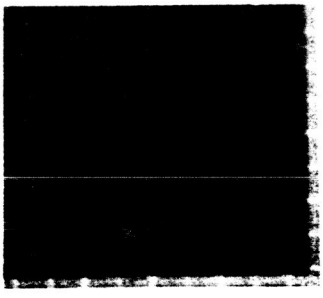

92 l/mm

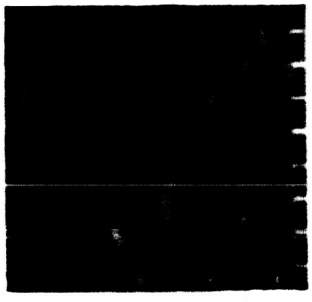

Sun Elevation 75°

Sun Elevation 15°

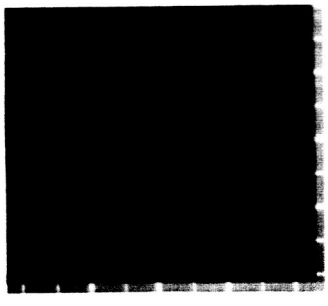

220 l/mm

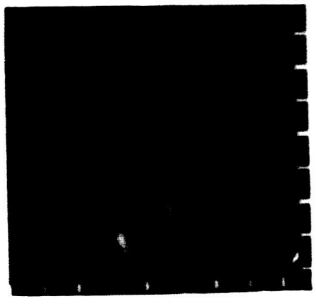

Sun Elevation 75°

Sun Elevation 15°

Enlargements made from the three photo systems at two sun elevations to show the relation of grain size to detail in the KLM6-65 photography

Figure B7-1

reading resolution targets. The details of reading and recording for each of the experiments are given in the later sections on evaluation.

8. Computer Plotting

After the readers completed notations on the data sheet, all of the responses were coded and put on punch cards for computer manipulation. A sample of the coding is shown in Figure B8-1. All of the mono and stereo photography obtained from the geometric slips was coded and punched into cards.

An IBM 7044 computer was programmed to sort and then rank the coded reader responses as follows:

Reader Response	Rank
No detection	0
Detection but no identification	1
Correct identification as to concavity or convexity (not full identification as to shape)	2

The responses of the three readers to each object were summed to develop a matrix of responses for eight sun altitudes and six object sizes. The sums, therefore, take values from 0 to 6. Zero represents a point in the matrix where all three readers indicate no detection, and 6 represents a point where all three readers correctly identified the surface type as either convex or concave. (The value of 2 for identification x 3 readers = 6).

A line was drawn through the matrix at values of 1, below which all readers failed to find any detectable image on the film, and another line through the values of 5 above which all the readers were able to correctly identify the image. In the area between 1 and 5, the readers were able to detect something but not identify it.

READER RESPONSE TO DUSTED SPHERICAL AND CONICAL SURFACES

Photography 0° (Target Pos.) 1 (Camera Pos.) System 1 Reader K Date 4-24-65 Sun Elevation 45°

Neg. # 57 - 18 (roll - frame)

Chart #

L/mm

Background Density 0.87

Position	20	19	18	17	16	15	14	13	12	11	10	9	8	7	6	5	4	3	2	1Δ
No Detection *			0										0							
Detection **	Λ						Λ		Λ	XS		V			V				V	
Identification***		SΛ		CΛ	SΛ	SΛ		SΛ			SV			SV		CV	SV	SV		SV
†	1	2	3	4	5	6	7	8	9	10	11	12	13	14	15	16	17	18	19	20	21	22	23	24	25	26	27	28	29	30	31	32
∓	1	1	2	5	0	5	7	1	8				5	9	1	7	9	9	5	9	5	2	8	4	1	8	4	6	8	8	4	8

* Write 0 for No Detection

** Write XS for something small detected, no identification
Write XL for something large detected, no identification
Write Λ for something convex detected
Write V for something concave detected

*** CΛ - conical convex
CV - conical concave
SΛ - spherical convex
SV - spherical concave

Neg. # 7 - 21 (roll - frame)

Chart #

L/mm

Background Density 0.87

Position	20	19	18	17	16	15	14	13	12	11	10	9	8	7	6	5	4	3	2	1Δ
No Detection *			0			0		0	0	0		0	0	0		0	0			
Detection **		Λ			XS		Λ	XS			V							V	V	XS
Identification ***	SΛ			CΛ											CV					
†	33	34	35	36	37	38	39	40	41	42	43	44	45	46	47	48	49	50	51	52	53	54	55	56	57	58	59	60
∓	0	0	7	2	1				9	5	1	7	2	1	5	2	1	1	4	1	1	1	6	1	1	4	4	2
									61	62	63	64	65	66	67	68	69	70	71	72	73	74	75	76	77	78	79	80

Δ These numbers refer to the target position on the model.

† These numbers refer to the punch card column.

∓ Coded Reader Response for the Computer. Entries under Nos. 1 - 12 and 33 - 40 are coded test conditions for computer use.

Figure B8-1 READER RESPONSE DATA SHEET

There are ten surface types for each resolution system as follows:

a. 26° Conical Concave
b. 7° Conical Concave
c. 2:1 Spherical Concave
d. 4:1 Spherical Concave
e. 8:1 Spherical Concave
f. 26° Conical Convex
g. 7° Conical Convex
h. 2:1 Spherical Convex
i. 4:1 Spherical Convex
j. 8:1 Spherical Convex

For the resolution systems, a total of 30 matrices were plotted by the computer to depict all of the surface types for the three systems. An index to these matrices is found in Table B8-1, items 1 to 30.

To condense the data further, matrices were made by combining the reader response for the concave surfaces for each resolution system and the reader response for the convex surfaces for each resolution system. In these matrices, a value of 30 represents five surface types correctly identified (the value of 2 for object identification x 5 surface types x 3 readers = 30). Lines were drawn through the arbitrary points 5 and 25 to separate the three areas of reader response. The index for these six additional matrices is also found in Table B8-1, items 31 to 36.

Finally, the reader response for both convex and concave surfaces for each resolution system was combined. Figure C1-2 is the reader response to all ten surface types recorded on a photo system resolving 220 lines per mm; Figure C1-3 is the reader response to all ten surface types recorded on a photo system resolving 92 lines per mm; and Figure C1-4 is the reader response to all 10 surface types recorded on a photo system resolving 53 lines per mm. In these graphs, vertical columns of data are for each of eight sun altitudes, while the horizontal rows are readings from six object sizes on the simulated lunar surface. The log scale is used to provide good separation in the smaller object sizes. The separations between no detection and detection were arbitrarily placed through the

Index to Matrices

Fig. No.	Matrix No.	System Resolution in 1/mm	Surface Type Analyzed
	1	220 1/mm	26° conical concave
	2	"	7° Conical concave
	3	"	2:1 spherical concave
	4	"	4:1 spherical concave
	5	"	8:1 spherical concave
	6	"	26° conical convex
	7	"	7° conical convex
	8	"	2:1 spherical convex
	9	"	4:1 spherical convex
	10	"	8:1 spherical convex
	11	92 1/mm	26° conical concave
	12	"	7° conical concave
	13	"	2:1 spherical concave
	14	"	4:1 spherical concave
	15	"	8:1 spherical concave
	16	"	26° conical convex
	17	"	7° conical convex
	18	"	2:1 spherical convex
	19	"	4:1 spherical convex
	20	"	8:1 spherical convex
	21	53 1/mm	26° conical concave
	22	"	7° conical concave
	23	"	2:1 spherical concave
	24	"	4:1 spherical concave
	25	"	8:1 spherical concave
	26	"	26° conical convex
	27	"	7° conical convex
	28	"	2:1 spherical convex
	29	"	4:1 spherical convex
	30	"	8:1 spherical convex
	31	220 1/mm	All concave (1-5) 220 1/mm
	32	"	All convex (6-10) 220 1/mm
	33	92 1/mm	All concave (11-15) 92 1/mm
	34	"	All convex (16-20) 92 1/mm
	35	53 1/mm	All concave (21-25) 53 1/mm
	36	"	All convex (26-30) 53 1/mm
C1-2	37	220 1/mm	All forms (1-10) 220 1/mm
C1-3	38	92 1/mm	All forms (11-20) 92 1/mm
C1-4	39	53 1/mm	All forms (21-30) 53 1/mm

Table No. B8-1

value 10, and through the value 50 to separate the area of identification from detection. A value of 60 represents identification for all readers and all surface types. (The value of 2 for identification x 3 readers x 10 surface types = 60). Near the lower left corner of each of these figures is a mark which indicates the pitch of the tri-bar target for limiting resolution at the lunar surface for that photo system, based upon 1/4 inch on the model being equivalent to 1 foot on the moon.

A copy of all 39 matrices was sent to Mr. Robert L. Jones, MSC, NASA, Houston, Texas, for use by persons in NASA who are interested in further study of the responses to each individual surface type. Duplicate matrices remain at Kodak.

C. GEOMETRIC SHAPES

1. Photographic Schedule and Records

Figure C1-1 is a copy of the data sheet used to record the photography. The procedure for photography was to record all the sun angles with one film, then repeat the test with changed aperture and different film, and finally to repeat the test with the third film and the proper aperture. This series completed all the monoscopic photography.

The stereo photography is taken with a single film and all sun angles, after which the model is tilted back 45° and additional mono and stereo photography taken to complete the resolution series.

At each sun elevation position, 5 exposures were taken nominal, ± one stop, and ± 2 stops. It was from the negatives taken at ± 2 stops from the nominal that a study was made of the effects of under and over exposure.

A 5-inch x 7-inch view camera with a 19-inch f/11 lens was then used to record the model at the various sun angles and in a limited stereo series. These record shots complete the photography of one model. The above procedure was repeated to obtain the photography for the 2nd model containing geometric shapes.

2. Reader Instruction

In order to provide a uniform basis on which the reader may judge the negatives, the following paragraphs were prepared and given to the reader before they started to read.

INSTRUCTIONS TO READER

What Is It All About?

Contract NAS9-3826 (Z3841), Lunar Photo Study, includes the development and construction of a model of the lunar surface consistent with present day knowledge. One purpose of the study is to find the best

Date of Photography
Target Photographed
Target Recline
Camera-Target Distance
Camera-Target Angle
Lines/mm Anticipated _____, Recorded _____
Film & Emulsion #
f/# Setting of Lens
Illumination at Target Plane (Foot Candles)

Film Development

1) Developer
2) Time
3) Temperature

ROLL # / Sun Elevation / Exposure Time	(✓) Ck Off	Frame #		(✓) Ck Off	Frame #		(✓) Ck Off	Frame #		(✓) Ck Off	Frame #		(✓) Ck Off	Frame #	
(Sec.)															
- .6 Log E															
- .3 Log E															
Log E Nominal															
+ .3 Log E															
+ .6 Log E															

ROLL # / Sun Elevation / Exposure Time	(✓) Ck Off	Frame #		(✓) Ck Off	Frame #		(✓) Ck Off	Frame #		(✓) Ck Off	Frame #		(✓) Ck Off	Frame #	
(Sec.)															
- .6 Log E															
- .3 Log E															
Log E Nominal															
+ .3 Log E															
+ .6 Log E															

Figure C1-1 Data Sheet for Lunar Photo Study

conditions for capturing lunar surface detail on film. The model will be studied photographically.

Presently the relationship of system resolution to detection of size and shape of lunar objects is being investigated. For this purpose a target was made consisting of idealized geometric shapes covering a range of sizes. These were dusted with a powder to give surface reflectance properties similar to those of the moon's surface. Exposures were made for a range of target illuminations and repeated with changes in system resolution.

Our Model and How to State Your Response

You are asked to view under a microscope at 100x magnification a number of negatives, each containing an image of the dusted target. A single light source, representing the sun, illuminates the target surface. The target consists of a flat area, a plane, that has been shaped at certain points to form the following four types of surfaces:

Conical Convex

Conical Concave

Spherical Convex

Spherical Concave

The four surface types appear in several diameters:

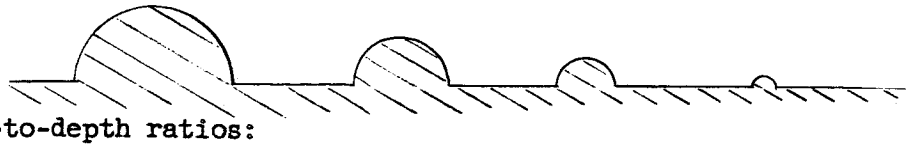

and diameter-to-depth ratios:

You are given the location of these deformations on the plane, Fig. B4-2, and are told the sun elevation. You are then to determine whether the shapes are not detectable, detectable, or identifiable.

A Morning on the Moon

Just as the sun rises from and sets below the horizon on earth, so the sun rises and sets on the lunar landscape. In fact, on the images you will be viewing the sun will move from a position just above the horizon (5° sun elevation) to a position approximately at noon (84° sun elevation). This excursion takes place in eight steps with sun elevations as follows: 5°, 10°, 15°, 30°, 45°, 60°, 75°, 84°.

The sun elevation is given by the number to the left and below the target for each image, or can be found on the reader response form.

The relationship of highlight (dark area on negative) to shadow (light area on negative) is a key to identification of surface details. For instance, at low sun elevations the shadow of a conical convex deformation comes to a point, while the shadow of a spherical convex deformation is rounded.

Study the photographs of the geometric shapes in Figures B4-3 and B4-4. Notice the amount and shape of the shadows cast by the convex and concave shapes. When you are ready to start reading you will be given a Reader Response Data Sheet (B8-1) to fill out. Follow the instructions on this sheet.

If you find that a change in magnification will help to detect or identify any object in the model, feel free to change the magnification to either a larger or a smaller value.

END INSTRUCTIONS TO READER

3. Reader Response - Evaluation and Analysis

Table C3-1 lists the figure numbers and the major parameters of the reader response Matrix Summaries for the geometric shapes. The method used to create these matrices is described in section B8, Computer Plotting. Note that the ordinate is a logarithmic scale.

It will be remembered that in the summaries the curves were drawn through a value 10 for detection and a value of 50 for identification.

Note that in all of the curves at low sun elevations (high phase angles) the readers were able to detect objects smaller than the pitch of the limiting tri-bar chart. This is possible because at the lower sun elevation the shadows cast by convex shapes are longer than the shape dimension. For example: at 5° sun elevation a 1 inch diameter, 26° Cone (.24" height) casts a shadow 2.8" long.

a. Vertical Monoscopic Photography of Geometric Shapes

A study of the reader response data for the individual geometric shapes shows that the diameter-to-height ratio determines the relative contrast of the geometric shapes. A shape of 2:1 ratio is more contrasty than the 8:1 shape, and the reader response data show that the 2:1 shape can be seen at higher sun elevations. The 26° cone has a diameter to height ratio of 4:1. The ability to detect and identify this shape is identical to that for the 4:1 sphere.

The reader response curves for the cones and spheres form a family of curves proportional to the diameter-to-height ratio which in turn are proportional to the slopes of the surface of the shape. The slopes are proportional to their apparent contrasts at the lunar surface. The 7° cone

Major Parameters for Reader Response

Matrix Summaries for the Geometric Shapes

Figure No.	Matrix No.	Limiting H.C. Resolution of Photo System Lines/mm	Pitch on the Moon of Limiting Tri-bar, feet	Type of Photography	Exposure	Remarks
C1-2	37	220	.91	Vert. Mono	Nominal	Similar if compared
C1-3	38	92	2.2	Vert. Mono	Nominal	to limiting tri-bar
C1-4	39	53	3.8	Vert. Mono	Nominal	see Fig. C1-15
C1-5	100	220	.91	± 10° Stereo	Nominal	Like C1-2, except better at
C1-6	101	220	.91	± 15° Stereo	Nominal	high sun elevation
C1-7	102	220	.91	± 20° Stereo	Nominal	
C1-8	141	220	.91	Oblique	Nominal	Like C1-2
C1-9	142	92	2.2	Oblique	Nominal	Like C1-3
C1-10	143	53	3.8	Oblique	Nominal	Like C1-4
C1-11	168	220	.91	Vert. Mono	2 stops under	Degraded from C1-2
C1-12	169	53	3.8	Vert. Mono	2 stops under	Like C1-4
C1-13	194	220	.91	Vert. Mono	2 stops over	Like C1-2
C1-14	195	53	3.8	Vert. Mono	2 stops over	Like C1-4

Table No. C3-1

has a diameter to height ratio of 16 : 1 and fits into this family of curves in its proper place.

A study of the summaries to the Reader Response for the three photo systems (Figures C3-2, C3-3, and C3-4) indicates that the ability to detect and identify a lunar object correlates directly with the capability of the photo system to resolve high contrast tri-bar charts. Figure C3-15 has been made by combining the above three curves using the pitch of the limiting high contrast tri-bar chart as the unit of measure for the ordinate. The measured departure of the three curves from Figure C3-15 is less than 20%.

In Figure C3-15 the abscissa has been converted to phase angle. In the vertical photography, with the camera and the sun in the plane of the ecliptic, the phase angle is 90° minus the sun elevation.

$$A = 90 - E$$

where A = Phase angle

E = Sun elevation

In the system where the camera is out of the plane of the ecliptic the phase angle is calculated from

$$\cos A = \cos B \cos (90-E)$$

where A = Phase angle

B = Camera angle from the Nadir

E = Sun elevation

This equation applies only when the camera is in a plane containing the Nadir at right angles to the ecliptic i.e. the spherical triangle is a right spherical triangle.

Figure C3-16 is made from information provided by C3-15 and shows the areas of Identification, Detection, and No Detection for photo systems resolving up to 220 lines/mm at sun elevations of 15° and 40°.

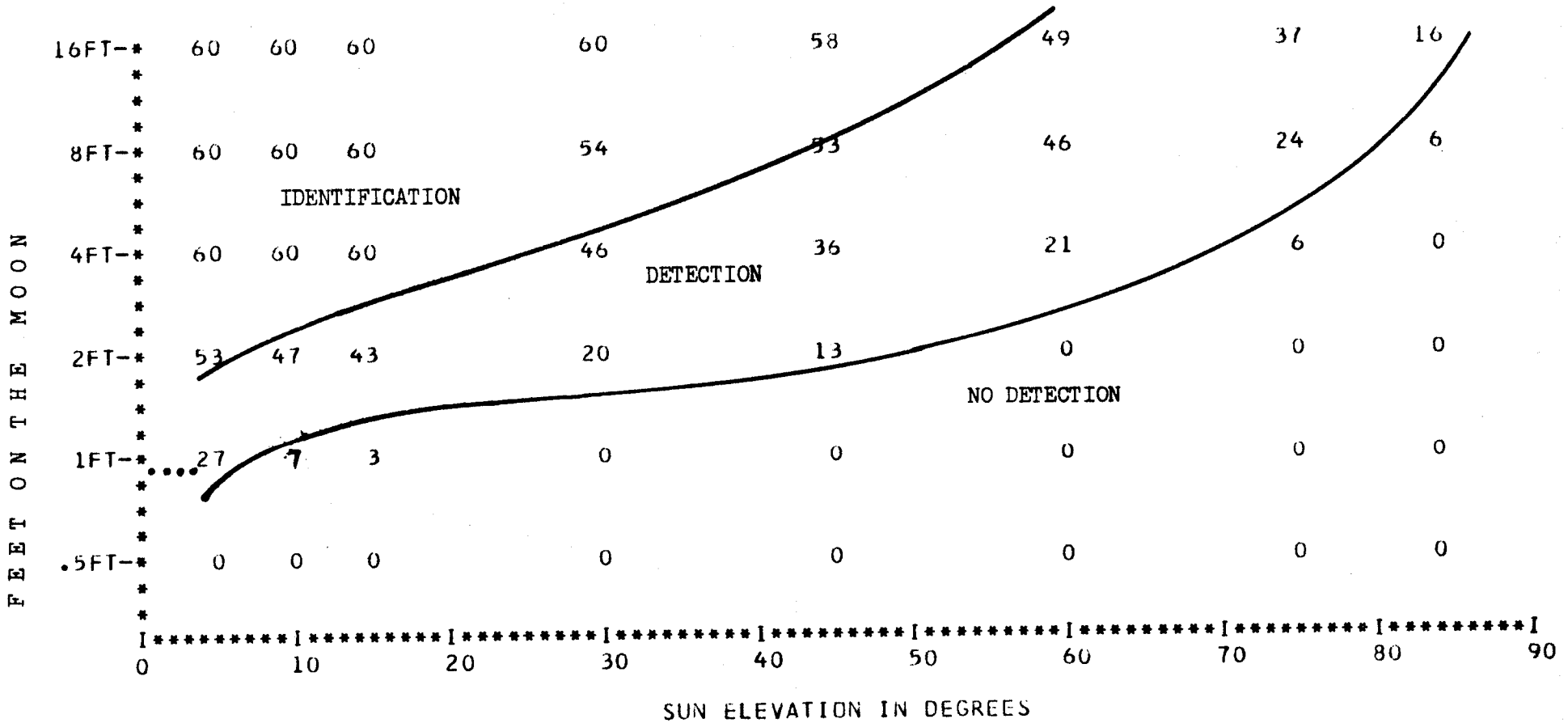

MATRIX NUMBER 37 READER RESPONSE FOR VERTICAL MONOSCOPIC PHOTOGRAPHY OF GEOMETRIC SHAPES

*PHOTOGRAPHY**VERTICAL MONOSCOPIC *SYSTEM**220 L/MM *SURFACE** ALL CONCAVE AND CONVEX
.... INDICATES PITCH OF LIMITING TRIBAR FOR A 220 LINE PER MILLIMETER PHOTO SYSTEM

Figure C3-2

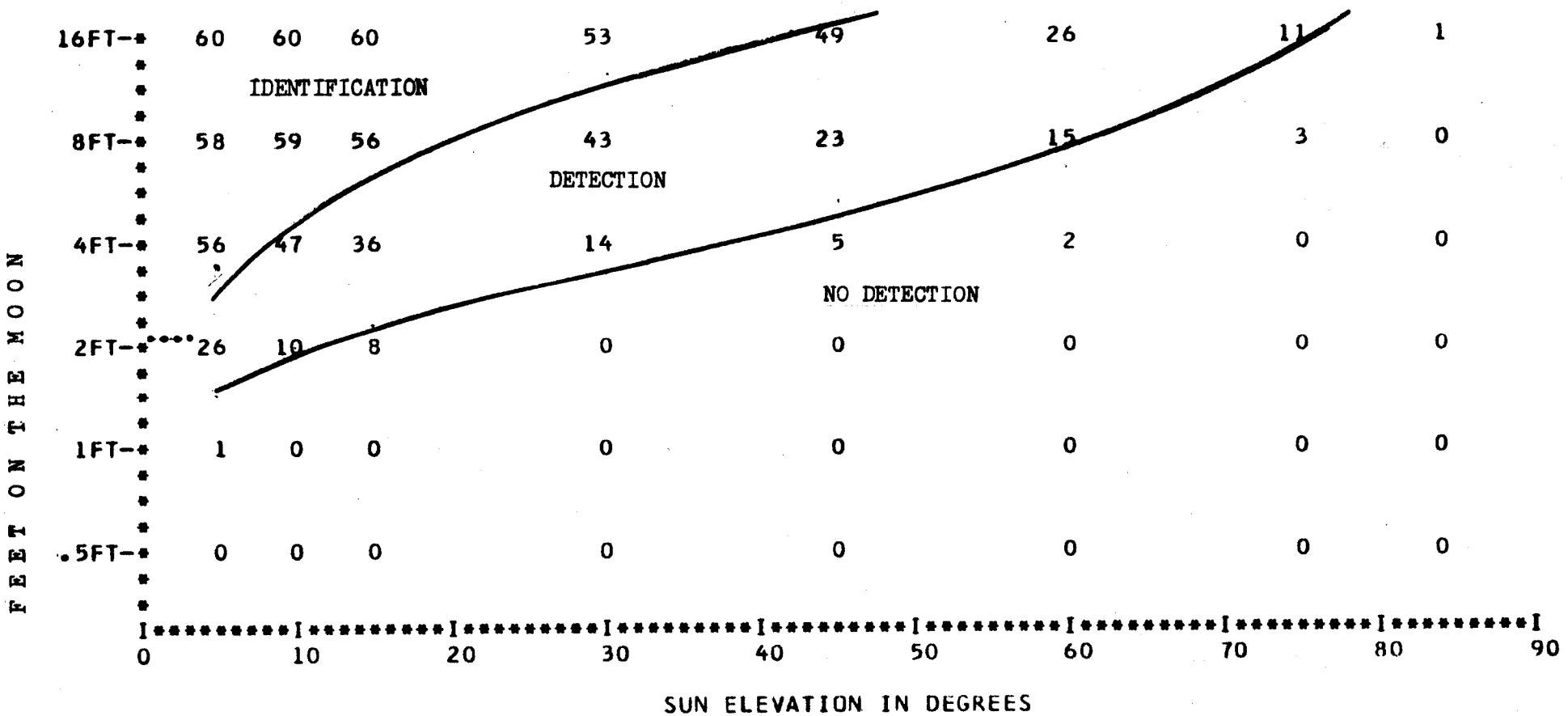

MATRIX NUMBER 38 READER RESPONSE FOR VERTICAL MONOSCOPIC PHOTOGRAPHY OF GEOMETRIC SHAPES

*PHOTOGRAPHY** VERTICAL MONOSCOPIC *SYSTEM** 92 L/MM *SURFACE** ALL CONCAVE AND CONVEX
.... INDICATES PITCH OF LIMITING TRIBAR FOR A 92 LINE PER MILLIMETER PHOTO SYSTEM

Figure C3-3

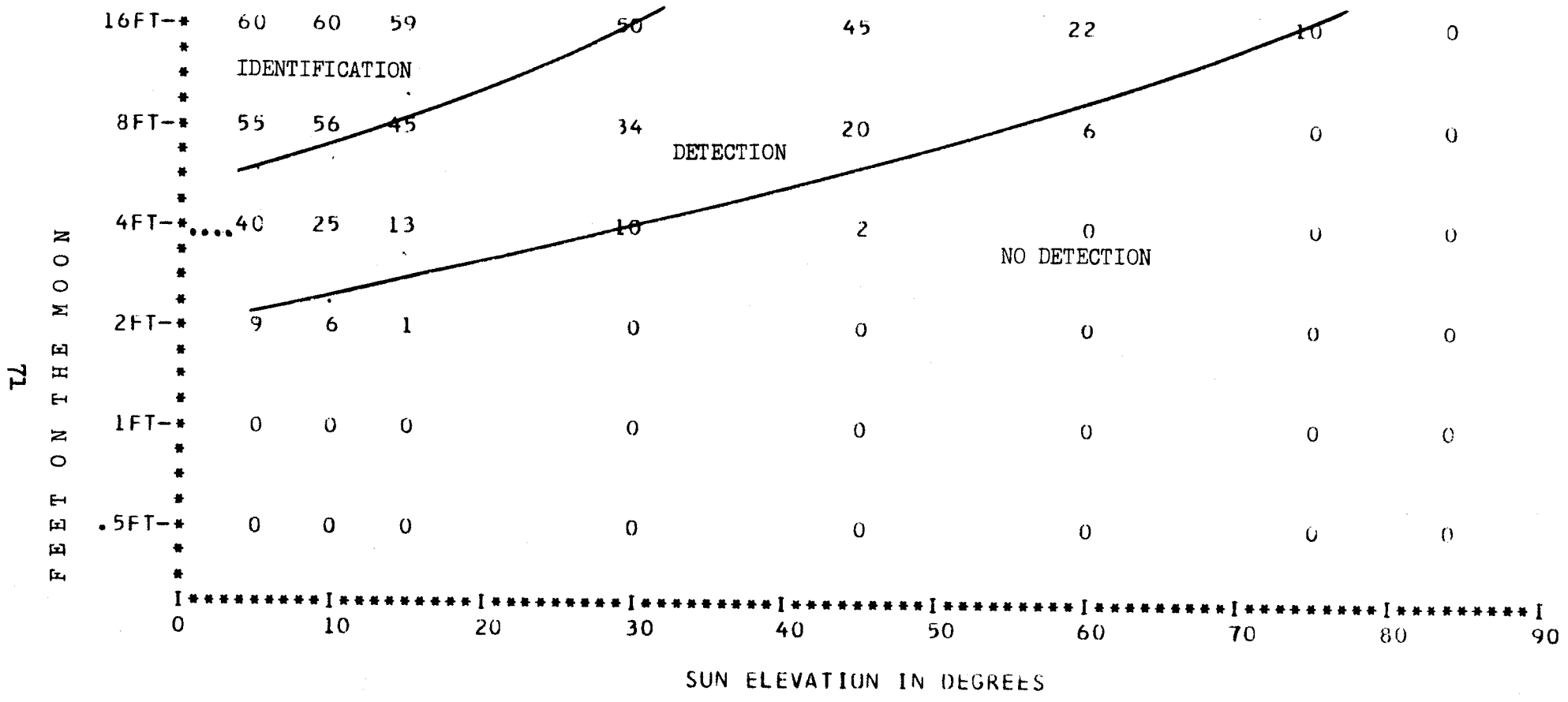

MATRIX NUMBER 39 READER RESPONSE FOR VERTICAL MONOSCOPIC PHOTOGRAPHY OF GEOMETRIC SHAPES

*PHOTOGRAPHY**VERTICAL MONOSCOPIC *SYSTEM** 53 L/MM *SURFACE** ALL CONCAVE AND CONVEX
.... INDICATES PITCH OF LIMITING TRIBAR FOR A 53 LINE PER MILLIMETER PHOTO SYSTEM

FIGURE C3-4

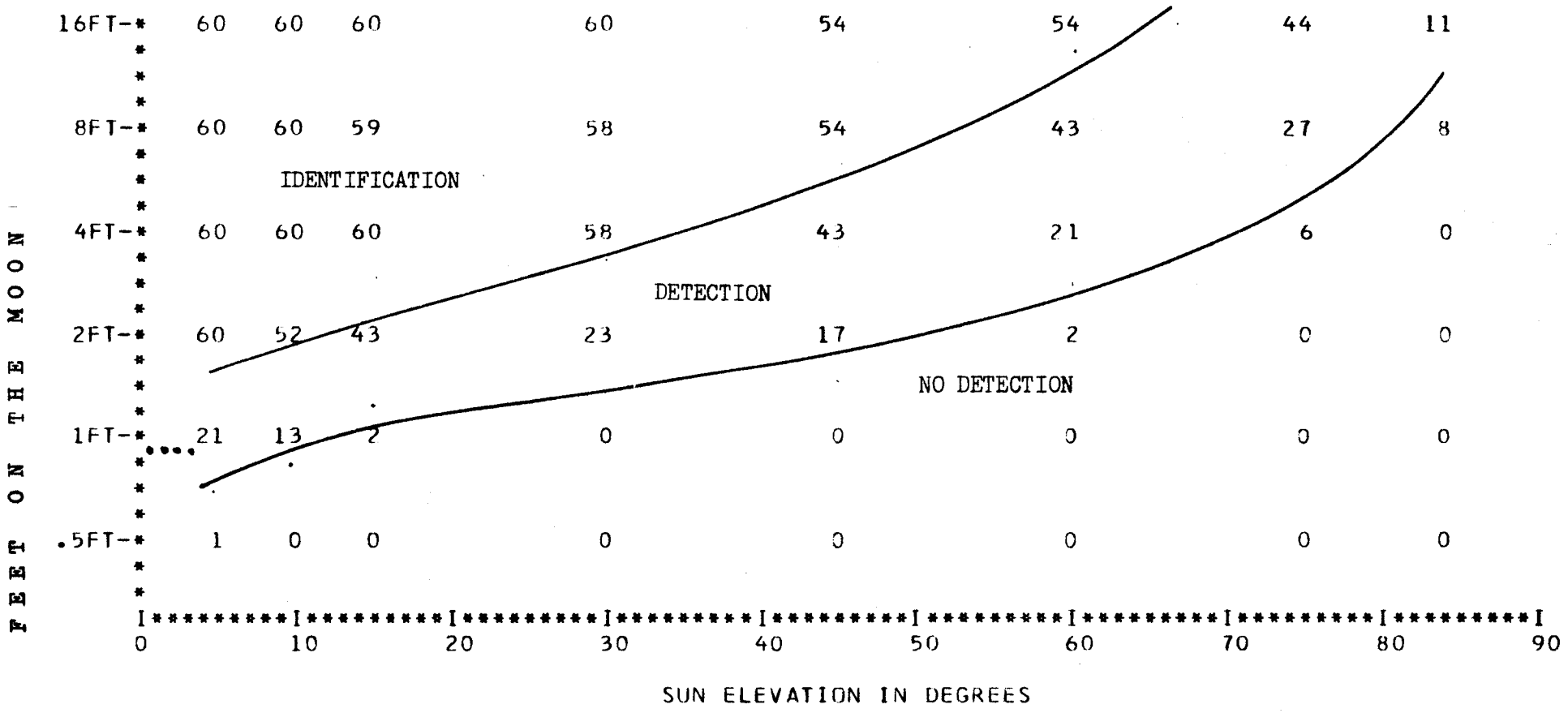

MATRIX NUMBER 100 READER RESPONSE FOR STEREO PHOTOGRAPHY OF GEOMETRIC SHAPES

*PHOTOGRAPHY**10 DEG STEREO HALF ANGLE *SYSTEM**220 L/MM *SURFACE** ALL CONCAVE AND CONVEX
.... INDICATES PITCH OF LIMITING TRIBAR FOR A 220 LINE PER MILLIMETER PHOTO SYSTEM

FIGURE C3-5

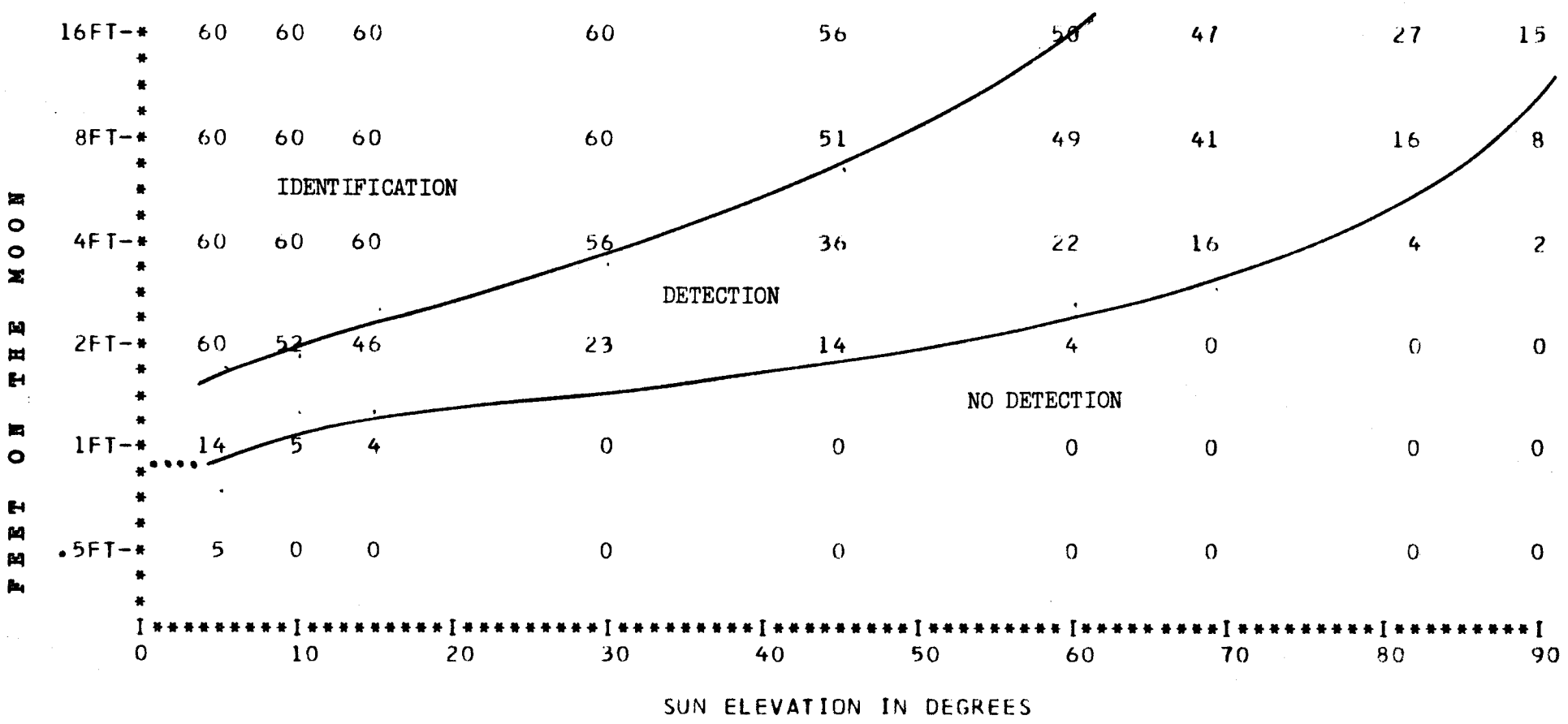

MATRIX NUMBER 101 READER RESPONSE FOR STEREO PHOTOGRAPHY OF GEOMETRIC SHAPES

*PHOTOGRAPHY**15 DEG STEREO HALF ANGLE *SYSTEM**220 L/MM *SURFACE** ALL CONCAVE AND CONVEX
.... INDICATES PITCH OF LIMITING TRIBAR FOR A 220 LINE PER MILLIMETER PHOTO SYSTEM

FIGURE C3-6

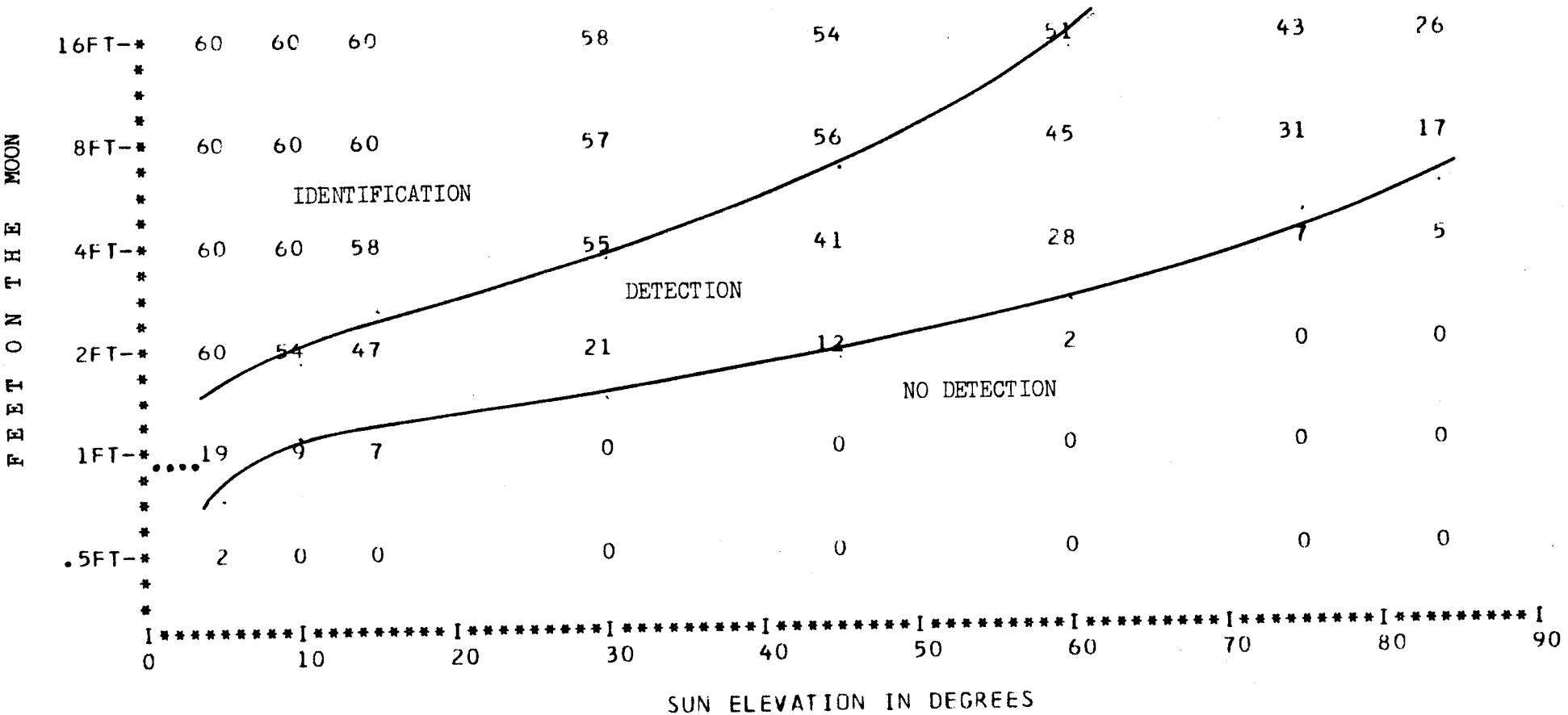

MATRIX NUMBER 102 READER RESPONSE FOR STEREO PHOTOGRAPHY OF GEOMETRIC SHAPES

*PHOTOGRAPHY**20 DEG STEREO HALF ANGLE *SYSTEM**220 L/MM *SURFACE** ALL CONCAVE AND CONVEX
.... INDICATES PITCH OF LIMITING TRIBAR FOR A 220 LINE PER MILLIMETER PHOTO SYSTEM

Figure C3-7

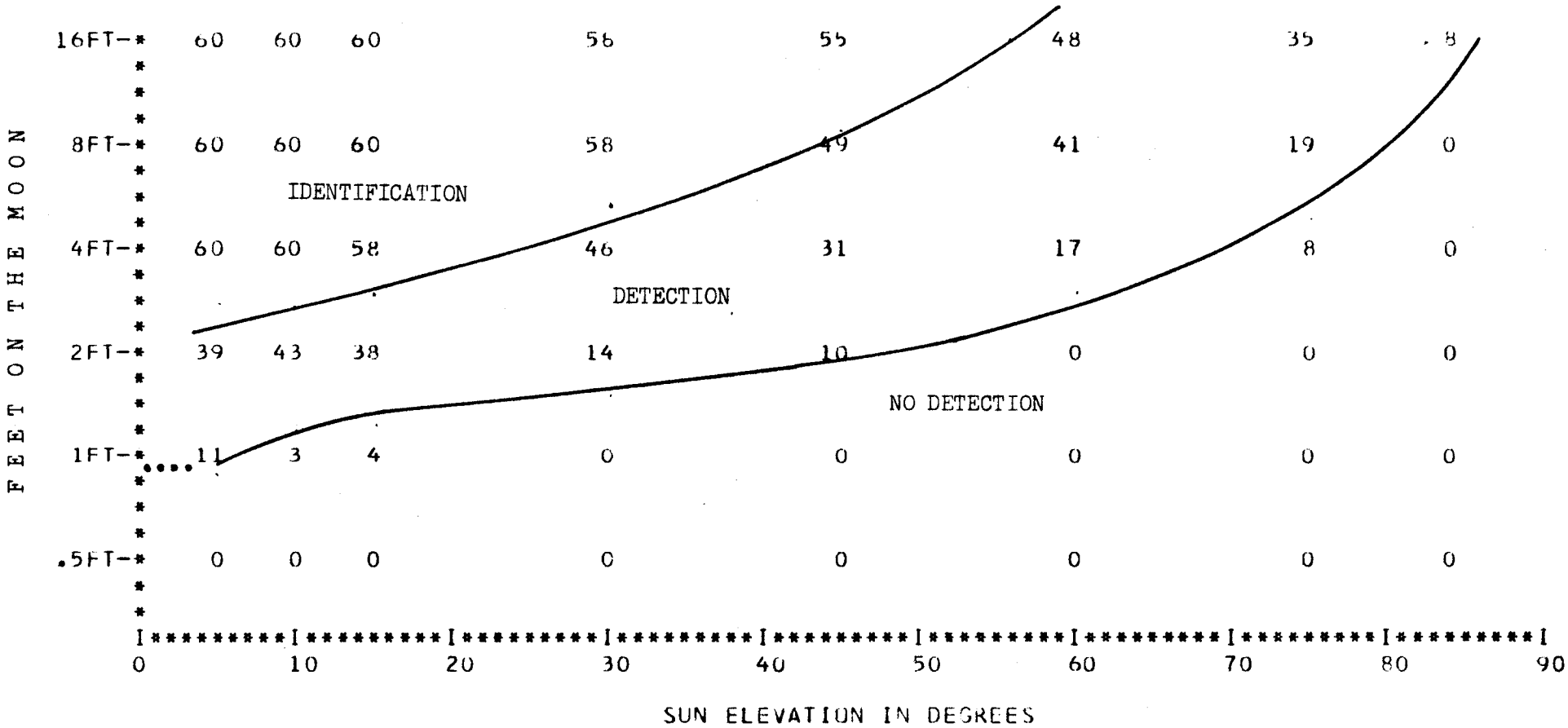

MATRIX NUMBER 141 READER RESPONSE FOR OBLIQUE MONOSCOPIC PHOTOGRAPHY OF GEOMETRIC SHAPES

*PHOTOGRAPHY**45 DEG OBLIQUE MONOSCOPIC *SYSTEM**220 L/MM *SURFACE** ALL CONCAVE AND CONVEX
.... INDICATES PITCH OF LIMITING TRIBAR FOR A 220 LINE PER MILLIMETER PHOTO SYSTEM

Figure C3-8

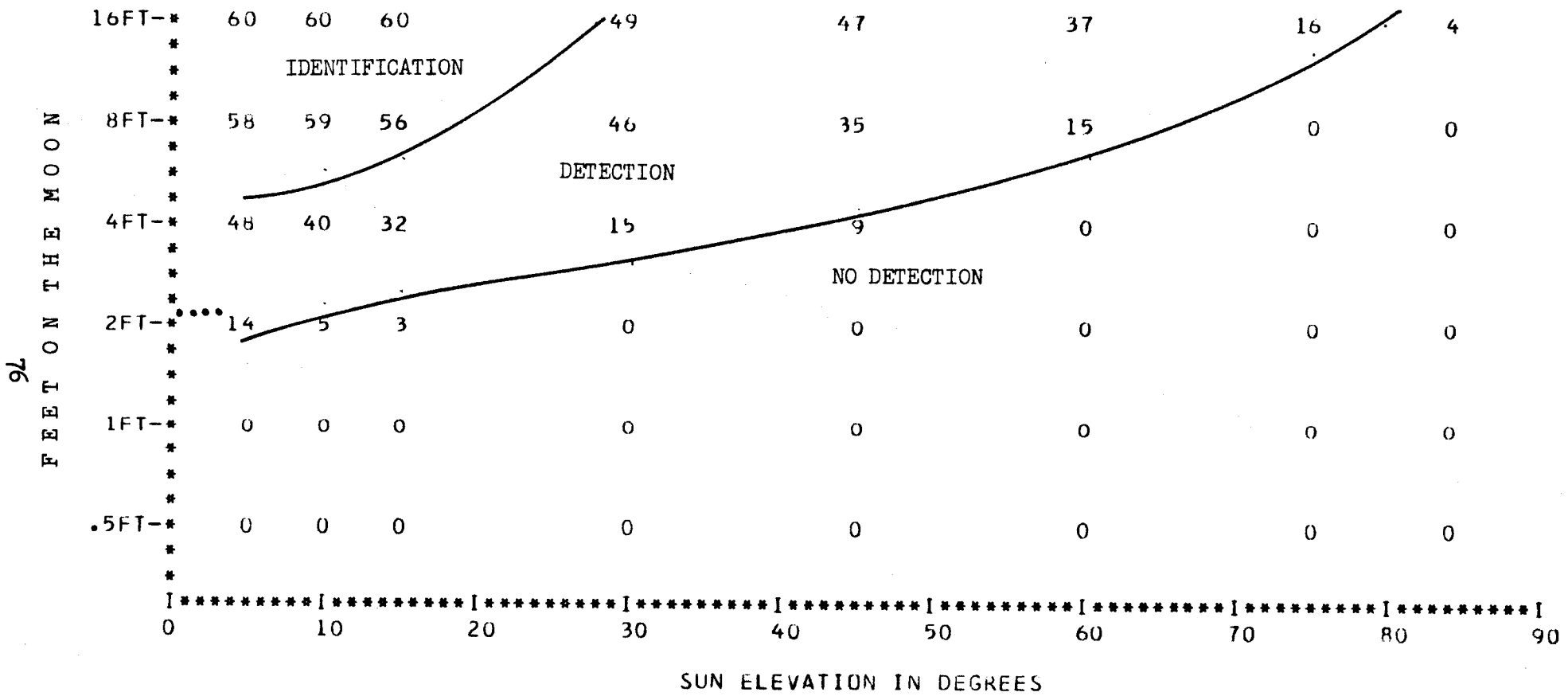

MATRIX NUMBER 142 READER RESPONSE FOR OBLIQUE MONOSCOPIC PHOTOGRAPHY OF GEOMETRIC SHAPES

*PHOTOGRAPHY**45 DEG OBLIQUE MONOSCOPIC *SYSTEM** 92 L/MM *SURFACE** ALL CONCAVE AND CONVEX
.... INDICATES PITCH OF LIMITING TRIBAR FOR A 92 LINE PER MILLIMETER PHOTO SYSTEM

Figure C3-9

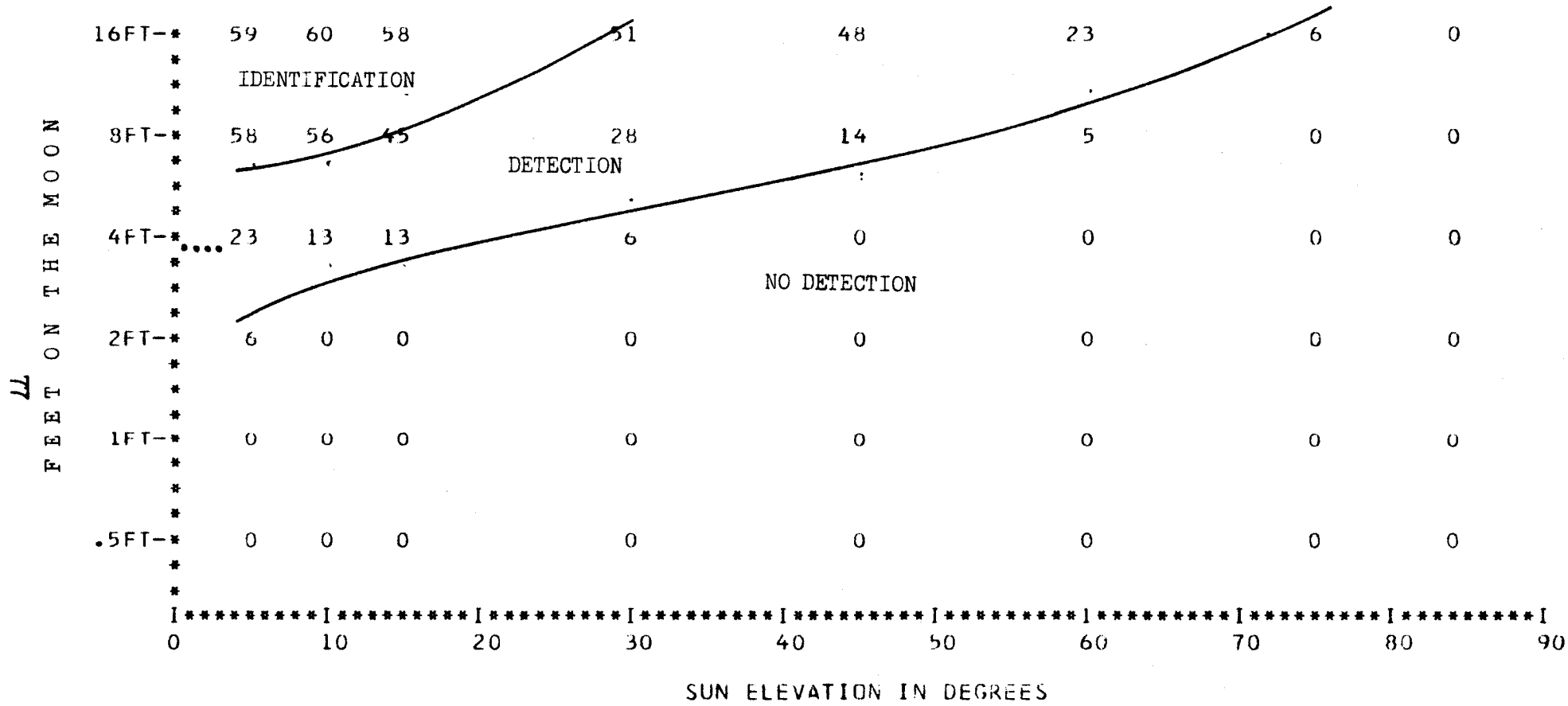

MATRIX NUMBER 143 READER RESPONSE FOR OBLIQUE MONOSCOPIC PHOTOGRAPHY OF GEOMETRIC SHAPES

*PHOTOGRAPHY**45 DEG OBLIQUE MONOSCOPIC *SYSTEM** 53 L/MM *SURFACE** ALL CONCAVE AND CONVEX
.... INDICATES PITCH OF LIMITING TRIBAR FOR A 53 LINE PER MILLIMETER PHOTO SYSTEM

Figure C3-10

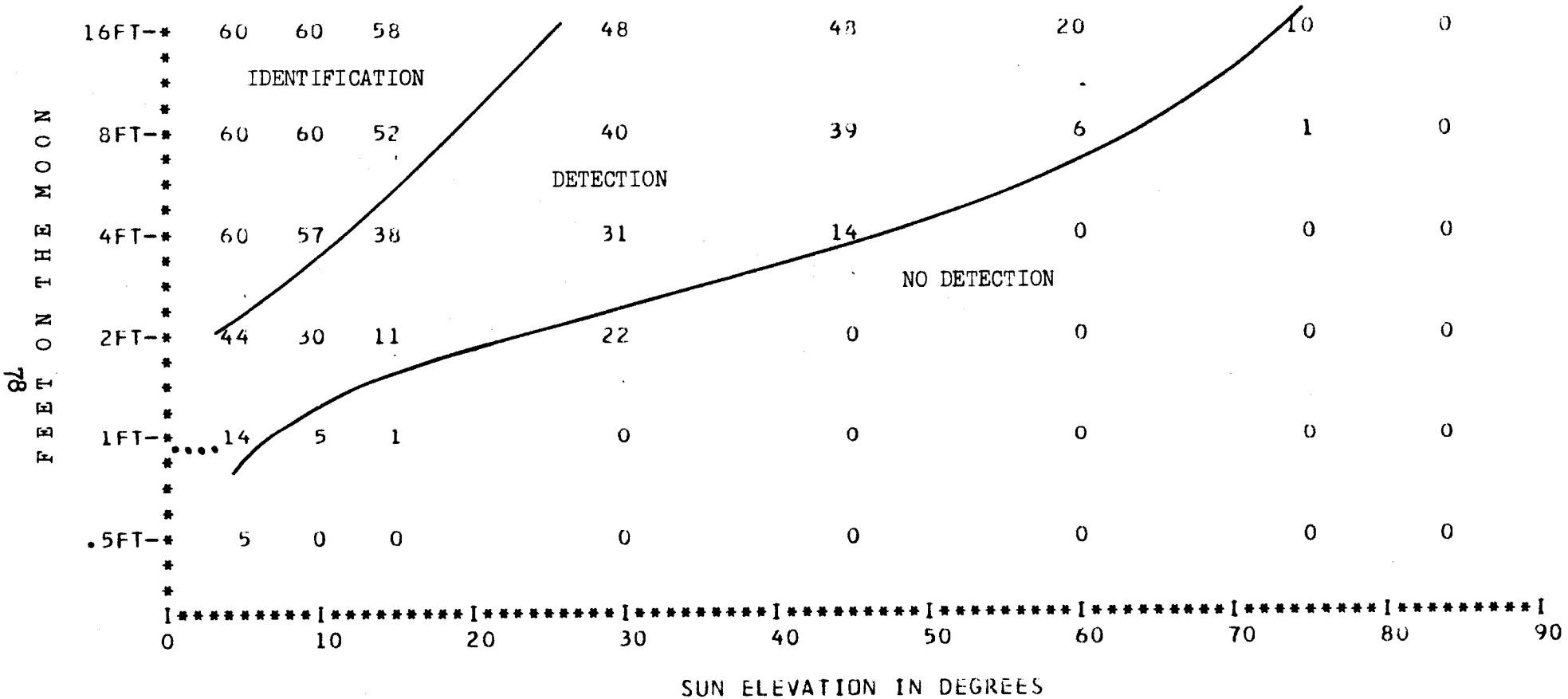

MATRIX NUMBER 168 READER RESPONSE FOR VERTICAL MONOSCOPIC PHOTOGRAPHY OF GEOMETRIC SHAPES, UNDEREXPOSED TWO STOPS

*PHOTOGRAPHY**VERTICAL MONOSCOPIC *SYSTEM**220 L/MM *SURFACE** ALL CONCAVE AND CONVEX
.... INDICATES PITCH OF LIMITING TRIBAR FOR A 220 LINE PER MILLIMETER PHOTO SYSTEM

Figure C3-11

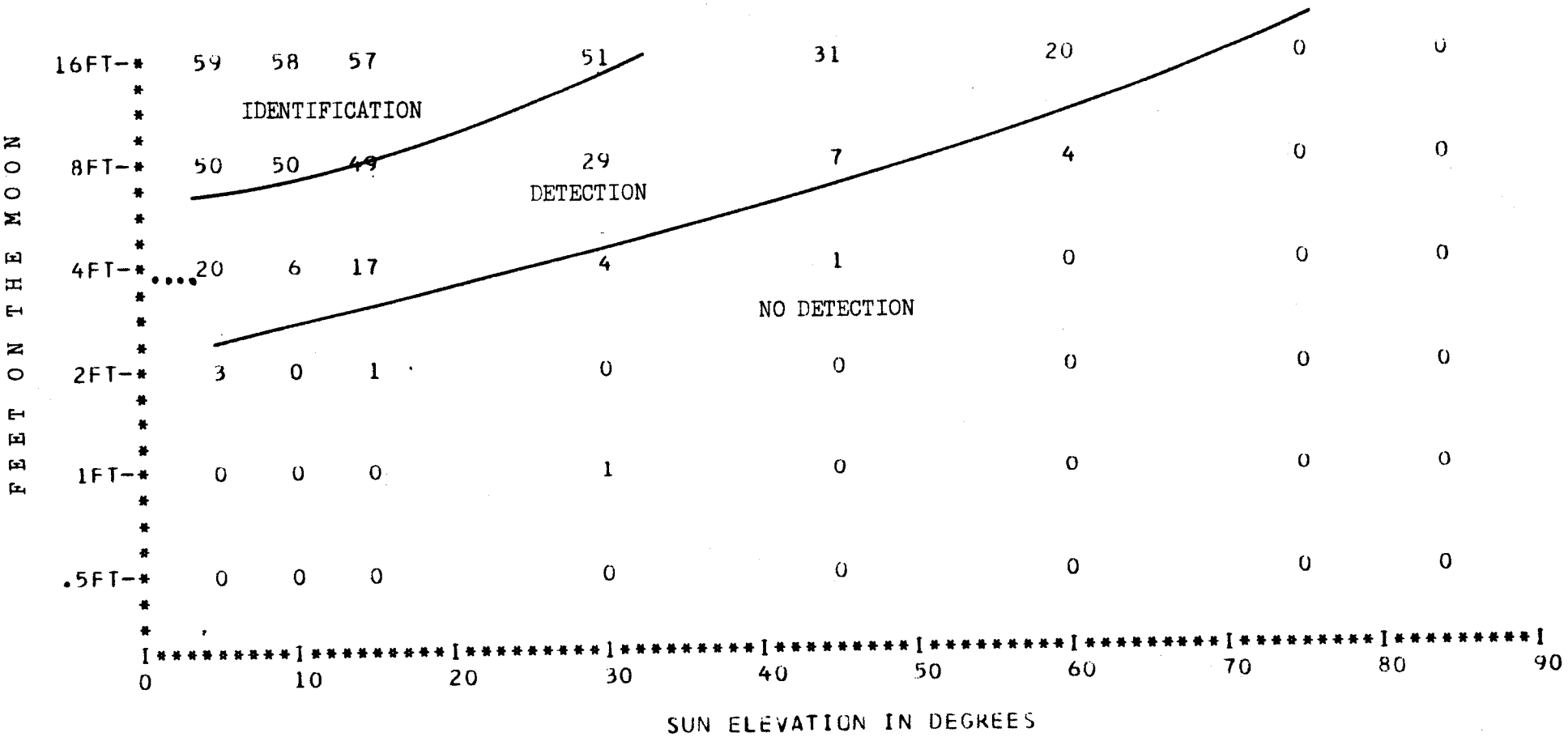

MATRIX NUMBER 169 READER RESPUNSE FOR VERTICAL MONOSCOPIC PHOTOGRAPHY OF GEOMETRIC SHAPES, UNDEREXPOSED TWO STOPS

*PHOTOGRAPHY** VERTICAL MONOSCOPIC *SYSTEM** 53 L/MM *SURFACE** ALL CONCAVE AND CONVEX
.... INDICATES PITCH OF LIMITING TRIBAR FOR A 53 LINE PER MILLIMETER PHOTO SYSTEM

Figure C3-12

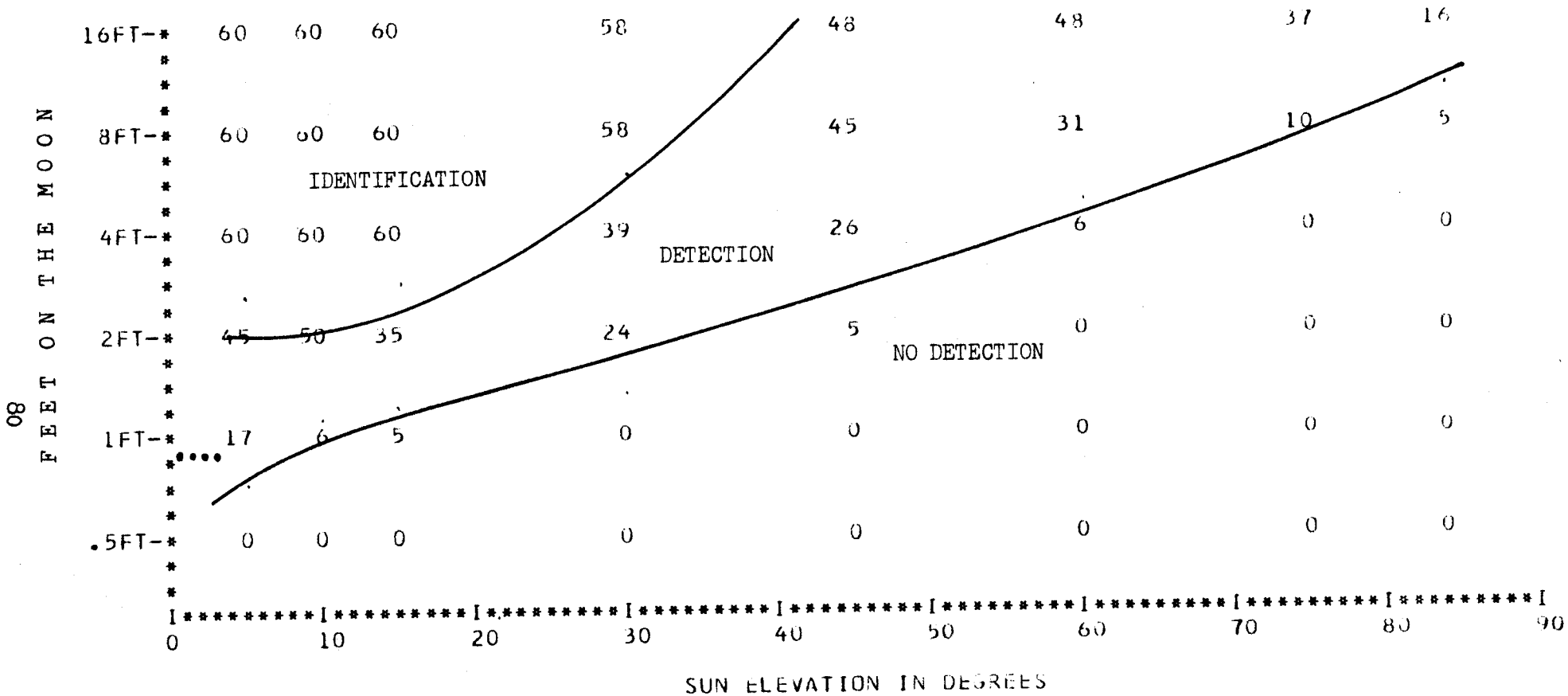

MATRIX NUMBER 194 READER RESPONSE FOR VERTICAL MONOSCOPIC PHOTOGRAPHY OF GEOMETRIC SHAPES, OVEREXPOSED TWO STOPS

*PHOTOGRAPHY**VERTICAL MONOSCOPIC *SYSTEM**220 L/MM *SURFACE** ALL CONCAVE AND CONVEX
.... INDICATES PITCH OF LIMITING TRIBAR FOR A 220 LINE PER MILLIMETER PHOTO SYSTEM

Figure C3-13

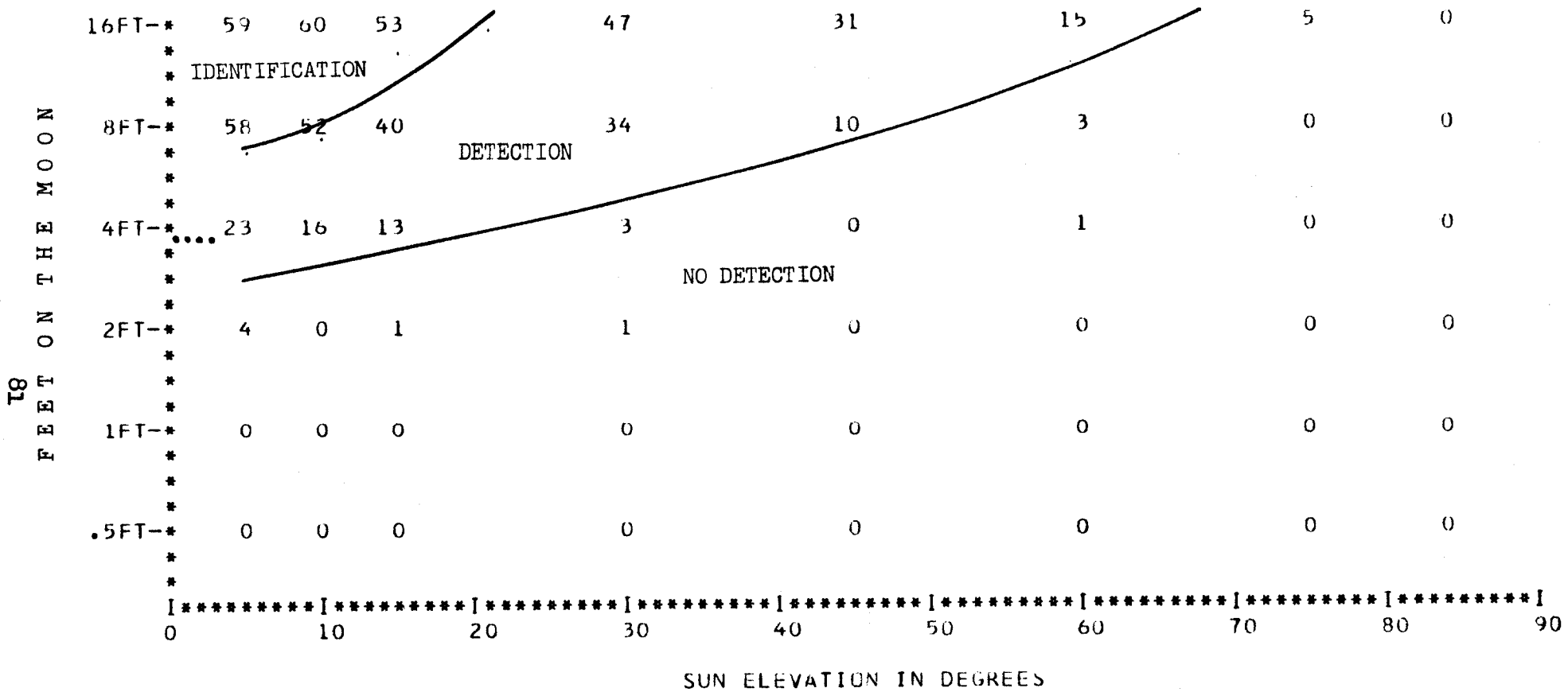

MATRIX NUMBER 195 READER RESPUNSE FOR VERTICAL MONOSCOPIC PHOTOGRAPHY OF GEOMETRIC SHAPES, OVEREXPOSED TWO STOPS

*PHOTOGRAPHY**VERTICAL MONOSCOPIC *SYSTEM** 53 L/MM *SURFACE** ALL CONCAVE AND CONVEX
.... INDICATES PITCH OF LIMITING TRIBAR FOR A 53 LINE PER MILLIMETER PHOTO SYSTEM

Figure C3-14

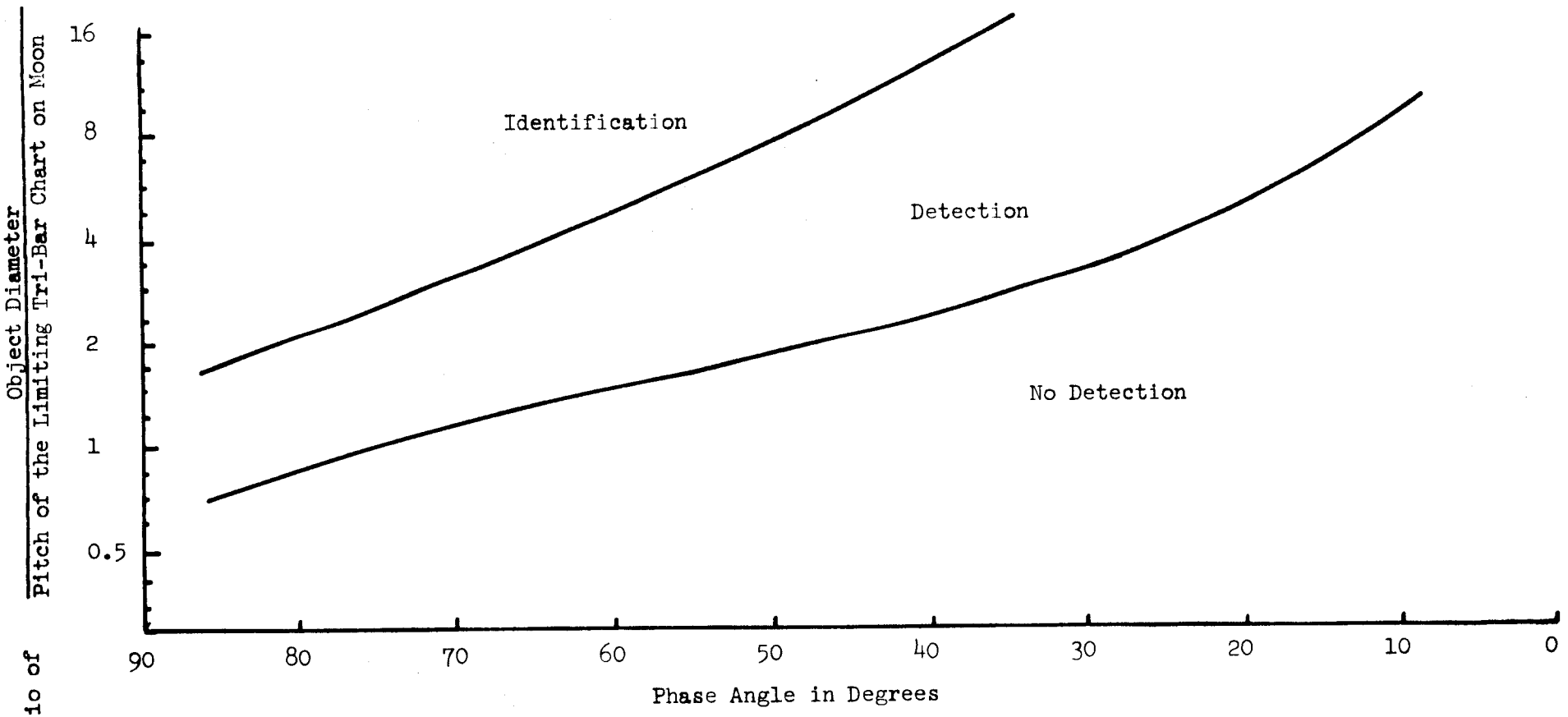

Relationship of phase angle to the pitch of the limiting tri-bar chart for identification and detection of geometric shapes using monoscopic vertical photography. Data obained from Figure C1-2, C1-3 and C1-4. Note the ordinate is a log scale. The abscissa is the phase angle between camera and sun measured at the lunar surface.

Figure C3-15

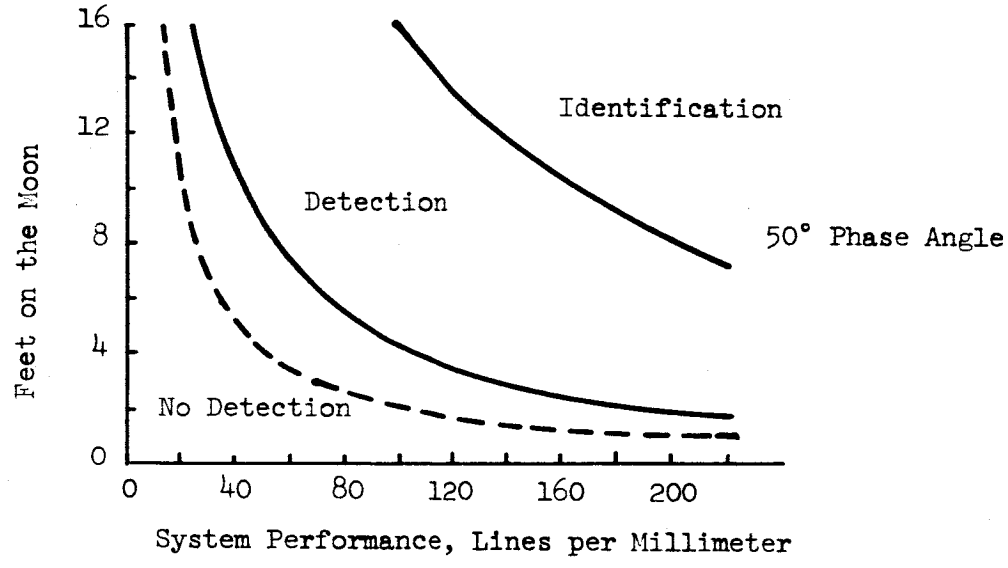

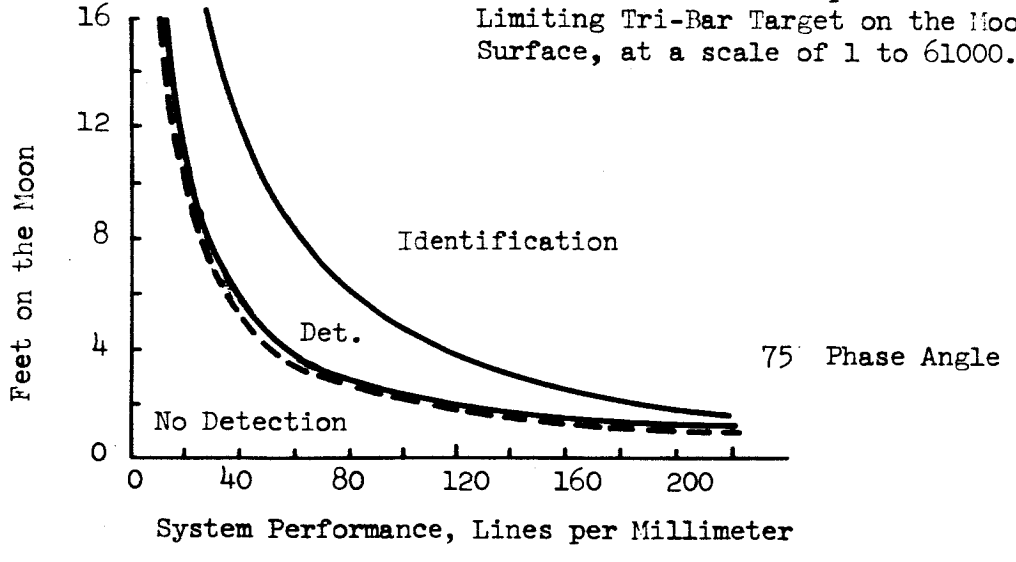

Resolution vrs. Lunar Distance for Phase Angles of 50° and 70° at Photographic Scale of 1 to 61000. Data Obtained from Figure C3-15.

Figure C3-16

The ordinate of feet on the moon is based upon a scale of 1 to 61,000 (1 foot on the moon = 1/200mm on the film). Note, however, that Figure C3-15 is not limited to this scale alone, but could be applied to any scale providing the pitch of the limiting tri-bar of the system is known at the surface of the moon.

In the example above the pitch of the limiting tri-bar at 220 lines/mm is .91 feet on the lunar surface, (assuming 1 to 61,000 scale) at a sun elevation of 15° the phase angle is 90° - 15° = 75°, the intersection of 75° and the line between detection and no detection is 1 for the limiting tri-bar. The limiting tri-bar from above is .91 feet so the geometric shape that should be just detectable at the lunar surface would be .91 feet. The intersection of 75° phase angle with the line separating identification and detection shows a value of about 2.5 x limiting tri-bar or 2.5 x .91 feet = 2.3 feet. Therefore at 15° sun elevation with vertical monoscopic photography a reader should be able to identify as either concave or convex a geometric shape 2.3 feet in diameter if the photographic scale is such that the limiting, high contrast tri-bar has a pitch of .91 feet on the moon. Geometric shapes between 2.3 feet and .91 feet will be detected under the same condition and shapes smaller than .91 feet will not be detected.

b. Stereo Photography of the Geometric Shapes

The parameters that effect photographic stereo acuity or the ability to detect changes in elevations are: photographic scale, system resolution, and stereo angle. In this study the scale was 1 to 61,000 and the system resolution was 220 lines/mm, but the stereo angle was either ± 10°, ± 15°, or ± 20°. The photographs are taken at the indicated stereo angles from the surface vertical and in the equatorial plane. As the sun is in the equatorial plane, the angles between the camera axis and the sun (phase angles) for a 60° sun elevation and stereo angles of ± 10° were 40° and 20°. Since the lunar photometric function is highly dependent upon the phase angle, pictures taken at the smaller phase angle have the least

contrast. Figure C3-5, C3-6 and C3-7 are the matrices of the reader response to the ± 10°, ± 15° and ± 20° stereoscopic photography respectively. In the Table C3-2, it can be seen that detail rendition improves with greater stereo angle, at least up to ±20°, and that most of this improvement is caused by increased scene contrast from the larger angle between the sun and camera axis. All of this evaluation was made from the negatives.

The readers failed to see any stereo except in the low sun elevations, probably because of the very low contrast of the lunar scenes at the high sun elevations. In this experiment as the sun elevation became smaller the contrast increased until at a sun elevation of 30° or 15° the readers were able to see a stereo image.

Following the evaluation of these stereo pairs, it was realized that the improvement in detection and identification was primarily because of the increased angle between the sun and camera axis (phase angle). In fact, the stereo reader response curves for ± 15° stereo can be nearly superimposed on the mono photography with a 15° displacement of the sun elevation axis. Apparently, the detail in the low contrast scene adds very little to the detection or identification of the lunar features under these experimental conditions.

Two suggestions are made to improve object detection and identification in lunar stereo photography:

1. The stereo photographs should be made out of the planes of the sun and the lunar equator. This has been done for KIM 6-65 and is evaluated in the next section.

2. Positives should be made of the scenes for this type of evaluation since it may be difficult for readers to see stereo in negatives. Positives have been made of the stereo photography for KIM 6-65, where the camera is out of the sun and lunar equator plane. This work is evaluated in the next section.

Stereoscopic Evaluation

Figure	Matrix	Geometric Forms	Photo System Lines/mm	Stereo Angle	Best Linear Detection at Max. Sun Elevation	Detection	Identification
	90	All concave	220	±10°	16' at 84°	A	A
	91	All convex	220	±10°	16' at 84°	A	A
	92	All concave	220	±15°	8' at 90°	B	B
	93	All convex	220	±15°	16' at 90°	B	B
	94	All concave	220	±20°	8' at 90°	B	B
	95	All convex	220	±20°	8' at 90°	B	B
C3-5	100	All forms	220	±10°	16' at 84°	A	A
C3-6	101	All forms	220	±15°	10' at 90°	B	B
C3-7	102	All forms	220	±20°	8' at 90°	B	B

Matrix #90 refers to the computer plot of reader response for all concave surfaces with the 220 lines/mm photo system at ±10° stereo angle from which curves are drawn separating the areas of no detection, detection, and identification. The parameters for the other selected matrices are given in the table above.

A = The curve made from the matrix is very close to the reader response curve made from the mono photography, except at the very high sun angles where mono photography cannot detect any objects at 90° sun elevation.

B = The curve made from the matrix is close to the mono photography except that the readers were able to identify (or detect) slightly smaller objects at any given sun elevation.

Table No. C3-2

c. Oblique Monoscopic Photography of Geometric Shapes

The oblique photography was made by tilting the model back 45° and keeping the camera and sun in the same plane. The phase angle between the camera and the sun in this oblique photography will be identical to the phase angle of the vertical monoscopic photography. A study of the Reader Response curves C3-8, C3-9 and C3-10 will show that the response to this oblique photography is very nearly the same as that to the vertical monoscopic photography; therefore, the curves in Figure C3-15 adequately describe the reader response to all of these photo systems.

This oblique photography keeps the camera, model and sun in the ecliptic plane and is like a surface at the lunar equator with an average slope of 45°. Since the reader response is the same for this oblique and the vertical monoscopic photography it is implied that the response to lunar geometric shapes is independent of the average slope of the lunar surface.

This experiment helps to confirm the singular importance of the phase angle in lunar photography.

d. Under and Over Exposure (± 2 Stops)

Two photo systems, the 220 lines/mm system utilizing SO-243 film and the 53 lines/mm system utilizing Kodak Tri-X film, were investigated to determine the effect of under and over exposure on lunar photography. The nominal exposure for each of the photo systems placed the background at a density of .8 which is satisfactory for low contrast lunar scenes and places the average exposure near the point of maximum resolution for each film. Referring to the characteristic curves for these films (Fig. B6-3), the densities and the gammas can be obtained for the background when the pictures are given 2 stops under and 2 stops over exposure. This information is tabulated in Table C3-3.

Density - Gamma Relationship for Two Photo Systems

Exposure Level	Photo System Lines/mm	Film	Density	Gamma	Fig. No.	Reader Response
2 stops under exposed	220	SO-243	.3	.31	C3-11	Degraded from C3-2
Nominal exposure	220	SO-243	.8	1.8	C3-2	
2 stops over exposed	220	SO-243	1.9	1.8	C3-13	Similar to C3-2
2 stops under exposed	53	Tri-X Pan	.4	.55	C3-12	Similar to C3-4
Nominal exposure	53	Tri-X Pan	.8	.6	C3-4	
2 stops over exposure	53	Tri-X Pan	1.16	.6	C3-14	Similar to C3-4

Table No. C3-3

Under Exposure

Referring again to the characteristic curve for the Tri-X Pan film, a two times under exposure of .6 log E (2 Stops) reduces the density of the background from .8 to .4 changing the gamma very little. Comparison of Fig. C3-12 with C3-4 shows that the reader response is nearly the same at this exposure level as the response at the nominal exposure levels. The luminance range of the lunar scene is small enough so that little information is lost below the toe of the characteristic curve. The density of this scene is everywhere about .4 less than for the nominal exposure, with the gamma nearly unchanged.

Since the SO-243 film is a material of higher contrast, an under exposure of .6 log E brings the background density down from .8 to .3 which is only .05 above the minimum density. Any portion of the scene with luminance less than the background will be lost. With this amount of under exposure the gamma has been reduced from 1.8 to .3. A comparison of Fig. C3-11 (the reader response for an under exposed, 220 lines/mm system) with Figure C3-2 (the nominally exposed, 220 lines/mm system) shows how much the under exposure has degraded the system. With this amount of under exposure at 5° sun elevation a geometric shape must be 2 times larger to be identified and at 25° sun elevation the shape must be at least 4 times larger before it can be identified. Detection is nearly the same at low sun elevation (5°) but a geometric shape must become 3 times larger at 60° sun elevation before it can be detected. To summarize, an under exposure of 2 stops using SO-243 film will seriously degrade the photographic record of lunar scenes.

Over Exposure

Using Tri-X film the background density is increased from .8 to 1.16 with 2 stops over exposure. The gamma is unchanged. The density of the image is everywhere increased by .36. Unless a low image density is required, the quality of the image has been degraded very little from

the nominal exposure (compare Fig. C3-14 with Fig. C3-4).

If the image is viewed directly, a slightly brighter light source on the microscope will compensate for the darker image.

In general however, there is some loss in resolution in areas where the density is greater than 1.5. If the image is to be read-out in an electronic system, increasing noise may place limitations upon maximum density that can be read.

With 2 stops over exposure the background density of the SO-243 film is changed from .8 to 1.9 but the gamma remains unchanged. Except for a small loss in resolution, the additional 1.1 density will not be detrimental provided there is enough light in the microscope to bring the image to a brightness comfortable for viewing. A comparison of Fig. C3-2 and C3-13 shows very little difference in reader response between the nominal and over exposed films. Apparently, the scene luminance range is low enough so that little is lost in over exposure.

Summary

It will be noted that the Tri-X film is a moderate gamma film designed for aerial reconnaissance where film latitude is required in order to cover a wide range of scene luminances. The image is printed on either paper or a transparent material where the contrast of the scene can be increased as desired. Consequently, small errors in the exposure of a lunar scene will not be serious.

The SO-243 however is a high contrast film designed for aerial reconnaissance of scenes with short luminance scales where the exposure will be properly made. It has a better capability for separating small differences in luminance than the Tri-X film but requires better exposure control. A small error in exposure (especially under exposure) of a lunar scene will be more serious with this high contrast film.

e. Reader Repeatability

To check the repeatability of the readers' responses, random selections of 10 negatives previously read by each reader were taken from the 48 vertical, monoscopic photographs for a second reading. Each reader re-read his photographs and gave responses which were ranked and compared with his previous responses in the statistical Sign Test*. It was found that there is no difference in the two sets of readings by each reader at the 95% significance level.

In addition to the Sign Test, Figure C3-17 was made to graphically present the data for the two sets of ranked responses from each reader. Points lying on the 45° line represent no change in response for the two readings. The graphs show that the readers were very consistent in reading the photographs.

4. Conclusions From the Geometric Shapes

1. Figure C3-15 shows an important relationship between phase angle and the detection and identification of geometric shapes in terms of the pitch of the limiting high contrast tri-bar. This figure combines in one curve the results from the reader responses to photography of the geometric shapes in three modes: vertical mono, stereo in the ecliptic plane, and oblique. Given the scale, the resolution capability of a photo system and the phase angle, this curve shows the sizes of geometric shapes that can be detected and identified on the lunar surface.

2. The phase angle, i.e. the angle between the camera and the sun measured at the lunar surface has a greater influence on detection and identification of geometric shapes than the sun elevation angle for nearly vertical photography. However the exposure required for a phase angle near 85° is about 32 times the exposure required at small phase angles (increased image smear).

* Ref: Introduction to Statistical Analysis
By W. J. Dixon & S. J. Massey Jr.

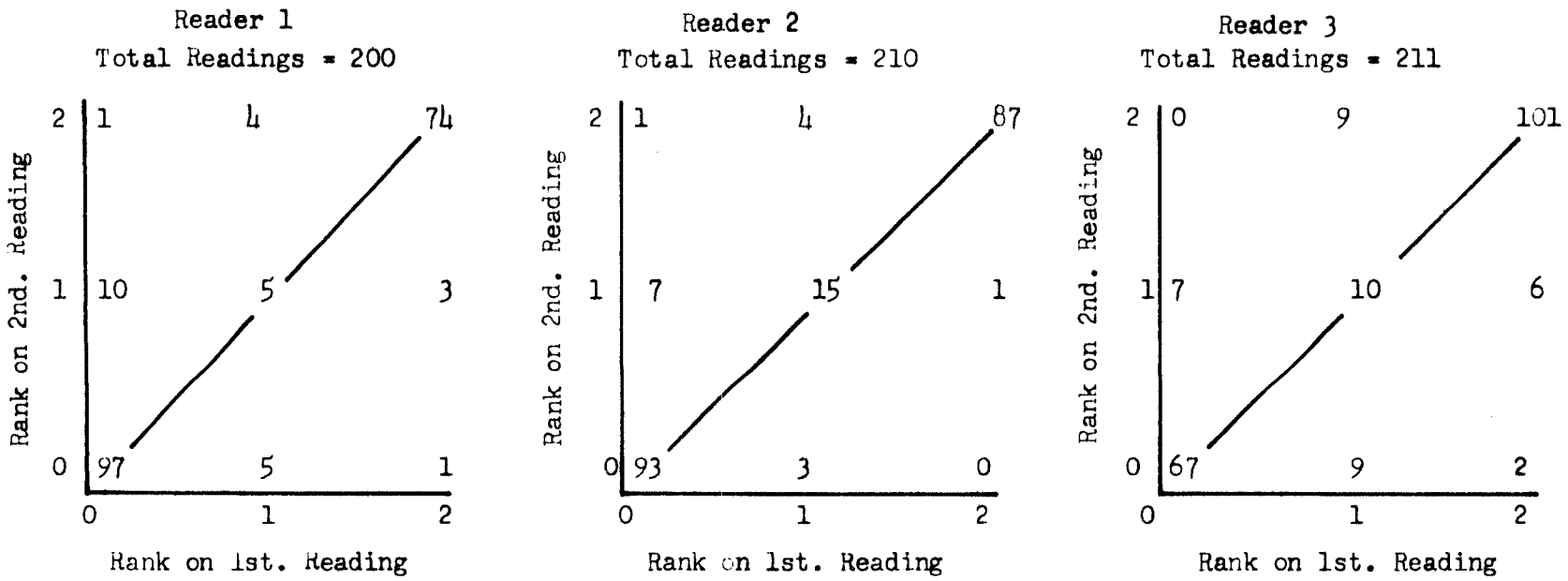

Plots of Ranked Responses on two Separate Readings (Rank of response on second reading vs Rank of Response of 1st. reading) for the three readers.

Figure C3-17

3. It was found that oblique photography does not influence the detection and identification of geometric shapes.

4. Contrast of the geometric shapes is approximately proportional to the slopes of their surface, i.e. the ratio of the diameter to the height.

5. The reader response to stereo photography in the ecliptic plane can be compared to vertical photography if the maximum phase angle of the stereo is used for the comparison. Apparently, the low contrast image of the stereo pair offers very little improvement in the detection or identification of geometric shapes with dimensions near the limiting high contrast tri-bar.

6. Statistical Tests indicate that the readers were consistent in their readings.

D. KODAK LUNAR MODEL 6-65 (KLM6-65)

1. Photographic Schedule and Records

The same data sheet was used for recording the photography of the KLM6-65 (Figure C1-1) as was used to record the geometric shapes. The schedule of photography was similar except that the oblique photography was made with the camera out of the ecliptic plane, and the stereo photography was made with the camera base line at right angles to the ecliptic plane.

A data sheet was made to record the reader responses from the several studies. An example of this sheet is shown completely filled out in Figure D3-1

2. Reader Instruction

The following paragraphs were prepared and given to the readers in order to provide a uniform basis on which the readers may judge the pictures.

INSTRUCTIONS TO READERS

The Kodak Lunar Model 6-65 (KLM6-65) is based upon our present knowledge of the moon including features which were observed in the Ranger photographs. This model was dusted to provide reflectances that closely match the lunar photometric function and was illuminated with a simulated solar source at a number of sun elevations during photography with three representative photo systems.

The negatives from these photo systems are to be evaluated in order to determine the parameters that will best show the hazards in landing areas on the lunar surface. The model represent a lunar area 160 ft. on a side with the largest crater 36 feet in diameter. The reader is requested to view the negatives at 100 power but he may, if he wishes, change the magnification of the microscope if by so doing it will help to bring out any of the details or help to integrate the grain structure of the film. An out of

focus image in the microscope may also assist the reader in this evaluation and is to be encouraged if it will help with this evaluation.

To bridge the gap between previous work done using geometric shapes and KLM 6-65, a number of geometric shapes have been included in this model as follows:

4-foot-diameter, 26° slope, conical convex surface

8-foot-diameter, 7° slope conical concave surface

8-foot-diameter, 8:1, spherical concave surface

8-foot-diameter, 7° slope, conical convex surface

In addition to these geometric shapes, the following lunar features have been included: boulders, fault line, crater chain, and a shallow ditch.

The order in which the photographs will be presented for evaluation is as follows:

Table D2-1 Order of Presentation

Order	Sun Elevation (degrees)	Resolution of Photo System (l/mm)	Order	Sun Elevation (degrees)	Resolution of Photo System (l/mm)
1	84	53	13	30	53
2	84	92	14	30	92
3	84	220	15	30	220
4	75	53	16	15	53
5	75	92	17	15	92
6	75	220	18	15	220
7	60	53	19	10	53
8	60	92	20	10	92
9	60	220	21	10	220
10	45	53	22	5	53
11	45	92	23	5	92
12	45	220	24	5	220

A data sheet and a set of blank maps have been prepared for this evaluation. The data sheet has one line for each photograph and many columns on that line. The first five to seven columns describe the photographs and list the order of evaluation; the remainder of the columns are for your response. The columns are listed below with a description of the reason for each.

1. Photo system - This will be either 53 lines/mm, 92 lines/mm, or 220 lines/mm and describes the resolution of the photo system that was used to take this photograph.

2. Pitch in feet of the limiting tri-bar chart projected on the lunar surface.

3. Sun Elevation - Angle between the plane of the model and the simulated solar source.

3a. Phase angle - Angle between the camera and the sun measured at the lunar surface.

4. Order of Evaluation - Since the reader has a good memory, it has been decided to present the photographs in an order that will start with the least detail in the scene and progress to the photographs with the most detail. In this way the reader will discover new features as the sun elevation changes, providing a good record of detail vs. sun elevation.

5. Negative Numbers - Each of the negatives has been numbered; this column provides a place to record the number. 5a. Record the left eye negative number of a stereo pair. 5b. Record the right eye negative number of a stereo pair.

6. Cone, convex, 4 feet in diameter, 26° slope - Record when this shape can be identified.

7. Cone, convex 8 feet in diameter, 7° slope - Record when this shape can be identified.

8. Cone, concave 8 feet in diameter, 7° slope - Record when this shape can be identified.

9. Spherical concave surface, 8:1 diameter to depth - Record when identified.

10. Shadow/Diameter ratio - Record this ratio for the spherical surface in 9 above.

11. Size - Estimate for the smallest crater observed.

12. Albedo - a streak of light material has been placed on this model - Record in this column the degree of contrast or ease of finding this albedo change.

13. Albedo - a blob of lighter material - Record the ease of finding this albedo change.

14. Albedo - an area of darker material - Record ease of finding this albedo change.

15. Albedo - a second area of darker material - Record ease of finding.

16. Number of Boulders - Record the number of boulders or protrusions that can be observed in the scene.

17. Craters 10 feet in diameter on left side - Record the number of craters 8 to 12 feet in diameter that can be counted on the left half of KLM 6-65.

18. Fault - Record the ease of finding this fault line.

19. Crater chain - This is a small chain of 5 craters - Record when this chain is observable.

20. Landing area - At sun elevations 75, 45, 30, 15, and 5° select an area in which you think a LEM could be landed safely, mark this area on the blank map provided, or mark on the blank map the areas that the LEM should avoid. The Lunar Excursion Module (LEM) weighs 29,000 earth pounds

(approximately 5,000 moon pounds or about twice the weight of your car, but with the inertia of a 15 ton truck) and has 4 legs on a radius of about 14 feet with 3-foot-diameter pads. It is designed to land two men on the lunar surface and should land on a nearly level area.

21. Ditch - There is a long, narrow depression several feet below the normal elevation - Record in column 20 the ease with which this can be identified.

After you have read these instructions, the 1st negative will be given to you for evaluation.

End of Instructions to Readers

3. Reader Response Evaluation and Analysis

In the study of the geometric shapes the sun elevation was used as the independent variable. In the last section it was shown (Figure C3-15) that phase angle is the important parameter that controls the contrast of the lunar scene. Consequently, the discussion that follows will emphasize the phase angle rather than the sun elevation. This will reduce the number of curves required to present the results of the reader response for KIM6-65 and increase the understanding of the factors involved. It should be remembered that this study is limited to nearly vertical photography with the camera never more than 45° from the Nadir. Also, except in the motion picture, the camera axis is never below the sun elevation, a condition where no shadows would be visible.

a. Monoscopic Photography in the Ecliptic Plane

Figure D3-1 is a summary of data of the reader responses for KIM 6-65. The headings and column numbers have been explained under Instructions to the Reader.

In the following discussion of the responses from the three readers, the paragraph numbers correspond to the column numbers on the data sheet. Column numbers 1 through 5 describe the photo system and list the sun elevation, phase angle, the order of evaluation, and the negative number.

Geometric Shapes (Column 6-10)

In general the geometric shapes were not discovered by the readers until the phase angle was large enough to cast a shadow which helped identify these shapes; however, once the location was known, it was possible to go back to considerably lower phase angles and identify these shapes.

(6) The 4-foot-diameter, 26° slope, convex cone was the first geometric shape to be identified, but it was classified as a boulder even with the 220 l/mm system until the sun elevation reached 15° and the object cast an identifying shadow. In the 53 l/mm and 92 l/mm photo system, the 4-foot size of this protrusion was at just about the limit of resolution, and this cone was never identified. This result agrees with the data obtained in the geometric shape experiment. The 220 l/mm photo system, however, gave enough detail to the readers to identify this shape as a cone at 15° sun elevation. At lower sun elevations, the shape of its shadow was lost in the background; however, the readers remembered the location and correctly identified the shape from the few remaining details. A 4-foot 26° cone was identified in the geometric shape experiment at 60° phase angle and can be identified in KLM 6-65 at this phase angle when the position is known.

(7) The 8-foot diameter, 7° convex cone was not identified in either the 53 l/mm or the 92 l/mm photo system. It was identified in the 220 l/mm system when the phase angle was increased to 80°. If the position of this target is known, it can be recognized as a cone at smaller phase angles. In the test using geometric shapes, a cone of this size was identified at a phase angle of 75°.

(8) The 8-foot diameter, 7° concave cone was not identified in the low resolution systems but was identified in the 220 l/mm photo system when the phase angles reached 85° and the object cast an identifying shadow. This shape, like the others, can be identified at lower phase angles if the location is known by the reader. In the geometric shape study it was identified at 75°.

(9) The 8-foot diameter, 8:1 (diameter to depth) spherical concave surface was not identified in the 53 l/mm photo system but was identified at 85° phase angle in the 92 l/mm photo system and at 80° and 85° phase angles in the 220 l/mm photo system. This geometric shape is very much like many of the craters located in the model and could be identified only because it has a smoother surface than the others. At very small phase angles, craters cannot be identified in any of the photo systems. With the 220 l/mm photo system, the largest craters can be identified at 15°; however, the sun must move to a 30° phase angle before these same craters can be identified in the 92 l/mm system and to 45° before they can be identified in the 53 l/mm system.

The 8-foot crater can be identified or recognized at much lower phase angles if its position is known. In the geometric-shape experiment, it was identified at 45° phase angle in the 220 l/mm photo system.

(10) The ratio of shadow to diameter in the 8:1 concave surface was estimated as .6 at 10° sun elevation and .8 at 5° sun elevation. This compares very favorably with the calculated values of .64 and .83 as given in Figure B4-9. At a sun elevation of 15° the shadow covers .34 of the diameter. At 30° sun elevation the side nearest the sun is darker and no distinct shadow should be seen. In the 53 l/mm photo system, all of these fine details are lost in the film grain.

(11) Column 11 gives the estimated size of the smallest crater that can be identified for each sun elevation. The size data for these photo systems follow the curves given in Figures C3-2, C3-3 and C3-4, providing

a very good correlation between the reader response to KLM 6-65 and the geometric shapes. The readers estimated the size of the craters from a rather crude scale with 20-foot divisions located along the bottom and right side of model. They were also told that the largest crater is 36 feet in diameter and the next largest is 28 feet in diameter.

Table D3-1 Estimated Smallest Craters (MONO)

Photo System 1/mm	P	Sun Elevation / Phase Angle	75 / 15	60 / 30	45 / 45	30 / 60	15 / 75	10 / 80	5 / 85
53	3.8	C*			27	11	6	5	5
		C/P **			7.1	2.6	1.6	1.3	1.3
92	2.2	C		24	13	9	5	5	5
		C/P		11	5.9	4.1	2.3	2.3	2.3
220	.91	C	18	7	6	3	1	1	1
		C/P	20	7.7	6.6	3.3	1.1	1.1	1.1

* Estimated smallest crater

** Ratio of crater diameter to the pitch of the limiting high contrast tri-bar chart projected on the lunar surface.

Table D3-1 has been prepared from the data in column 11. For comparison the table shows the calculated value of this crater size divided by the pitch of the limiting tri-bar. This ratio has been plotted in Figure D3-6 and shows a very good agreement with the data from the geometric shape experiment.

(12 and 13) Albedo Changes - The areas of light albedo, which were made by dusting silver chloride over the copper oxide, were easily seen at the high sun elevations (low phase angle) and were, in fact, the only features that could be identified. These areas were seen in pictures made by the low resolution system, but since this was the first target presented to the readers, they were not sure that the image represented a

a change in albedo. The albedo in the light area was 0.091.

(14 and 15) Albedo Change - The albedo change in darker areas on the model was small and was never correctly identified by any of the readers for any of the systems. The change was made by dusting Will copper oxide over two areas that were already dusted with the Fisher copper oxide, the Will copper oxide having a somewhat lower albedo as follows:

Fisher copper oxide albedo:	.055
Will copper oxide albedo:	.048

The Will copper oxide was dusted very lightly in order not to cause an avalanche when the model was turned into a vertical position; and it can just be seen in the large record photographs (Figure B4-11, 84° sun elevation). The above albedo measurements were made from samples of all the same material. A light dusting of the Will over the Fisher copper oxide will not bring the albedo all the way to .048.

(16) Number of Boulders - Column 16 lists the number of boulders counted by the observers at each sun elevation. The criterion for identification of a boulder is that the shadow is away from the sun and the bright side is next to the sun in contrast to the appearance of a crater. In general, a boulder cannot be found until a shadow is present, but once the reader found it, he would look carefully in the area on later photos for details that would permit identification. A number of false boulders were noted, and the geometric cones were frequently counted as a boulder since they met the above criterion. There were only six boulders placed on the model, but careful examination of the photography at 10° sun elevation shows a number of other places on the model where the above criterion would indicate a boulder.

(17) Craters 10 feet ± 2 feet in diameter on left side of model. Table D3-2 has been constructed from column 17. It lists the number of craters 8 to 12 feet in diameter in the left half of the model that can be identified for each phase angle.

Table D3-2

Photo System Lines/mm	P	Ratio of 10 Ft. to Pitch of the Limiting Resolution	Number of 10 Ft. Craters Counted in Left Half of KLM6-65 Phase Angle 30°	45°	60°	75°	80°	85°
53	3.8	2.6			2	6	8	10
92	2.2	4.5		2	4	9	10	10
220	.91	11.	1	6	12	13	13	13

The 53 1/mm and the 92 1/mm photo systems can give only a few details of an object of 10-foot size. The 220 1/mm photo system, however, is capable of resolving details in a 10-foot crater. The above table agrees reasonably well with the geometric shape experiment.

Most of the craters in KLM 6-65 have a diameter-to-depth ratio of 8 to 1, which corresponds to the lunar features measured from Ranger photography (see Figures B4-6). Craters with 8:1 diameter-to-depth ratio should just begin to cast a shadow as the sun elevation sinks below 30° (see Figure B4-9). Thus, the 220 1/mm photo system should be able to identify all these craters at 30° sun elevation (60° phase angle) in agreement with the above table. One of the 10-foot craters can be identified at a phase angle as small as 30° in this high-resolution photo system.

In the 53 1/mm and 92 1/mm photo systems, shadows are needed for object identification as these systems require more contrast in object details before 10-foot objects can be clearly identified. The readers were able to detect the first 10-foot craters in the 53 1/mm photo system only after the phase angle reached 60°.

The readers used the 20-foot scale divisions on the bottom and right side of the model to estimate the size of craters. Since this is not a very precise scale, it will account for some of the variation in reader response.

The data from this section is plotted in Figure D3-7. A few of the craters about 12 feet in diameter were counted and on this chart are plotted in the area of detection. All of the rest of the counts are in the area of identification, and as the phase angle becomes larger more craters can be identified, i.e. the farther away from the detection area (up and to the left) that a point occurs the more certain it is that all of the craters will be counted.

(18) Fault Line - The following table was constructed from reader response to identification of the fault line.

Photo System l/mm	Tri-Bar Pitch at Surface P	Phase Angle Above Which the Fault Line Was Identified	Phase Angle Above Which the Fault Line was Easily Identified
53	3.8	30	75°
92	2.2	30	60°
220	.91	15	45°

These data show that the higher resolution system can identify the fault line at a smaller phase angle. The original intent was to have the fault line 30 or 40 feet in length, but the junction between the left and right portions of the model shows a discontinuity which was considered by the readers to be a fault line running from top to bottom on the model.

(19) Crater Chain - This item consists of 5 craters with the following diameters: 15-feet, 12-feet, 11-feet, 9-feet and 6-feet with the 6-foot crater overlapping the 9-foot crater.

Table D3-3 Crater Chain

Photo System (1/mm)	Pitch of the Limiting Tri-Bar at the Lunar Surface (feet) = P	Ratio 6ft. P	Phase Angle Above Which the Crater Chain Was Identified
53	3.8	1.6	75°
92	2.2	2.7	75°
220	.91	6.6	30°

The readers were able to find some of these craters at much smaller phase angles than those listed in table D3-3 but it was necessary to resolve and detect the smallest crater before the five craters could be identified as a crater chain with confidence.

(20) Map of Landing Area - At small phase angles, the readers chose to stay away from the areas of light albedo since it was not known what dangers these areas represented. Other than this, they could not detect any hazards to landing. As the phase angle was increased, the readers selected the N.E. quadrant in which to land the LEM, avoiding the largest crater in the S.E. quadrant, the next largest in the N.W. quadrant, and the albedo change in the S.W. quadrant. At larger phase angles, more and more details and potential hazards began to show and one reader said he would try to straddle the large crater (adjacent to the 8-foot-diameter cone) in the N.E. quadrant with the feet of the LEM. The others also selected the N.E. area as the best possible LEM landing area on the model.

(21) Ditch - The ditch which occupies an area 60 feet long by 10 feet across and about 1 foot deep on the right-hand side of the model can be identified when the phase angle exceeds the following values:

Photo System 1/mm	Pitch of the Limiting Tri-Bar, Feet	Phase Angle Above Which the Ditch is Identifiable
53	3.8	75°
92	2.2	60°
220	.91	45°

It should be noted that the ditch can be identified when the phase angle reaches a value where 5- to 6-foot craters and the largest boulder (2 feet high, 6 feet across) can be identified.

Photo System 1/mm	Pitch of the Limiting Tri-Bar Feet	Sun Elev. Degrees	Phase Angle Degrees	Eval. Order	Neg. No.	CONES Convex 4',26°	CONES Convex 8',7°	CONES Concave 8',7°	Spherical Concave I	Spherical Concave S/D	Est. Smallest Crater Diam. Ft.	ALBEDO Light #1	ALBEDO Light #2	ALBEDO Dark #1	ALBEDO Dark #2	Number Boulders	Number of Craters of 10' Diam. on Left Side	Fault	Crater Chain	Landing Site	Ditch
1	2	3	3a	4	5	6	7	8	9	10	11	12	13	14	15	16	17	18	19	20	21
53	3.8	84	6	1	M5-4	0	0	0	0	0	0	I	I	0	0	0	0	0	0	0	0
53	3.8	75	15	4	M5-11	0	0	0	0	0	0	I	I	0	0	0	0	F	0	X	0
53	3.8	60	30	7	M5-17	0	0	0	0	0	0	I	I	0	0	0	0	DI	0	0	0
53	3.8	45	45	10	M5-25	0	0	0	0	0	27	I	I	0	0	0	0	I	0	X	0
53	3.8	30	60	13	M6-3	0	0	0	0	0	11	I	I	0	0	0	2	I	0	0	0
53	3.8	15	75	16	M6-10	0	0	0	0	0	6	I	I	0	0	1	6	EI	I	X	I
53	3.8	10	80	19	M6-18	0	0	0	0	0	5	DI	DI	0	0	1	8	EI	EI	X	EI
53	3.8	5	85	22	M6-25	0	0	0	0	0	5	L	L	0	0	2	10	EI	EI	X	EI
92	2.2	84	6	2	M3-4	0	0	0	0	0	0	EI	EI	0	0	0	0	0	0	0	0
92	2.2	75	15	5	M3-11	0	0	0	0	0	0	EI	EI	F	F	0	0	0	0	X	0
92	2.2	60	30	8	M3-18	0	0	0	0	0	24	EI	EI	0	0	0	0	DI	0	0	0
92	2.2	45	45	11	M3-25	0	0	0	0	0	13	EI	EI	0	0	1	2	I	0	X	0
92	2.2	30	60	14	M4-3	0	0	0	0	0	9	EI	EI	0	0	1	4	EI	0	0	DI
92	2.2	15	75	17	M4-11	0	0	0	0	0	5	I	I	0	0	2*	9	EI	EI	X	I
92	2.2	10	80	20	M4-18	0	0	0	0	0	5	DI	DI	0	0	3*	10	EI	EI	X	I
92	2.2	5	85	23	M4-25	0	0	0	I	.8	5	L	L	0	0	5*	10	EI	EI	X	I
220	.91	84	6	3	M1-5	0	0	0	0	0	0	EI	EI	0	0	0	0	0	0	0	0
220	.91	75	15	6	M1-11	0	0	0	0	0	18	EI	EI	0	0	0	0	DI	0	X	0
220	.91	60	30	9	M1-19	0	0	0	0	0	7	EI	EI	0	0	0	1	I	DI	0	0
220	.91	45	45	12	M1-25	0	0	0	0	0	6	EI	EI	0	0	2	6	EI	I	X	I
220	.91	30	60	15	M2-4	0	0	0	0	0	3	EI	EI	0	0	3	12	EI	EI	0	EI
220	.91	15	75	18	M2-12	I	0	0	0	0	1	EI	EI	0	0	7*	13	EI	EI	X	EI
220	.91	10	80	21	M2-18	I	I	0	I	.6	1	I	I	0	0	7*	13	EI	EI	X	EI
220	.91	5	85	24	M2-25	I	I	I	I	.8	1	DI	DI	0	0	7*	12	EI	EI	X	EI

I = Identified
L = Lost or camouflaged
0 = No response from the readers

EI = Easily identified
DI = Difficult to identify
F = False identification

X = Lunar landing site selected; map drawn showing this selected area.
*4 Foot 26° or 8 Foot 7° Cone Counted as a Boulder

Summary of the Response From Three Readers For KLM6-65, Monoscopic Photography

FigureD3-1

b. Stereoscopic Photography in the Ecliptic Plane

The three camera systems photographed the KLM6-65 model at ±15° stereo angle in the ecliptic plane. The summary of the reader responses is given in Figure D3-2.

A study of these data shows that the reader response is very similar to that from the monoscopic vertical photography, especially if the larger phase angle of the stereo pair is compared with the phase angle of the vertical monoscopic photography. The data in Column 11 (estimated smallest crater) are shown in Table D3-4, and along with the ratio of crater size to pitch of the limiting tri-bar chart, is plotted in Figure D3-6. The data in column 17 (number of 10 ft. craters) are shown in Table D3-5 and are plotted in Figure D3-7. The data from this experiment show very good agreement with that from the geometric shape experiment. The readers failed to see the model in three dimensions except in the 220 line/mm system used at low sun elevations (large phase angles), probably because of the low contrast at high sun elevation angles and because the photo systems record the height of objects on the model too near the limit of resolution.

Table D3-4

Estimated Smallest Crater - Stereo in Ecliptic

Photo System Lines/mm	Pitch of Limiting Tri-Bar, Feet	Sun elevation / Max. Phase angle	60 / 45	15 / 90	5 / 105
53	3.8	Est. Smallest Crater, feet		8	7
		Crater size/pitch		2.1	1.8
92	2.2	Est. Smallest Crater, feet	36	4	4
		Crater size/pitch	16.4	1.8	1.8
220	.91	Est. Smallest Crater, feet	8	2	2
		Crater size/pitch	8.8	2.2	2.2

Table D3-5

Number of 10 ft. Craters Counted - Stereo in Ecliptic

Photo System	Pitch of Limiting Tri-Bar - feet	Ratio 10 ft./P	Max. Phase Angle 45	90	105
53	3.8	2.6		6	8
92	2.2	4.5		8	8
220	.91	11	5	12	12

Photo System 1/mm	P	Sun Elev. Degrees	Phase Angle Degrees	Eval. Order	Neg. No. Left	Neg. No. Right	CONES Convex 4',26°	CONES Concave 8',7°	CONES Concave 8',7°	Spherical Concave Obs.	Spherical Concave S/D	Est. Smallest Crater Diam. Ft.	ALBEDO Light Streak	ALBEDO Blob	ALBEDO Dark #1	ALBEDO Dark #2	#B**	Number of Craters of 8-12' Diam. on Left Side	Fault	Crater Chain	Landing Site	Ditch
1	2	3	3a	4	5a	5b	6	7	8	9	10	11	12	13	14	15	16	17	18	19	20	21
53	3.8	90	15	1	M-11-3	M-17-3	0	0	0	0	0	0	EI	EI	0	0	0	0	0	0	AE	0
53	3.8	82	23/7																			
53	3.8	69	36/6																			
53	3.8	60	45/15	4	M-11-22	M-17-21	0	0	0	0	0	0	I	I	0	0	0	0	0	0	AE	0
53	3.8	45	60/30																			
53	3.8	30	75/45																			
53	3.8	15	90/60	7	M-12-14	M-18-11	0	0	0	0	0	8	I	I	0	0	2	6	EI	EI	UR	EI
53	3.8	10	95/65																			
53	3.8	5	100/70	10	M-12-24	M-18-25	0	0	0	d	.6	7	L	L	0	0	3	8	EI	I	UR	EI
92	2.2	90	15	2	M-9-3	M-15-3	0	0	0	0	0	0	EI	EI	0	0	0	0	I	0	AE	0
92	2.2	82	23/7																			
92	2.2	69	36/6																			
92	2.2	60	45/15	5	M-9-22	M-21-4	0	0	0	0	0	36	I	I	0	0	0	0	EI	0	AE	0
92	2.2	45	60/30																			
92	2.2	30	75/45																			
92	2.2	15	90/60	8	M-10-13	M-16-12	0	DI	0	d	.4	4	I	I	0	0	4	8	EI	EI	UR	EI
92	2.2	10	95/65																			
92	2.2	5	100/70	11	M-10-28	M-16-26	I	DI	0	I	.6-.8	4	DI	DI	0	0	5	8	EI	EI	UR	EI
220	.91	90	15	3	M-7-3	M-13-3	0	0	0	0	0	0	EI	EI	0	0	0	0	EI	0	AE	0
220	.91	82	23/7																			
220	.91	69	36/6																			
220	.91	60	45/15	6	M-7-19	M-13-17	0	0	0	0	0	8	EI	EI	0	0	1	5	EI	I	UR	DI
220	.91	45	60/30																			
220	.91	30	75/45																			
220	.91	15	90/60	9	M-8-12	M-14-10	I	I	I	d	.4-.6	2	EI	EI	0	0	6	12	EI	EI	UR	EI
220	.91	10	95/65																			
220	.91	5	100/70	12	M-8-27	M-14-22	I	EI	I	I	.8	2	DI	DI	0	0	7	12	EI	EI	UR	EI

I = Identified
L = Lost or camouflaged
O = No response from the readers

EI = Easily identified
DI = Difficult to identify
AE = Anywhere except on the items identified
#B** = Number Boulders

d = Reader was directed to this shape and asked to estimate shadow to diameter ratio
UR = Upper right quadrant
P = Pitch of the limiting Tri-Bar, feet

Summary of the Response From Three Readers For KLM6-65, Stereo (±15) Photography in the Ecliptic

FigureD3-2

c. Stereo Photography out of Ecliptic Plane

In this experiment the model was arranged so that the camera axes were 15° from the nadir and at right angles to the plane of the ecliptic. A study of the data in Figure D3-3 shows good agreement with results from the mono vertical photography and the stereo photography taken in the plane of the ecliptic, provided that the comparisons are made against the larger phase angles of the stereo pairs. This result agrees with that from the geometric shape experiment; again the readers were not able to see three dimensions until the phase angle reached a value of 75° and then only in the higher resolution photo systems. The readers did say, however, that this experiment had better stereo than previously evaluated systems.

The phase angle is the important criterion determining the lunar contrast and is apparently more important than the additional information supplied by two negatives viewed with both eyes.

The data from column 11 are plotted in the proper place in D3-6 and that from column 17 is in D3-7.

Reader Remarks:

In general, the boulders were found by contrast logic, highlight on the sunney side and shadow away from the sun, rather than stereo techniques.

The shadow of the largest boulder falls into a crater shadow making it difficult to identify at lower sun elevations.

All photo systems give the impression that craters are hills on some occasions.

The fault line was very contrasty because of model shrinkage before the photographs were taken.

Photo System 1/mm	P	Sun Elev. Degrees	Phase Angle Degrees	Eval. Order	Neg. No. Left	Neg. No. Right	CONES Convex 4°,26	CONES Convex 8°,7°	CONES Concave 8°,7°	Spherical Concave I	Spherical Concave S/D	Est. Smallest Crater Diam. Ft.	ALBEDO Light Streak	ALBEDO Light Blob	ALBEDO Dark #1	ALBEDO Dark #2	#B**	Number of Craters of 8-12' Diam. on Left Side	Fault	Crater Chain	Landing Site	Ditch
1	2	3	3a	4	5a	5b	6	7	8	9	10	11	12	13	14	15	16	17	18	19	20	21
53	3.8	90	15	1	M-23-3	M-35-3	0	0	0	0	0	0	EI	EI	0	0	0	0	EI	0	AE	0
53	3.8	82	17																			
53	3.8	69	19																			
53	3.8	60	33	4	M-27-2	M-23-2	0	0	0	0	0	28	EI	EI	0	0	0	0	EI	0	AE	0
53	3.8	45	47																			
53	3.8	30	61																			
53	3.8	15	75	7	M-39-2	M-30-2	0	0	0	0	0	7	I	I	0	0	1	8	EI	I	UR	EI
53	3.8	10	80																			
53	3.8	5	85	10	M-39-16	M-30-17	0	0	0	0	0	6	L	L	0	0	2	8	EI	I	UR	EI
92	2.2	90	15	2	M-24-1	M-36-3	0	0	0	0	0	0	I	EI	0	0	0	0	EI	0	AE	0
92	2.2	82	17																			
92	2.2	69	19																			
92	2.2	60	33	5	M-26-3	M-32-3	0	0	0	0	0	25	EI	EI	0	0	0	0	EI	0	UR	0
92	2.2	45	47																			
92	2.2	30	61																			
92	2.2	15	75	8	M-38-3	M-29-3	0	0	0	d	.4-.5	5	I	DI	0	0	2	10	EI	I	UR	EI
92	2.2	10	80																			
92	2.2	5	85	11	M-38-18	M-29-25	I	0	0	I	.8	4	L	L	0	0	5	10	EI	EI	UR	EI
220	.91	90	15	3	M-22-4	M-34-4	0	0	0	0	0	0	EI	EI	0	0	0	0	EI	0	AE	0
220	.91	82	17																			
220	.91	69	19																			
220	.91	60	33	6	M-35-4	M-31-4	0	0	0	0	0	7	EI	EI	0	0	1	4	EI	I	UR	0
220	.91	45	47																			
220	.91	30	61																			
220	.91	15	75	9	M-37-5	M-28-5	EI	DI	DI	I	.4-.5	3	I	DI	0	0	5	11	EI	EI	UR	EI
220	.91	10	80																			
220	.91	5	85	12	M-37-20	M-28-20	I	I	I	I	.7-.8	3	L	L	0	0	6	12	EI	EI	UR	EI

I = Identified
L = Lost or camouflaged
O = No response from the readers

EI = Easily identified
DI = Difficult to identify
AE = Anywhere except on the identified items
#B** = Number Boulders

d = Reader was directed to this shape and asked to estimate shadow to diameter ratio
UR = Upper right quadrant
P = Pitch of the limiting Tri-Bar feet

Summary of the Response From Three Readers For KLM6-65, Stereo (15° Half Angle) Photography Out of Ecliptic Plane (Negatives)

FigureD3-3

d. Oblique Photography Out of the Ecliptic Plane

This experiment was made with the camera axis 30° from the nadir and at right angles to the ecliptic plane and with the sun in the ecliptic plane. Exposures were made only in the 220 lines/mm photo system. The data in Figure D3-4 compare very favorably with the vertical monoscopic photography if the phase angles are used for the comparison.

If an orbiting vehicle rolls to obtain oblique photography the scale of the photography will change unless the altitude is also changed. The comparison of the results of this experimental oblique photography with vertical monoscopic photography was made at the same photographic scale.

This oblique photography of KLM6-65 differs from that made of the geometric shapes in that in oblique photography of the geometric shapes the model, sun and camera were all in the ecliptic plane, while in this experiment the camera was 30° out of the ecliptic plane. However, the results from these two experiments are nearly identical if comparisons are made with phase angle as the independent variable.

The data from column 11 are plotted in the proper place in Figure D3-6 and that from column 17 is in Figure D3-7. These plots show good agreement with the previous experiments.

Photo System 1/mm	Pitch of the Limiting Tri-Bar Feet	Sun Elev. Degrees	Phase Angle Degrees	Evol. Order	Neg. No.	CONES Convex 4',26°	CONES Concave 8',7°	CONES Concave 8',7°	Spherical Concave I	Spherical Concave S/D	Est. Smallest Crater Diam. Ft.	ALBEDO Light #1	ALBEDO Light #2	ALBEDO Dark #1	ALBEDO Dark #2	Number Boulders	Number of Craters of 10' Diam. on Left Side	Fault	Crater Chain	Landing Site	Ditch
1	2	3	3a	4	5	6	7	8	9	10	11	12	13	14	15	6	17	18	19	20	21
220	.91	84	31	1	M-19-4	0	0	0	0	0	30	EI	EI	DI	0	0	0	EI	0	UR	0
220	.91	75	33	2	M-19-11	0	0	0	0	0	13	EI	EI	0	0	1	2	EI	0	UR	0
220	.91	60	41	3	M-19-18	0	0	0	0	0	10	EI	EI	0	0	1	3	EI	DI	UR	0
220	.91	45	52	4	M-19-25	0	0	0	d	(0)	6	EI	EI	0	0	2	8	EI	I	UR	0
220	.91	30	64	5	M-20-3	I	DI	DI	d	.2	3	EI	EI	0	0	4	10	EI	EI	UR	DI
220	.91	15	77	6	M-20-10	I	DI	DI	I	.4	3	EI	EI	0	0	5	11	EI	EI	UR	I
220	.91	10	81	7	M-20-17	I	I	DI	I	.6	2	I	I	0	0	6	12	EI	EI	UR	EI
220	.91	5	86	8	M-20-25	I	I	I	I	.8	2	L	L	0	0	6	12	EI	EI	UR	EI

I = Identified
L = Lost or camouflaged
0 = No response from the readers

EI = Easily identified
DI = Difficult to identify
UR = Upper right quadrant

d = Reader was directed to this shape and asked to estimate shadow to diameter ratio
(0) = Shadow length is zero

Summary of the Response From Three Readers For KLM6-65, Oblique Monoscopic Photography Camera 30° From Nadir (Negatives)

FigureD3-4

e. Positive Stereo Photography out of the Plane of The Ecliptic

It is possible that positive images would be easier for the readers to evaluate than the negatives. To study this question a set of positive photographs was made from the stereo photography taken out of the plane of the ecliptic. In printing the positives the resolution dropped from 220 lines/mm to about 120 lines/mm making the limiting tri-bar about 1.7 feet on the lunar surface.

All of the readers said they would rather evaluate positive images, but the data (Figure D3-5) show that the evaluation is somewhere between the 93 lines/mm and the 220 lines/mm photo systems. The data from column 11 are plotted in the proper place in Figure D3-6 and from column 17 in Figure D3-7 showing that these data agree with the previous experiments.

It is concluded that while the readers, prefer positive images, they can do as well with negative images of lunar scenes when judging detail rendition in the pictures.

Photo System l/mm	P	Sun Elev. Degrees	Phase Angle Degrees	Eval. Order	Neg. No. Left	Neg. No. Right	CONES Convex 4',26°	CONES Convex 8',7°	CONES Concave 8',7°	Spherical Concave I	Spherical Concave S/D	Est. Smallest Crater Diam. Ft.	ALBEDO Light Streak	ALBEDO Blob	ALBEDO Dark #1	ALBEDO Dark #	#B**	Number of Craters of 8-12' Diam. on Left Side	Fault	Crater Chain	Landing Site	Ditch
1	2	3	3a	4	5a	5b	6	7	8	9	10	11	12	13	14	15	16	17	18	19	20	21
120	1.7	90	15	1	M-22-4	M-34-4	0	0	0	0	0	0	EI	EI	DI	0	0	0	EI	0	AE	0
120	1.7	82	17																			
120	1.7	69	19																			
120	1.7	60	33	2	M-25-5	M-31-5	0	0	0	0	0	17	EI	EI	0	0	1	0	EI	0	UR	0
120	1.7	45	47																			
120	1.7	30	61																			
120	1.7	15	75	3	M-37-5	M-28-5	I	I	0	I	.3-.4	5	DI	L	0	0	5	11	EI	EI	UR	EI
120	1.7	10	80																			
120	1.7	5	85	4	M-37-20	M-28-19	EI	EI	I	I	.6-.8	3	L	L	0	0	6	13	EI	EI	UR	EI

I = Identified
L = Lost or camouflaged
0 = No response from the readers

EI = Easily identified
DI = Difficult to identify
AE = Anywhere except on the identified items
#B** = Number Boulders

UR = Upper right quadrant
P = Pitch of the limiting Tri-Bar, feet

Summary of the Response From Three Readers For KLM6-69, Stereo (15 Half Angle) Photography Out of Ecliptic Plane (Positives)

Figure D3-5

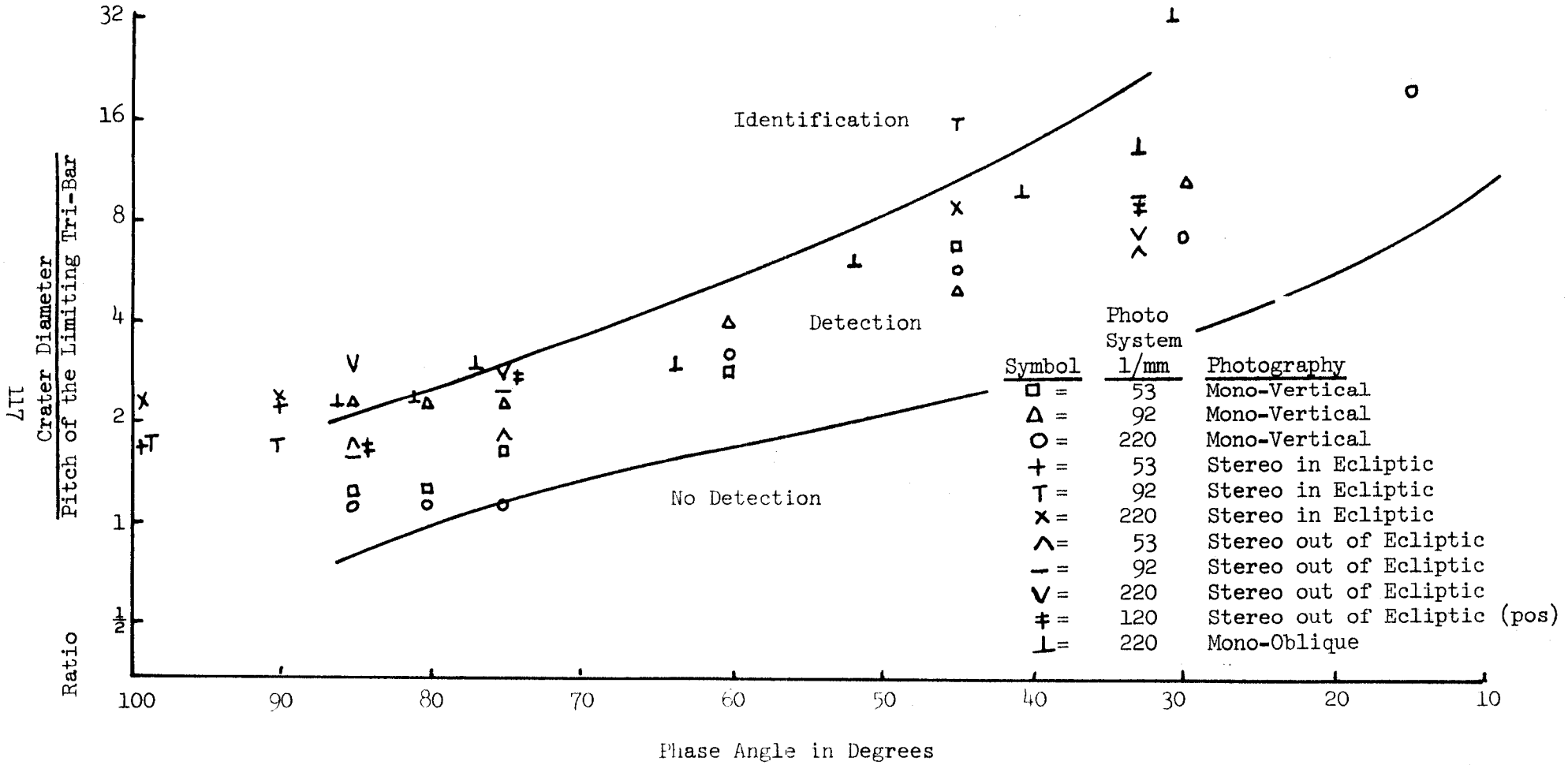

Estimated smallest crater identified by readers observing photography of KLM6-65. Several types of photography and several photo systems are represented - Data obtained from Column 11 in Reader Response Summaries of KLM6-65. Coordinates and lines separating identification, detection and no detection taken from Figure C3-15.

Figure D3-6

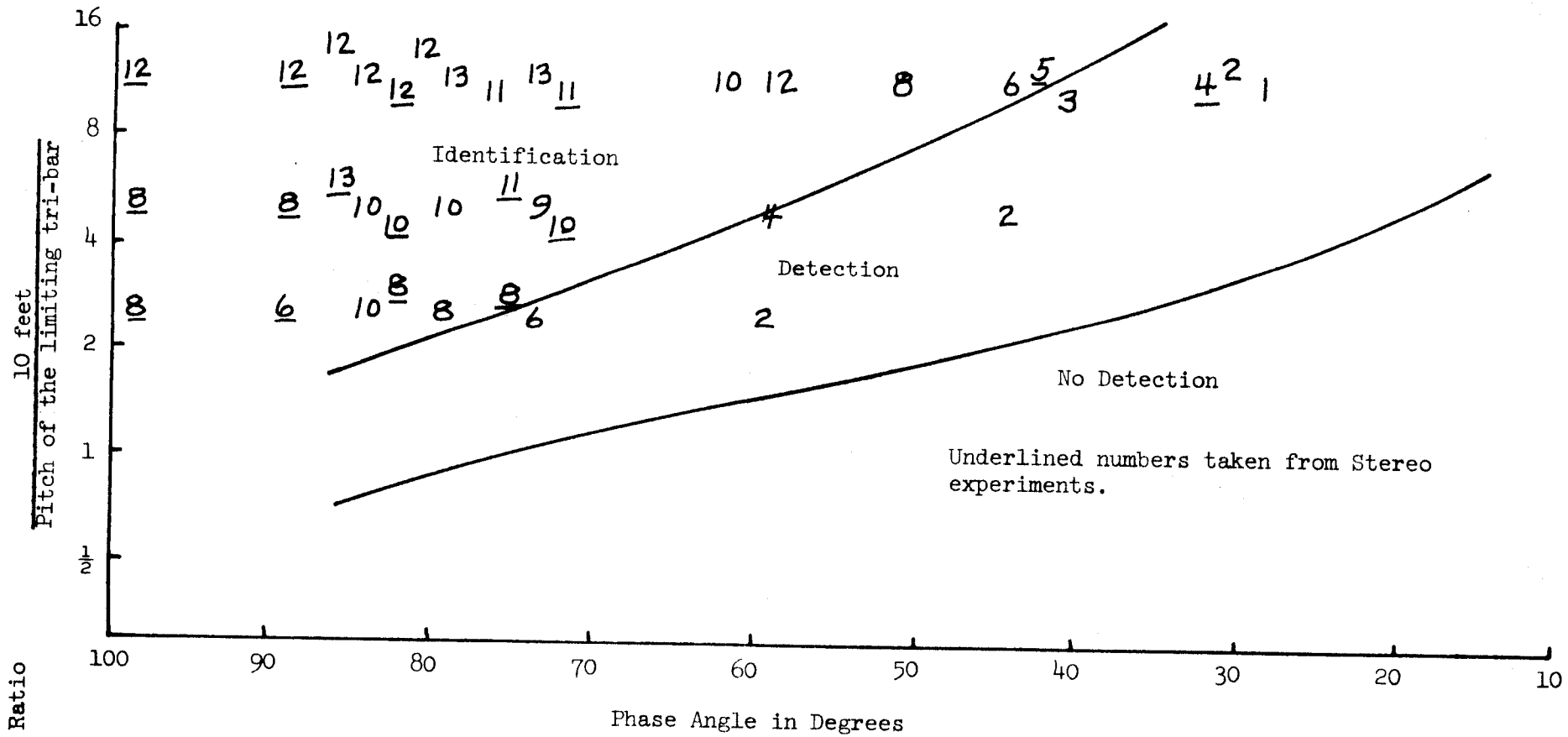

Number of craters 8 to 12 feet in diameter counted on the left half of KLM6-65 vs Phase Angle. Data obtained from column 17 of reader response summaries. Coordinates and lines separating identification, detection and no detection are taken from Figure C3-15.

Figure D3-7

4. Conclusions from KLM6-65

(1) The Kodak Lunar Model 6-65 has features that match the lunar surface as revealed by studies of Ranger photography and, when dusted with copper oxide, is a realistic model for photographic studies.

(2) Detection and identification of objects on KLM6-65 agree very well with results from the experiment using geometric shapes. Therefore, there is reason to believe that Figure C3-15 adequately describes the reader response to images of lunar detail.

(3) The data from the estimated smallest crater identified by the readers (column 11 in Summaries) is plotted in Figure D3-6 on the coordinates of C3-15 and shows that there is good agreement between the reader response to crater size on the KLM6-65 and the response to the geometric shapes.

(4) The data from the number of 10 foot craters that can be identified by the reader (column 17 in Summaries) is plotted in Figure D3-7 on the coordinates of C3-15 showing that there is good agreement between the reader response to KLM6-65 and the response to the geometric shapes.

(5) The albedo changes are the only features that can be identified at low phase angles. They become masked or camouflaged in KLM6-65 at phase angles greater than 75° to 85°.

(6) There are thirteen 10 foot craters on the left side of KLM6-65. If the percentage of identified 10 foot craters divided by the pitch of the photo system is plotted against the phase angle, we obtain a matrix of points as shown in Figure D3-8. The matrix contains all the data in column 17 from all of the KLM6-65 experiments. A family of curves may be drawn for several multiples of D/P where D is the crater diameter and P is the pitch of the high contrast tri-bar chart at the limiting resolution for the photo system.

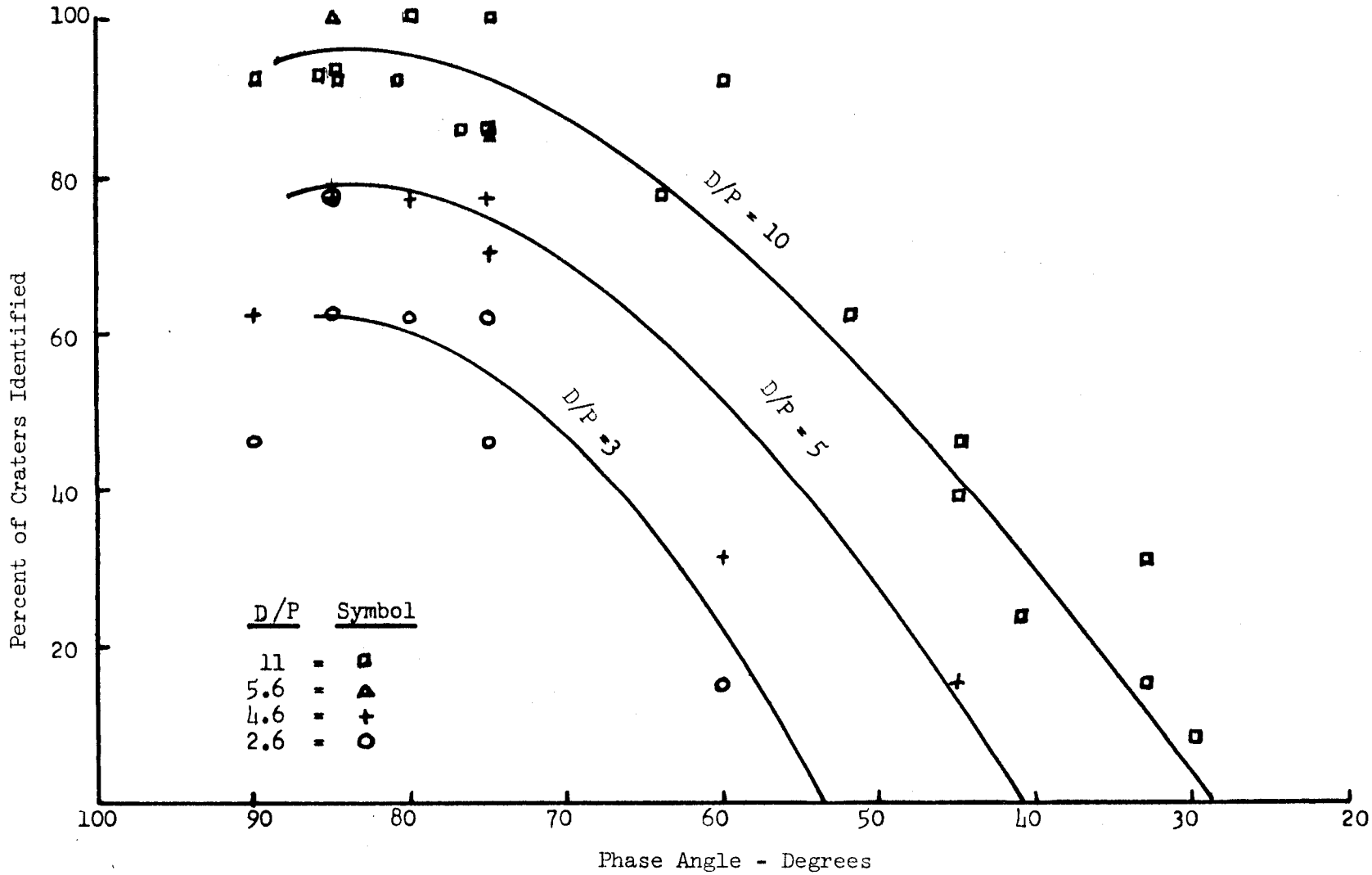

Percent of craters identified vs phase angle for a number of photo systems. D is crater diameter, P is the pitch of the limiting high contrast tri-bar chart on the lunar surface. Data for this curve obtained from column 17 in reader response summaries - number of 10 $\pm$ 2 foot craters counted in the left half of KLM6-65.

Figure D3-8

As an example of the interpretation of these curves, the curve labeled D/P=10 shows that for a photo system of 1 foot limiting resolution a phase angle of at least 75° is required to identify 95% of the 10 foot craters. Also a photo system with 3.3 foot limiting resolution D/P=3 can identify a maximum of about 60% of the 10 foot craters even at high phase angles. At phase angles below 55° the photo system of quality D/P=3 cannot identify a 10 foot crater; and below 30° the D/P=10 photo system cannot identify a 10 foot crater.

These curves can be applied to identification of other sizes of craters provided the diameter to depth ratio (contrast) of the craters remains near 8:1 as in KLM6-65. If this ratio changes then the contrast will change, and the family of curves would move to the right for higher contrast lunar objects and to the left for lower contrast lunar objects. For instance, to identify 95% of the 5 foot craters in a lunar scene at a phase angle of 75° requires a photo system that can resolve a high contrast tri-bar chart with a pitch of 1/2 foot i.e., D/P=5/.5=10 .

(7) The phase angle is the important criterion determining the contrast of a lunar scene and is apparently even more important than the additional information supplied by two stereo negatives viewed with both eyes. This seems to be true in the experiment with the stereo pair taken out of the plane of the ecliptic and is certainly true for the stereo pair in the plane of the ecliptic.

(8) The readers failed to see three dimensions in most of the stereo photography of KLM6-65 except with the 220 lines/mm system, and then only at high phase angles.

(9) No significant difference was found between reader response to positive and negative stereo images.

(10) Small changes in slope are best detected with the sun near grazing incidence, but a considerable increase in exposure is required at large phase angles.

(11) Perhaps one of the best visual means for determining distance to the lunar surface will be to observe the shadow of the LEM on the lunar surface. The shadow is not visible when it is farther away than d (csc $1/2^{\bullet}$), where d is the LEM diameter presented to the sun. When looking at the surface in a direction $180^{\bullet}$ from the sun, the viewer will see a bright spot from the high lunar backscatter. When the LEM reaches a distance equal to d (csc $1/2^{\bullet}$), the shadow will just begin to appear in the center of the bright spot and will grow larger as the LEM approaches the surface. The shadow of an object with a 10 foot diameter just appears at 1440 feet away from the surface and grows larger as the object approaches, reaching full size on contact with the surface.

(12) Boulders are difficult to identify until the sun is low enough to cast a shadow.

(13) The readers expressed a fear of landing the LEM in the area of light albedo. At high sun elevations the contrast of craters, boulders and fault lines is reduced, making them look like a smooth plane. The area of light albedo then appears as an unknown and an undesirable place on which to land.

(14) The readers chose the upper right of the model on which to land the LEM. The lower right and upper left had the largest craters and the lower left included the area of high albedo.

E. MOTION PICTURES

1. Lambert Reflectance vs. Lunar Reflectance

Two motion pictures were made for this photo study. The first showed a comparison of two balls illuminated from a simulated sun source. One ball was dusted with copper oxide to simulate the lunar photometric function and the second ball simulated a Lambert diffuse reflector. The simulated light source traversed a complete orbit about the balls illustrating the reflectance at all phase angles. Figure A-1 shows four still photographs made of these balls at phase angles of 3°, 45°, 90°, and 155°.

2. Motion Picture from Descending LEM

The second motion picture was made to illustrate the view from the descending LEM.

a. LEM Descent Trajectory

The descent trajectory simulated in the motion picture was taken from the Design Reference Mission - DRM*. The parameters describing LEM position and orientation for the last 10,000 feet of this trajectory are given in Figures E1-1 and Table E1-1. LEM position is specified by altitude and range to the landing site, while LEM orientation is described by the pitch angle.

The time to descend from 10,000 feet to the surface is 180 seconds for this mission. Four major events occur in this period: (1) a rapid pitch maneuver at 10,000 feet which brings the lunar surface into view, (2) a rapid pitch maneuver at 200 feet which brings the landing site into full view, (3) a pitch-up of 10° at 50 feet to decrease forward velocity, and (4) touchdown. The lunar surface can be seen through the LEM Window, only during these last 10,000 feet of the descent trajectory.

* Design Reference Mission, Apollo Mission Planning Task Force Vol. I, LED-540-12, Grumman Aircraft Engineering Company, Bethpage, New York.

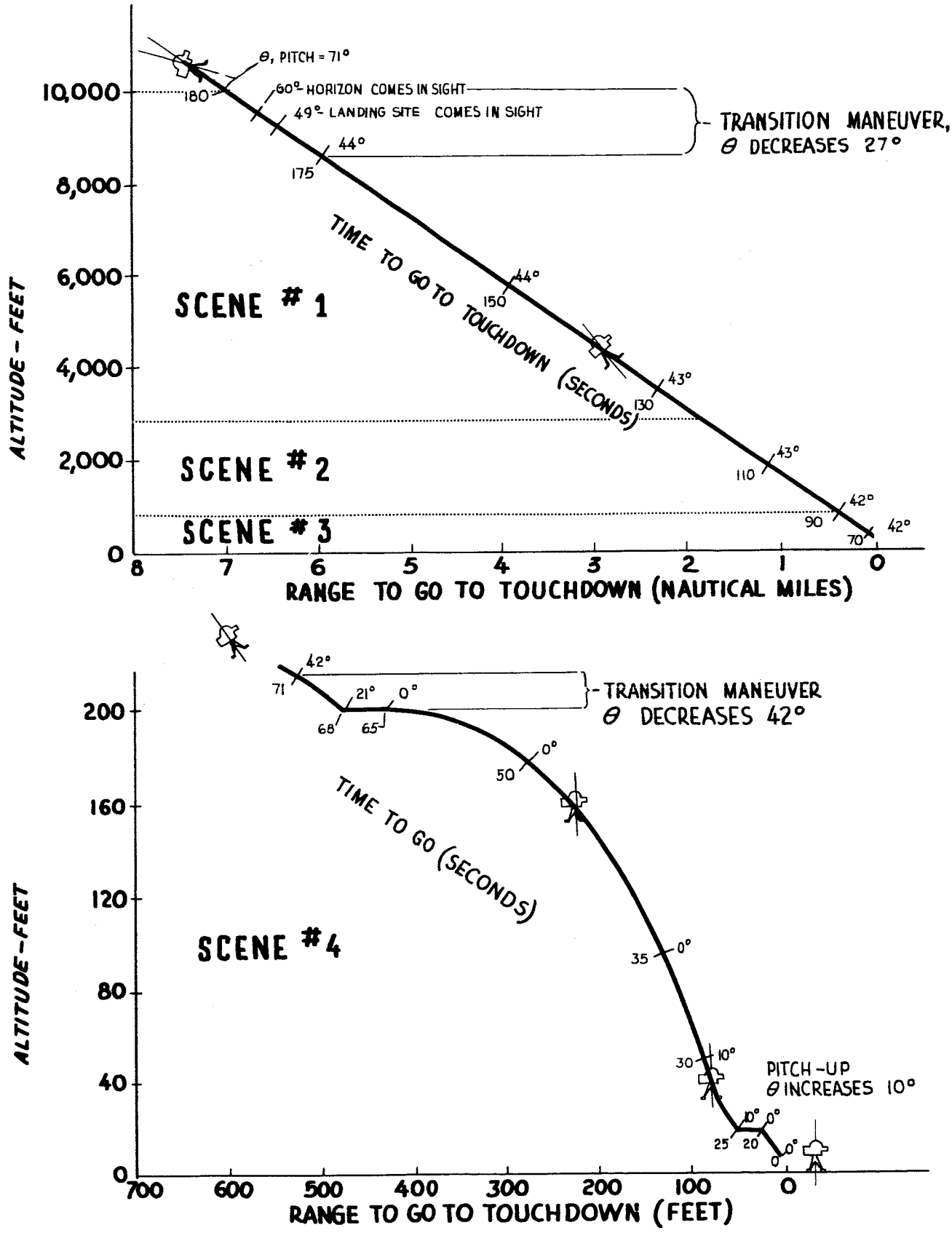

FIG. E1-1 - LEM DESCENT PARAMETERS FROM DESIGN REFERENCE MISSION USED IN PLANNING KODAK MOTION PICTURE SIMULATION

PARAMETERS OF LEM DESCENT FOR USE IN MOTION PICTURE

Scene #	Design Reference Mission LEM Descent				Simulated LEM Descent					
	Time To Go To Touchdown (sec.)	Altitude (Feet)	Range To Landing Site (Feet)	Pitch Angle* (Deg.)	Frame Number	Feet of Film	Altitude Above Model (Inches)	Range To Landing Site (Inches)	Angle of Camera Axis With Respect To Horizon	Scale Model To Moon
1. Begin	180	10,000	43,500	71	0	0	11	49	20°	1/11,300
End	125	2820	11,800	43	1320	33	3	13	- 8°	
2. Begin	125	2820	11,800	43	1321	33	11	48	- 8°	
End	94	770	2,920	42	2032	71	3	13	- 9°	1/3080
3. Begin	94	770	2,920	42	2033	51	11	49	- 9°	
End	70	208	460	36	2640	66	3	13	-15°	1/890
4. Begin	70	208	460	36	2641	66	42	103	-15°	
End	0	10	0	0	4320	104	2	0	-51°	1/60

*Pitch Angle = angle between LEM Vertical Axis (X axis) and local vertical.

TABLE E1-1

b. Constraints of Model and Equipment

A number of factors were operating to contrain the choice of model size, sun elevation, film, and method of producing the film. They are discussed in succeeding paragraphs. The positions of the sun and camera relative to the plane of the model are shown in Figure E1-2.

(1) The Illuminant

A Kodak 500-watt projector simulated the sun. It was placed 21 feet from a point 20 inches in from the front edge of the model so that the two inch diameter of the lens subtended 1/2 degree at this point.

To avoid having the shadow of the camera show in the field-of-view, it was necessary to choose a sun elevation of 37°, somewhat higher than that desirable for a landing. The projector illuminates an area 70 inches wide in the front, 95 inches wide in the back, and 120 inches deep. The size of the model is limited to these dimensions.

(2) The Model

Replicas of the surface used in constructing KLM 6-65 were smoothly joined together to form an 80 by 80 inch main section of the model used in the simulation. The scale of this surface is 1 to 48, where 1 inch equals 4 feet on the moon. This section was used in the background for the first half of the photography and later was used in the foreground. An earlier model, built to a scale of 1 inch equaling 80 feet on the moon, or 1 to 960, was joined to the main section and used in the foreground for the first half of the simulation. The problem of transferring from the surface of greater scale to the one of lower was partially solved by matching a small crater in the front section to a larger one in the main section.

(3) Lens, Camera and Film

A 15mm Cine Ektar Lens yields a field-of-view of 38° by 28° on 16mm film. This high quality lens was used on a Cine-Kodak Special Camera with time exposures of 5.5 seconds per frame using Tri-X Reversal Film.

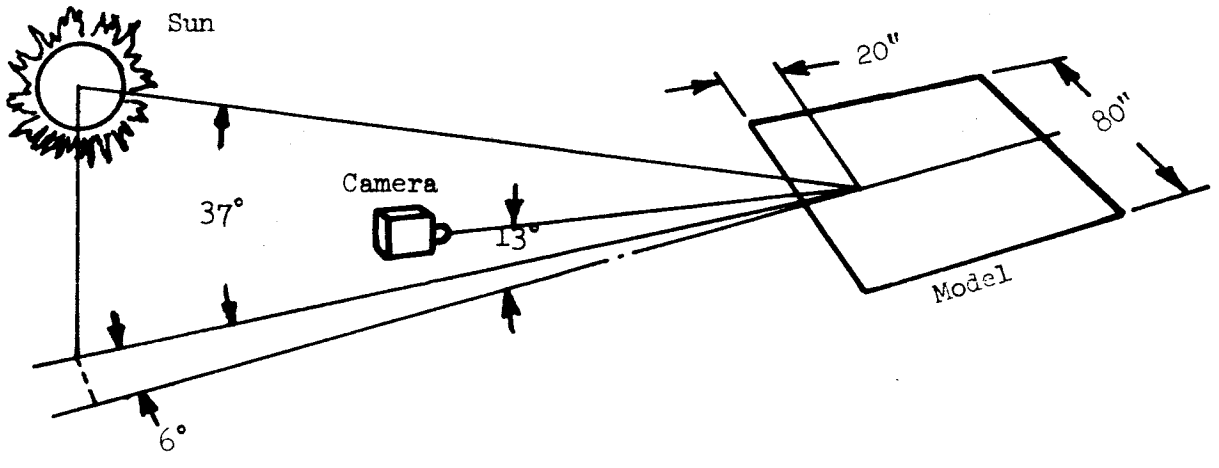

Relationship of Sun Simulator,
Camera, and Model for Motion Picture Simulation

Figure E1-2

(4) The Camera View

Placed at the design eye point of the LEM window, the 15mm lens covers from the bottom of the LEM window, or 25° from the vehicle vertical, to a point 53° from the vehicle vertical. By pointing the lens axis 7.5° to the left of the trajectory plane, the right limit of the camera view just meets the right edge of the LEM window.

This camera view was held for the entire simulation. To frame the LEM window as it appears in this view, a mask was made and placed in the focal plane of the motion picture camera. The mask blocks light from the film in the area beyond the edge of the window. Figure E1-3* shows that the lunar horizon remains in view in the LEM window for the entire section of the descent, but disappears from view in the simulation during the rapid pitch maneuver at 200 feet altitude because of the choice of camera view.

(5) Camera Motion

The 38° field of the 15mm lens limits the distance that the camera can be placed away from the back edge of the model. At 116 inches from the back edge, or 36 inches from the front edge, the 80 inches along the back edge (the horizon) fills the field of view. Depth of focus, on the other hand, limits the near distance to the model. To make this distance as small as possible the lens was set at f/22 to obtain the greatest depth of field for this lens. This setting allows the camera to move to 3 inches above the model's surface, at which point the nearest object in view is 8 inches away and the farthest is 88 inches, with the last few inches of the model slightly out of focus. Moving nearer the surface would cause an objectionable portion of the

*Taken from Figure 4.10.5-3, Pg. 4.10-25, Design Reference Mission, Ibid

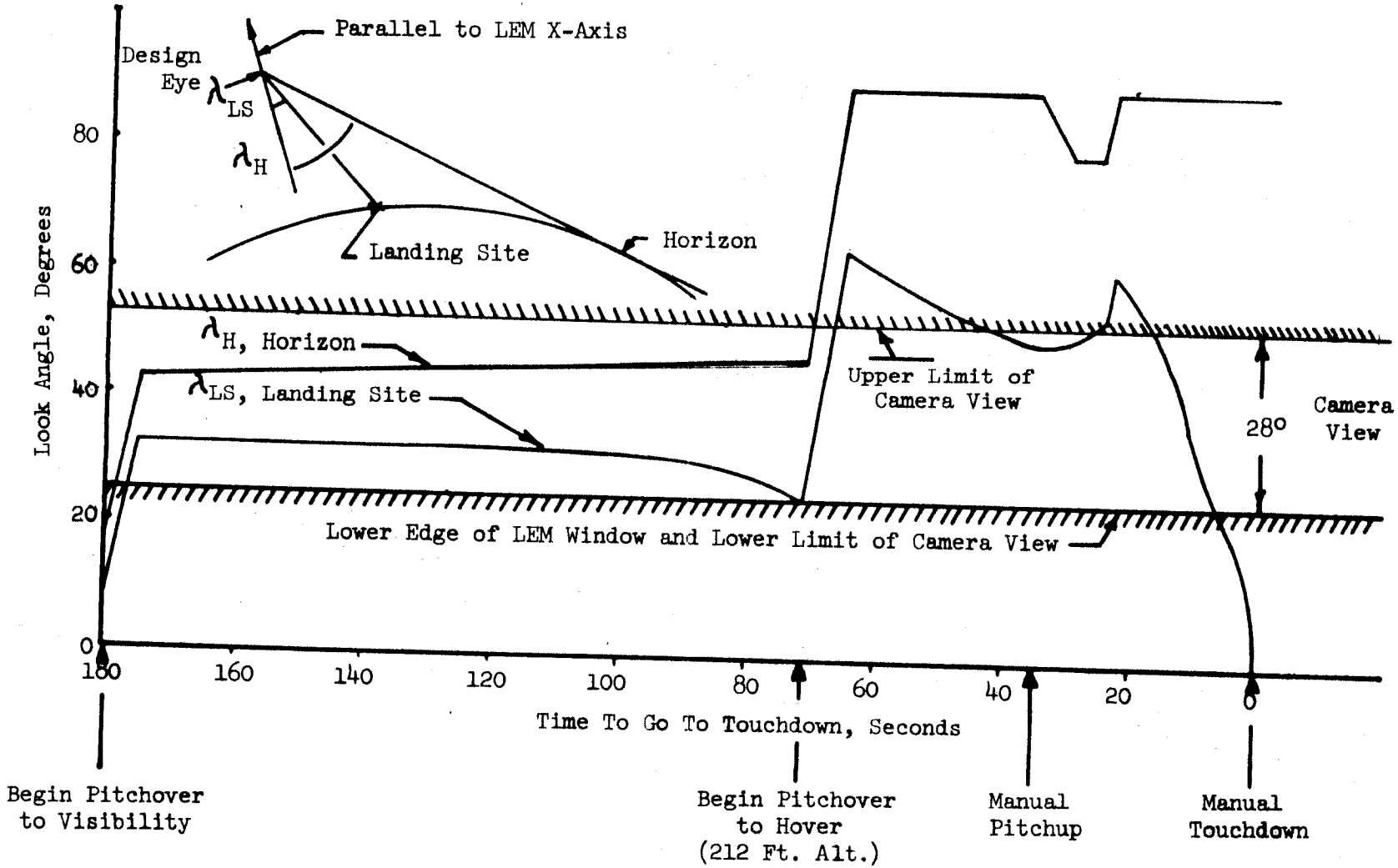

Figure EL-3 Positions of Horizon and Landing Site in LEM Window During Powered Descent Visibility Phase (Manual Touchdown)

picture to be out of focus. Letting the nearest approach position of the camera be at the model's edge and 3 inches above the surface, there was then available a range change of 36 inches or an altitude change of 8 inches on which to build the simulation.

For altitudes from 10,000 feet to 200 feet the flight path is along an almost constant slope of 13°. The elevator of a photographic tripod extending down at this angle of approach was used to simulate motion for this part of the descent. Motion for the descent from 200 feet, some of which is parallel to the surface and some of which is on a parabolic arc, was simulated by operating two tripod elevators welded together at right angles. Pitch changes were made through adjustments on a hand-cranked panning head. The camera was specially mounted on this panning head so that the axis of rotation for pitch changes passes through the nodal point of the lens.

c. Making the Motion Picture

The motion picture was filmed to show the events in real time sequence when projected at 24 frames per second. That is, 24 frames were exposed for each second of the descent. The limitation of 8 inches of altitude change ending 3 inches above the model made it necessary to photograph the simulation in four scenes with an assumed change in scale between each scene. The descent parameters for the beginning and end of the four scenes are given in Table E1-1. The altitude and range were plotted against frame number for each of the four scenes, and a schedule of focus settings, camera movement in inches, and pitch angle change in degrees for each frame was made.

The Cine-Kodak Special Camera was actuated every 5.5 seconds by an electronic release control, so that the shutter remained closed for the same length of time that it remained open. The procedure was to expose a frame, make the scheduled adjustments while the shutter was closed, expose a frame, make the next adjustments, and so on to the end of the scene.

d. Suggestions for Improving Simulations

First, a summary of the constraints of this simulation. The solar elevation was restricted to values higher than 37° to eliminate the shadow from the field of view. The size of the model, in turn, was constrained by the choice of solar simulator and its placement at 39° elevation. A 15mm lens was selected to obtain a wide angle of view and was set at f/22 for greatest depth of focus. Model size, lens view angle, and lens depth of focus then determined the range over which the camera could be moved. This range in turn dictated that the motion picture simulation be made in four scenes, each at a different scale. Since a lens setting of f/22 requires long exposures, with the 500 watt solar simulator, Tri-X reversal film was chosen to keep exposure times as short as possible and to keep the total filming time of the simulation within reason. However, Tri-X Reversal Film has a large grain structure which limits the quality of the final film.

Several changes which will improve the motion picture simulation are now apparent. First, a better quality motion picture can be generated from the set-up used by exposing Plus-X Reversal Film at f/16 using a 1000 watt light source in the sun simulator. This arrangement compensates for the lower speed of Plus-X Reversal Film and allows the film to be produced in the same time as

the one on Tri-X. Although stepping down to f/16 reduces the depth of field, the finer grain of Plus-X film may partially offset this loss by producing a sharper, clearer picture.

A second suggestion for improvement without seeking to reduce the contraints, is to build the foreground sections of the model to the scale of each scene. This could be done in such a way as to make the transition between scenes smooth and consistent.

A third suggestion is to increase the size of the model and use a solar simulator of larger diameter at a greater distance. The larger illuminated model would permit fewer changes in scale during the simulation.

Finally, one notes that changes in the relative positions of sun, LEM, and moon would free some of the restraints on the motion picture set. For example, illumination at right angles to the descent path would allow a sufficient width of model to be illuminated so that a three-or possibly two-scene simulation could be made. Also, by having the LEM land into the sun, the camera shadow does not fall on the model, and approaches at low sun elevations may be simulated.

Further work on simulating the DRM or other descent paths, will produce better quality and more informative motion pictures.

3. Conclusions

1. Under the constraints of the laboratory set-up, the motion picture is a good simulation of the final section of LEM descent trajectry. The film shows the very low contrast of the lunar surface when the observer has the sun at his back and is below the sun elevation angle. Under these conditions no shadows will be present.
2. The motion picture was processed to a gamma of 1.5 which gives an impression of greater contrast than will be seen by an observer.
3. Motion pictures of other trajectories should be made to find the optimum configuration for revealing maximum lunar detail.

F. FOLLOW-ON WORK

The following suggestions outline areas in which the present study has shown the need for additional investigation or has pointed out new topics for investigation. These suggestions are separated into three categories:

1. Application of Lunar Photometry
2. Detection and Enhancement of Photographic Detail
3. Methods of Rating Picture Quality

1. Applications of Lunar Photometry to Image Interpretation

a. Mapping of the moon by satellite photography will be done either by photoclinometry or by contour plotting from stereo pictures. The precision and accuracy of maps made by these two methods should be determined in experiments using pictures of realistic lunar models.

b. There is a need for information on the appearance of the lunar scene when viewed through color or polarizing filters. A realistic lunar model should be dusted with volcanic or other suitable powders in a manner duplicating the lunar photometric function. Photographs of this model should be taken using color or polarizing filters at several sun altitudes, and should be studied for possible improvements in our ability to detect landing hazards.

2. Detection and Enhancement of Photographic Detail

a. The investigations in the present study should be extended in several areas. These include a more thorough evaluation of the value of stereo photography in revealing lunar details, especially when pictures are taken in a plane not containing the sun; the appearance of a lunar landscape in photographs taken with a wide angle lens; and photography of models containing several values of albedo.

b. Multiple pictures of a possible landing site presented to a viewer in rapid sequence may offer increased information over that available in a single picture. This technique should be explored especially using pictures taken at high sun altitudes.

c. Low contrast images will be obtained in lunar photographs taken at high sun altitudes or after exposure of the film to sufficient penetrating radiation. Methods of increasing image contrast should be studied. These techniques include use of high contrast print materials, printing with a specular light source, chemical reducers and masking.

d. Several motion pictures should be made to illustrate the lunar scene as viewed from the landing LEM with favorable positions of the sun and the observers. Improvements in the method of filming the simulations could also be made.

3. Methods of Rating Picture Quality

Operational photography seldom includes pictures of calibrated test patterns to allow a precise measure of photo system performance. Three methods for measuring performance using images of lunar scenes are suggested below:

a. The Modulation Transfer Function (MTF) of a photographic system may be determined by Fourier analysis of traces made on images of sharp edges in the scene. The intersection of the MTF curve with the Aerial Image Modulation (AIM) curve for the photographic film yields a prediction of the limiting resolution of the system. This technique should be explored using images of lunar scenes to determine the precision of this method and to learn the correct size and shape for the mircodensitometer aperture.

b. The MTF curve for a system may also be found by autocorrelation, a method in which two identical transparencies of a scene are placed in exact register, then one moved laterally while their integrated transmission is measured. Performance ratings determined using this method should be compared with those obtained from tri-bar readings and edge trace analysis.

c. Comparison pictures are a simple but useful approach to the determination of photographic quality. A file of scenes from the lunar model could be prepared showing the effect on image

quality of degrading factors such as image motion, defocus, image scale, sun altitude, and film gamma. Comparison of pictures from the file with those from actual operations should permit estimation of a performance rating.